NTNU

Norwegian University of
Science and Technology

Analysis of Drift-off During Drilling on Deep Water

Ke Gao

Marine Technology
Submission date: September 2015
Supervisor: Carl Martin Larsen, IMT
Co-supervisor: Gullik Anthon Jensen, Kongsberg Oil & Gas Technologies

Norwegian University of Science and Technology
Department of Marine Technology

M.Sc. thesis 2014

for

Stud.tech. Ke Gao

ANALYSIS OF DRIFT-OFF DURING DRILLING ON DEEP WATER

During drilling from a floater with dynamic positioning system (no anchor lines) it is the thrusters that keep the vessel in position. If all power is lost (black-out) the vessel will start to drift due to forces from wind, current and waves. This is known as a drift-off situation. If this happens when the drilling riser is connected to the wellhead at the seabed, the riser might be damaged before an emergency disconnection can be accomplished. The time window between power loss and serious riser damage depends on the environmental condition and riser parameters. The purpose of this project is to carry out simulations of drift-off situations in order to identify this time window, and also to identify reliable analysis models for this type of analyses.

Two types of simulations may be carried out – one with prescribed vessel drift-off in combination with wave induced motions, and the other by use of a coupled model for vessel motions and riser dynamics.

The first model is uncoupled and will apply prescribed surge motions found by adding first order surge to a current induced component. Heave at the drill floor will also be known, while vertical motion of upper riser end must be calculated by a time domain simulation of riser dynamics. The first occurrence of maximum pull-out of the heave compensator can then be identified, and simulation may continue with riser end fixed to the floater for all translation degrees of freedom.

One effect that can be studied by use of the coupled model is the influence from current forces on the riser on drift-off speed. The riser may act like a "sail" due to its large area and hence also large current forces. After some time, when the vessel has gained speed and the heave compensator has reached its maximum stroke, the riser will start to act as an anchor to slow down the vessel speed. Further drift may give a rapid increase of riser stresses and lead to failure.

The work might be divided into tasks as follows:

1. Literature study that should cover deep water drilling technology and methods for simulation of riser dynamics and floater motions

2. Find data for a drilling unit including riser, and identify relevant environmental conditions for simulation of drift-off situations
3. Carry out a set of stochastic simulations of drift-off by use of an uncoupled model, and change the boundary condition for riser connection on the floater at the time instant when maximum stroke capacity is exceeded
4. If time allows a set of coupled analyses should be carried out in order to identify the influence from forces on the riser on drift-off behaviour

The work may show to be more extensive than anticipated. Some topics may therefore be left out after discussion with the supervisor without any negative influence on the grading.

The candidate should in her/his report give a personal contribution to the solution of the problem formulated in this text. All assumptions and conclusions must be supported by mathematical models and/or references to physical effects in a logical manner.

The candidate should apply all available sources to find relevant literature and information on the actual problem.

The report should be well organised and give a clear presentation of the work and all conclusions. It is important that the text is well written and that tables and figures are used to support the verbal presentation. The report should be complete, but still as short as possible.

The final report must contain this text, an acknowledgement, summary, main body, conclusions and suggestions for further work, symbol list, references and appendices. All figures, tables and equations must be identified by numbers. References should be given by author name and year in the text, and presented alphabetically by name in the reference list. The report must be submitted in two copies unless otherwise has been agreed with the supervisor.

The supervisor may require that the candidate should give a written plan that describes the progress of the work after having received this text. The plan may contain a table of content for the report and also assumed use of computer resources.

From the report it should be possible to identify the work carried out by the candidate and what has been found in the available literature. It is important to give references to the original source for theories and experimental results.

The report must be signed by the candidate, include this text, appear as a paperback, and - if needed - have a separate enclosure (memory stick or DVD/ CD) with additional material.

Supervisor is professor Carl M. Larsen

Trondheim, October 2014

Carl M. Larsen

Submitted: October 2014
Deadline: 15th Sepetember 2015

Acknowledgement

First and foremost, I would like to thank my supervisor, Professor Carl Martin Larsen of NTNU. His patience and motivation enlightened my pursuit in the riser analysis. His immense knowledge guided me through the obstacles and frustration encountered during the thesis writing. His professional dedication inspired the attitude and tranquility. Even I have very limited knowledge regarding the steel top risers, I succeeded acquiring the useful mechanical responses knowledge.

I would like to thank Senior Scientist Elizabeth Anne Passano of MARINTEK for her help with the Sima program installation, trouble shooting. Also thanks to PhD Gullik Anthon Jensen of Kongsberg for providing me the detailed modelling data, and Senior Research Scientist Knut Mo of MARINTEK for helping to achieve the platform modelling data.

Last but not least, I would like to thank my mother for supporting me all my life.

Department of Marine Technology

September 9th, 2015.

Ke Gao

Summery

For drilling operation in the deepwater, dynamic positioning system is used for platform to maintain the position. In case drift off (positioning system don't function), the drilling system might be damaged before an emergency disconnection can be performed. The time window between the beginning of the drift off and critical riser damage depends on the many facors. The purpose of the thesis is to identify the influence of coupling effects between the riser and platform on the time window and identify a reliable model for this type of analysis.

The dynamic nonlinear analysis is carried out in Sima for both coupled and uncoupled conditions. The critical scenario is defined that wind, current, and wave acting in the same direction. 300 m, 1000 m, 3000 m water depths are investigated. Different current speed is also researched in the parameter analysis.

Tension level is mainly dependent on the offset. The coupling effects on the time before tensioning stroke running out is very limited but it tension don't increase as fast as the uncoupled analysis. Different currents are found only important for the drift off speed. Since the limited coupling effects, a simple analytical solution is proposed. The results proved to be way conservative considering the tension.

Table of contents

Notation

TTR: Top tension riser
VIV: Vortex induced vibration
FEM: Finite element method
SCR: Steel catenary riser
LWR: Lazy wave riser
TDP: Touch down point
DNV: Det Norske Veritas
BOP: Blowout preventer
LMRP: Lower marine riser package
RAO: response amplitude operator
WT: weight
DAT: Direct acting tensioner
EDS: Emergency disconnect sequence
TLP: Tension leg platform
MODU: mobile offshore drilling unit
EDP: Emergency disconnect package
RSP: Riser safety package
NPV: Nitrogen pressure vessel
CAPEX: Capital expenditure
OPEX: Operating expenditure
RKB: Rotary Kelly bushing
DP: Dynamic positioning
DOF: Degrees of freedom
COG: Center of gravity

1. Motivation

Being evolved during the recent several decades from many other branches, the pipeline and riser technology fairly matured (Bai Y. and Bai Q. 2005). With the requirement of transferring to the deeper water and more hostile weathers, more technical challenges follows and needs to be solved. On the other hand, only robotic forces can be used under many circumstances, the design strategy is highly demanded which would cut the expense significantly if no inspection and fixation after the installation. With dynamic positioning being widely used, the pipeline and riser technology is becoming more and more critical. Gas production percentage on Norwegian continental shelf is increasing, the pipeline and riser are becoming more and more important in the operation (Factpages 2015).

2. Introduction

For a drilling floater working in the deep water, dynamic positioning system keeps the platform in position. When the platform lose power it will drift off due to wave, wind and current forces. If the riser is still connected during the drift off the riser and the wellhead down on the seafloor will have the possibility to be damaged. The aim of the thesis is to identify the time window between the power lost and possible damage.

Two types of modelling should be carried out. The first model is uncoupled which do not consider the interaction between the riser and the floater. The second model on the contrary account for the coupling effects between the riser dynamics and floater motions.

For the uncoupled model, the motion of the vessel is calculated by the program Sima and the motion of the upper and of the riser model is controlled by the vessel. The main part of riser body configuration is affected by the forced induced by winds, currents, and waves. For coupled modelling, the forces in the top of the riser is considered when calculating the vessel motion and on the other hand the upper hand motion of the riser is affected.

3. Previous Work Summary and Review

3.1 Review of a thesis regarding the different marine riser analysis program comparisons and Riflex computation verification (Zhan 2010)

Part 1

With all the development of the marine riser technology for many years, back analysis still shows the poor ability of analysis even with the advanced analysis programs. The more and more complexity of the programs today make it more difficult for the designers to feel the confidence. Verification thus should be processed to verify the results. Furthermore, understanding of the computation mechanism is also necessary.

Riser analysis tools are special purpose programs exclusive for slender structures including top-tensioned risers (TTRs), catenary risers, flexible risers and other types of slender structures like pipelines and mooring lines. The most popular marine riser programs reviewed involved are OrcaFlex, Deeplines, Flexcom, Riflex. Though the modelling environment and graphical user interface manifest differently, the solution principles do not vary much.

The common structural features shared between the programs are unlimited rotation and translation in 3D space, small bending stiffness, large deflection, large upper end motion excitation, nonlinear cross section properties, and complex cross section structure. Typical analysis are strength analysis, fatigue analysis, vortex induced vibration (VIV) analysis, and Interference analysis. And the results from finite element method (FEM) are nodal point coordinates, curvature, axial forces, bending moments, shear forces, and torsion.

Considering the load mode, regular waves are with Airy or Stoke wave theory. Irregular waves are depicted by various wave spectrums. Current are characterized by 3D time and space constant or space linear piecewise profile (Orcaflex offers a time varying profile option.). Hydrodynamic forces are calculated through Morison equation (Riflex provides a linear drag force option.). Rigid and elastic seabed contact model are determined by Coulomb friction, seabed profile, seabed suction, trenching and lateral seabed stiffness. Soil model could be linear elastic or non-linear hysteretic. Vessel motions are generated through transfer function or motion history files.

In the static analysis, both catenary and FEM analysis are used. Catenary method ignored the contact, bending and torsion stiffness and provides a quicker and preparatory result. FEM is more computation demanding and accurate. There is no unique solution when resisting compression for the catenary method, because the line will be slack under compression (Orcina, 2009). In the dynamic analysis, simulations are operated over a specified time period starting from the static analysis position.

Force equilibrium is achieved by iteration. Various integration methods are employed. The programs above focus on the global response and local stresses and strains are not considered.

The robustness of the above industrial software are trustworthy, the numerical shortages are unavoidable and noteworthy for engineers to make wise decisions. Catenary method can only serve as a time saver for preparatory stage of static configuration because of the accuracy shortage.

Newton-Raphson method iteration as an effective non-linear problem solver may encounter non-convergence problem when passing a limit point. More advanced technique like Riks should be employed if required. Spurious high frequency response caused by intrinsic FEM principle needs to be counteracted by target damping or integration damping. There is balance dilemma between the computation time and accuracy due to the fine or coarse discretization of FEM so parameter analysis should be taken to adjust a good balance. Similarly to the discretization problem, many widely used integration method is conditionally stable which requires time step to be small enough especially for some particular stages. To reach a good balance between computation and accuracy, smaller time steps are used when needed. Mass, damping and stiffness of frequency domain method are assumed to be not changed. Thus it is suitable for problems without involving much non-linearity. Top tension riser, for example, the beam rotations of which are less than 6 degree, generally use frequency domain method. To account for the post buckling behavior which can't be fully addressed in the FEM analysis model, the principle is to reduce the segment length sufficiently to a sensible length and make sure the Euler bucking is not exceeded in each element. Soil-pipe interaction model also have some limitations: linear model is effective in the view of global analysis but when it comes to the touch down area where fatigue should be considered, non-linear soil model should be used. However, non-linear model is not suitable for cap rock conditions. The coefficients in the hydrodynamic forces model are constant and will not be able to reflect real force. Also the vortex induced forces are ignored by many programs. Though the effect of axial drag force might be negligible, in some case it might lead to some non-conservative results (Patel 1995).

Part 2

To verify the reliability of Riflex, two type of analysis are carried out including static analysis and dynamic analysis. The principles in the static analysis to be verified is general FEM. Euler-Cauchy increment and Newton Raphson iteration is used in the FEM. In the static analysis, the verification method for steel catenary riser (SCR) and lazy wave riser configuration (LWR) are from Faltisen which neglects the bending stiffness and cable elasticity (Faltisen 1990). When considering the LWR, two approaches are used for determination of initial tension and suspended cable length.

The first is from Larsen C.M. (1996). The second is from Peyrot and Goulois (1979) which is the same principle adopted by Riflex catenary analysis.

The distribution of static configuration, effective tension, and bending moment reach a reasonable agreement. The top tension components also reach some acceptable results even with the current force which generated from no current configuration directly superposed on the current configuration.

In the dynamic analysis, an analytical approximation by Aranha (1997) is adopted to find the dynamic bending moment at the touchdown point. The approach as catenary method from Faltinsen neglects bending stiffness too and assumes no impact phenomenon. The approximation results shows a conservative shift with the Riflex outputs. Meanwhile, the location of the mean touch down point (TDP) don't coincide. In conclusion, the results are not comparable and verification of the dynamic part fails.

3.2 Review of a thesis regarding the detailed modelling of marine tensioning system (Sten 2012)

The demand of oil and gas industry moving towards deeper water set up the new boundary for the heave compensators. The stroke needs to be long enough to sustain a relative constant tension and compensate the relative motions between the platform and the riser upper end. Severe damages caused by forces, corrosion, wear and fatigues are found after in operation a few months or at most a few years. Replacement and maintenance of the large piston rods is very demanding and costly. Therefore, it is in demand that a more trustworthy material and sealing system can withstand the challenge. Then accurate forces the hydraulic systems are subject to needs to be known. Lateral deformations from lateral forces and accelerations are assumed exist because severe damage is observed on the pack box and cylinder rod.

The tensioning system are coupled with risers by six inclined cylinders. The inclination will account for the environmental lateral loads but also will cause lateral forces on the barrel and rod. To keep a relatively constant tension, cylinders are connected to a large volume nitrogen pressure vessels. There will be dynamic effects like pressure loss in the pipes.

The thesis mainly discuss the dynamic modelling of the drilling riser, especially the tensioner part. Traditional top tension is either constant or simple spring damper system to provide an approximate tension. Now a more realistic, accurate modelling is proposed which includes the following procedure:

1. Via global analysis of riser and prescribed motions of the platform, dynamic stroke was calculated firstly in Riflex. Pipe-in-pipe model was verified as a trustworthy modeling and adopted.

2. The motions from the Riflex was input into Simulation X to get the dynamic tension. Parameters of a simple spring-damper model was calculated by the dynamic tension results.

3. The spring-damper model was input back into Riflex to compare the results from the second step.

Hydraulic system is modelled using SimulationX and is composed of 7 parts: nitrogen pressure vessel, nitrogen/oil accumulator, shut-off valve, piping and hoses between shut off valve and cylinder, low pressure volume, cylinder, input from Riflex. Main focus is the pressure variations through the 7 parts. The results shows that the pressure variation leads to a significant cylinder force variation. The force variations and stroke variations are used to find the parameters of a simple spring-damper model. Though the simple model did not exert the same small non-linear effect as the SimulationsX results, it is considered correct enough to be used in the Riflex model for global analysis.

Traditionally Morison equation is adequate enough to address the issues because riser diameters are at least one order magnitude smaller the wave lengths of interest. The publications regarding slamming issues (Nestegård et al. 2004; Campbell et al. 1980) suggest that local slamming may have a noticeable influence on the tensioner response. The short duration and damping will not lead to noteworthy global response. Theories and parameter influences from the two articles are used in the current thesis which characterized by a combination of impact load term and a conventional Morison load model term. The model can be described as two parts, partially submerged part will endure slamming force, fully submerged Morison force. Det Norske Veritas (DNV) in-house program Waveslam is adopted for the slamming force calculation and the results are input in Riflex. The slamming force is shown to be have a great influence on the tensioning system which leads to larger forces on the cylinders. The impact of the forces on the risers and the associate parts are not of concern in the thesis. All data used are from platform Aker Spitsbergen support the conclusion. The heave compensator was instrumented for recording the response data.

In the thesis three kinds of modelling (bar, beam, and pipe-in-pipe) are developed for three water depth (206m, 1300m, 3000m) with tension tuned to 600KN between blowout preventer (BOP) and lower marine riser package (LMRP) for all water depths. The pressure in three water depths are 30, 60 and 100 bar. Bar and Beam modelling almost shows the same results. Modelling with slamming and modelling without slamming are compared. The slamming have a very minimal influence on the stroke as vertical motion of the tension ring is very small and main influence comes from the platform motions. Same goes to the stroke velocity and stroke acceleration. What is noticeable is that for significant wave height equals to 8m and peak period of 12s, the stroke velocity is far below the design limit. The pack box lateral acceleration of slamming direction is of concern as the slamming inclusion increase the acceleration

a significant amount. Shift from beam model to pipe-in-pipe model shows the same trend as pipe-in-pipe model experience longer distance between upper and lower end of the cylinder. Pack box vertical acceleration is mainly influenced by the platform motions so the difference is minimal. The vertical and slamming direction of the tension ring acceleration increases a large value as tension ring is close to slamming and more infected by slamming. Bending moment illustrates a large rise when slamming is included, but largest moment of both beam and pipe-in-pipe model exhibit similar results. Pipe-in-pipe modelling provides a more realistic mechanism relative motions and shows more accuracy by measured response. Therefore pipe-in-pipe modeling are used thereafter. The main interest which is lateral acceleration breached design criteria of lateral evenly distributed acceleration of 1.5 $\mathrm{m/s^2}$. Then all cylinders in operation of earlier design are replaced to withstand the higher acceleration up to 10 $\mathrm{m/s^2}$. Then tension variations from SimulationX are also beyond expectation which should be taken into account for analysis references.

Tension variations are large and larger pressure leads to larger pressure drop hence large tension variations. The situation of two cylinders out of six cease to function are investigated, the pressure and thus tension in the left four cylinders increase to compensate the loss of the two cylinders. Acceleration on the contrary decreases because of more stiffness because of the higher pressure and tension. Large moment in the rod/pack box and piston/cylinder contact are uncertain because local contact force, and thus a detailed model in Abaqus are to be investigated further. The maximum bending moment in the Abaqus is a bit higher than in the Riflex because Abaqus is more accurate when it comes to contact force and forces in guide bands are considered.

Measurements from the platform Aker Spitsbergen were recorded. The zero value of the strain gauge were impossible to find, but the tension force variation range seems to fit the range of the simulation results. With the limitation of the measurements recorded, comparison of the pack box accelerations will be made between the 206m water simulation results and 380m measurement results as environmental data are very similar. Cumulative distribution and sample history of frequency content of the calculations of the lateral acceleration appears to be comparable. Slamming component to wave component ratio from the simulation are much larger than from the measurement and this is may be caused by the nonlinearities of the slamming. However measurement confirm that the significant component other than the wave frequency is highly probably from slamming.

For future work, an integrated modeling of the hydraulic system and riser could be developed. It should meet the following requirement: global analysis of riser subject to vessel motions and environmental forces, hydraulic-pneumatic system simulation to provide the tensioner system pressure variation, detailed analysis of the contact forces between cylinder/piston and rod/pack box, instrumentation of riser system and real-time online assistant regarding operations and critical scenarios. An option could

be the two programs used in the thesis, and a real time communication between should be established. Even both measurement and simulation suggest the significant influence from slamming, the magnitude is still uncertain so the slamming model should be reviewed. The high quality measurement should be of concern in the future which greatly influenced the outcome of the study. Another factor that should be implemented is the platform offset which have shown great influence on the cylinder forces.

3.3 Review of a thesis regarding the tensioner stroke locking under unexpected platform offsets (Hermanrud 2014)

New financial and technological challenges is rising and deeper water depth and less new reservoirs leads to requirement of higher recovery rate. Workover riser is used for production or maintenance or optimization and thus highly related to the challenges

More complex marine operations and severe loss and damage caused by accidents urge the industry to level with higher standards and safer protocols. A workover system should be able to satisfy safety barriers to keep the operations safe and secure. Riser tension is highly related to the safety barriers. The thesis deals with a workover riser with two compensators. The riser is connected to support vessel at the upper end. The heave motions caused by the platform and translational displacements are compensated by the compensators and DP system respectively. In drilling operation normally risers aligned vertically above wellhead, deviations may occur during drift-off or drive off during which most critical scenario that can happen is under concern.

The critical scenario is defined as the drift-off condition and lock up of the compensator at the time interval when support vessel endure the maximum vertical velocity. Significant rise in the tension will be of a main concern. To make the max vertical velocity trackable, regular analysis is carried. Wave heights and period are based on the compensation limit of the compensators, scatter diagram for the operational area and support vessel response amplitude operator (RAO).

Analysis are carried out for three different water depth, 309. 4m, 1300m, and 3006.88m. Because sharp increase of the riser tension is need to be monitored, load impulse that travel from riser top to bottom should be considered. The speed of the impulse depends on the steel type. In the process, static analysis is used to find the initial position of the riser. Effective tension is used to modeling the geometric stiffness. Material nonlinearity is of minimal effect. Equilibrium is found be incremental loading procedure with iteration at each load step. Updated Lagrangian method is used without displacement limitations. Volume forces and current forces are standard displacement dependent modelling. In the dynamic analysis, airy wave theory is adopted for regular analysis. Wave potentials are stretched and compressed at the instantaneous position. Morrison model is accounting for the external force model. Time domain analysis is used to solve the nonlinearities involved. Newmark beta

family-Wilson Theta method, and Newton-Raphson iterative procedure are adopted for numerical calculations.

Modelling of the stack-up of 309.4m and 3006.88m is by adding or subtracting light weight (WT) riser joints in between of the 1300m one. Current profile of the 309.4m and 3006.88m are extended or truncated from 1300m one. From the top equipment to the bottom well head, all are modeled using circular beam element and an increased hydrodynamic diameter are accounted for the sharp edges and flow separation of the submerged equipment. Riser tensioner system is modelled as ideal with constant tension. Direct acting tensioner (DAT) system is not included and only the top compensation system is considered. Due to the uncoupled analysis, horizontal support of the tension system is not included but the results will minimal infected. As flow around the riser is not essential so umbilical modeling is not included.

From the limit of the compensating system, heave motion amplitude is stipulated. The regular wave height and period are assumed to be the significant wave height and peak period from the platform's working environment scatter diagram. The significant wave height and peak period are chosen from the transfer function. The lock up of the critical scenario can be either hydraulic fluid lock or spare stroke running out. The support vessel motion is examined from the wave trough to wave crest and if the vessel maximum speed reached before the spare stroke running out, the lock will be hydraulic fluid lock. Otherwise, stroke lock up will be the case (without reaching the vertical maximum velocity). Lock up will be modelling as vertical fix from riser top end to the vessel before which only the translational direction follow the vessel motion.

After the lock up, tension will increase rapidly with oscillations which will flatten as the floater reaches the wave crest except the cases with stroke running out because of large offset only. Because for large offsets in the dynamic analysis there is no boundary change and thus no accumulated inertia to raise the tension. Statically, because more offset means larger geometrical stiffness, larger offset yields a slightly larger tension even though the declined angle will have smaller forces perpendicular to the riser. Dynamically, lock up is earlier and velocity is smaller such that the tension increase is smaller than the zero offset case. Also from the results, there is no indication of much additional tension from the drag, added mass, and the offset caused angle. It can be concluded that if the riser can sustain the tension increase of zero offset, larger offset can be either. It can be seen that the difference between the offset riser tension and no offset riser tension are larger at the bottom and top sides.

The impulse oscillations were created by the reflection of the impulse. The longer the riser, the more time it needs to reflect. Hence the oscillation periods are longer for longer riser. The magnitude of the tension increase depends on the vertical velocity at the lock up interval. Because of the rapid increase of tension, fine time discretization is needed to capture it. The worst scenario is a combination of various factors and hence is very unlikely to occur. It do have the meaning of use reference and this

situation should be considered from humane and regulatory point of views. Further work like weak link design, statistically short term and long term analysis can be expected.

3.4 Review of a thesis regarding the marine riser recoil analysis (Grønevik 2013)

As drilling is moving towards deeper water, the extreme hydrostatic pressures imposes new challenges. Dynamic positioning is replacing the traditional mooring as the dimension and cost of mooring system increases as the water depths. The deeper water depths leads to larger and heavier drilling riser, more tension, more drilling mud quantity. The Macondo accident sounded the alarm.

Riser recoil analysis is mandatory for all offshore drilling unit for planned or planned disconnect. When environmental conditions have the potential of exceeding operation limits or uncontrolled platform motion scenarios (e.g. drift-off, drive-off) occur, the floater needs to be disconnected from the well head to keep well head from being damaged by exceeding forces. Next to the moment that tensioned riser is released, lower end will act as tensioned rubber and move upwards due to released stored elastic energy (non-dominating) and forces at the upper end (dominating).

Considerations needs to be taken that the recoiled the lower end of the riser don't come back and strike the wellhead. Also on the drilling deck the recoil needs to be slowed to not hitting the equipment on the deck. Emergency disconnect is more demanding than the planned disconnect because of no time to retrieve drilling string, circulate the drilling mud, and lower the tension. When emergency disconnection sequence is initiated, LMRP is lifted off and BOP is left to seal off the wellhead. If drill string is in place then blind shear rams will cut through the piping. For some situations even the positioning system can hold the floater in position, disconnect still needs to be done to avoid damaging equipment or wellhead (Kavanagh et al. 2002; Nguyen et al. 2006). Uncontrolled gas leak from seabed may endanger the platform buoyancy and a riser disconnect and platform pull off is needed (Dolphin Drilling 2013).

General procedures for an emergency disconnect sequence (EDS) would be cut the drilling pipe, sealing the well, opening annular to discharge mud, release the LMRP, activating anti-recoil system. Mud is discharged because retaining the mud will make riser enter the natural frequency of wave and lower the sea state required for buckling (Young et al. 1992). Timing is important for the impact between BOP and LMRP. It would highly possible if platform has a larger velocity than the recoil velocity. The practice for disconnecting is mostly because of platform offset, then due to large damping the LMRP will not swing back and hit the BOP according to conjecture. Another concern would be the buckling as longer riser are prone to buckle with lower compression forces. With the tensioners damping effect decelerating the upper part and lower part moving upwards from the bottom, an ill-tuned anti-recoiled system would cause buckling.

Modelling of such recoil scenario is of main concern, including the varying top tension, shut-off valve damping and vertical hydrodynamic damping, mud discharge mass loss and corresponding friction. All the modelling can't be modelled directly in Riflex and needs pre-processing and simplifications. Modelling of mud discharge friction is done by linear global nodal force time history. Assuming the seawater is refilled from above the riser, the friction force is calculated by dynamic equilibrium between hydrostatic pressure, mud weight, and friction force. Top tension is modelled by assuming adiabatic process and calculated by the internal pressure considering the effects of volume change. Damping effects are modelled as a function of strain rate squared. Due to the malfunction of the slug model for complex riser, another modeling by specifying dynamic nodal force upwards representing the force loss but mass still remain the same.

Due to friction force is applied in the wrong direction, most analysis is incorrect. For the future work, muds discharge study in a CFD program and a comparison in other FEM program should be performed.

4. Riser system

4.1 Main configuration

Marine risers are long slender structures and the cross section properties are constant in long sections. They are constructed with steel cylindrical pipes between the BOP and the floating drilling platform. On the sea floor the flex-joint or ball joint allows for rotation and affordable bending moments. Near the sea surface flex-joint and slip joint allows for rotation and riser axial displacement respectively. A typical top tension riser system can be seen from the picture below (AKER KVÆRNER STORD AS, 2007).

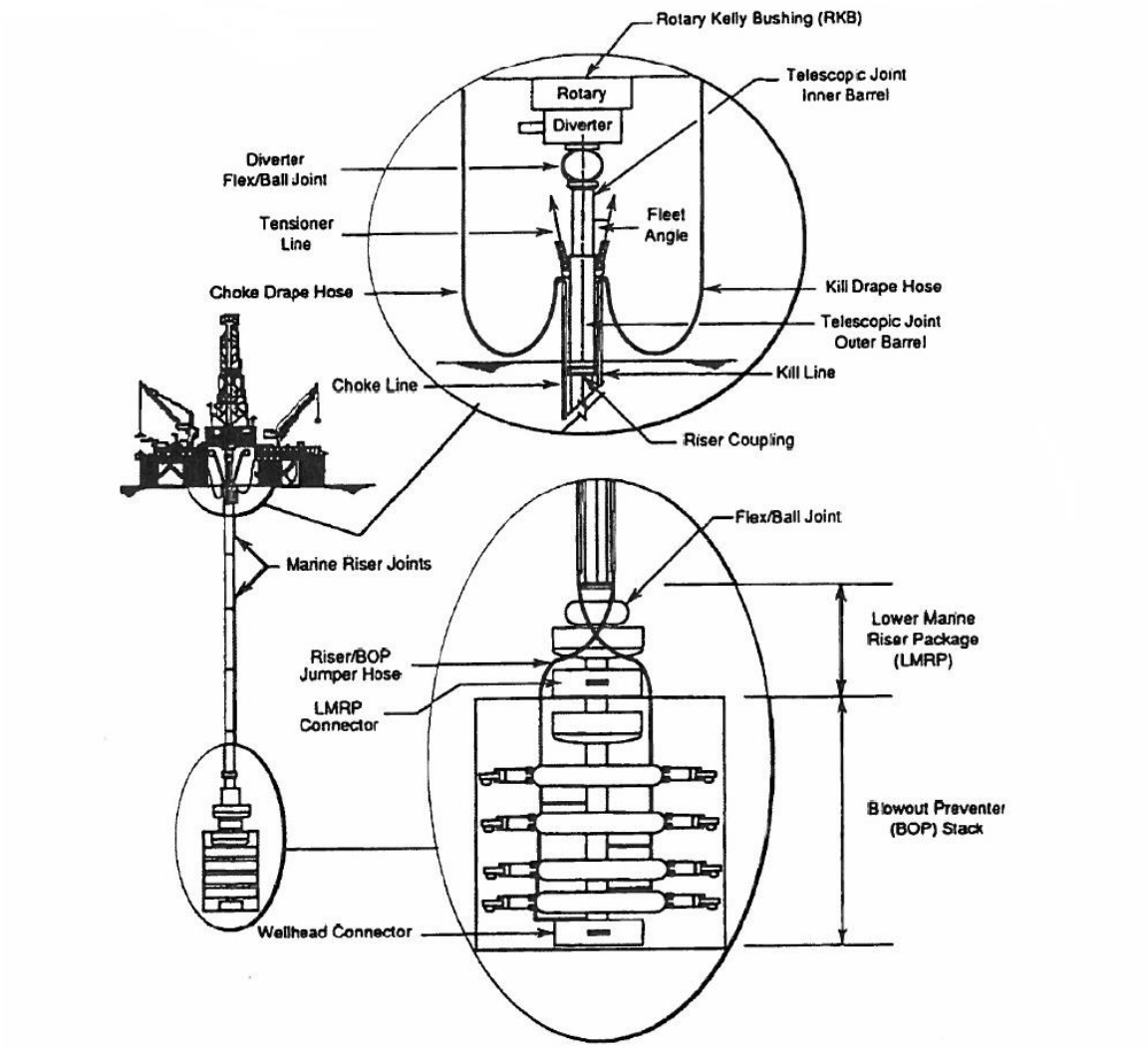

Figure 1 Top tension riser system

4.2 Riser types

The risers should be as short as possible to reduce the material and installation costs. But enough flexibility is also needed to allow for the floater excursion.

The riser the history could be dated from 1951 and after 1961 risers have been used for 4 main following purposes, and within each purpose, they varies with regards to detail, dimensions and materials.

*Drilling
*Completion (workover)
*Production (injection)
*Export

By architecture categorization, risers are divided into two types, namely rigid risers and flexible risers. And a hybrid riser is the combination of aforementioned two (Sparks 2011).

4.2.1 Categorization by purpose

4.2.1.1 Drilling riser

Drilling risers includes two types: low-pressure type and high pressure.

4.2.1.1.1 Low-pressure drilling riser

The standard drilling riser nowadays is the low pressure riser. Pressure at the upper end is atmospheric which won't be exceeded because of the mud weight. A typical drilling riser is made up of a central tube and several peripheral lines. The peripheral lines include kill, choke, booster and hydraulic lines. Kill and choke lines communicate with the well and circulate in case of gas kick, and then BOP is closed. Booster lines inject fluid at the riser lower end and accelerate floor to better evacuate cuttings. Hydraulic line of which the diameter is small power the BOP.

Drilling risers are usually embedded with buoyancy modules on the upper part to reduce the apparent weight. The riser parts near the surface are usually left bare to reduce hydrodynamic forces. The lower parts normally are also left bare because the density and cost of the syntactic foam increases depth.

The connector between the riser joints have different types like breechblock type and flanged type. Between the connectors peripheral lines are reinforced by guides to prevent them from buckling because of internal pressure. Risers usually are deployed from the top end by drill ships, semi-submersibles, Tension leg platforms (TLP), Spar. The drill ships and semisubmersibles are usually called mobile offshore drilling units (MODU). In case of emergency BOP will close the well head and the LMRP above the BOP will cut the drill string. A flexible joint between the riser and LMRP permits a limited rotation and thus prevent bending moment concentration.

4.2.1.1.2 High-pressure drilling riser

BOP is situated at the top end and thus kill and choke lines are not need and the architecture are much more simplified. However, the risers have to sustain the well pressure. The surface BOP configuration are mostly used for moderate environmental conditions. But Seabed emergency disconnection is also needed since the surface BOP brings more risks.

4.2.1.2 Completion riser

Completion risers are a combination of features of high-pressure drilling risers and low-pressure drilling risers. The upper end is equipped with BOP featuring the high-pressure drilling riser design. When deployed from a MODU, the lower end is equipped with packages featuring the low pressure drilling riser with emergency disconnection. The packages are powered by an umbilical and consist of emergency disconnect package (EDP) for cutting the string and riser safety package (RSP) for closing the well.

4.2.1.3 Production riser

Production risers which are used to connect production facilities are categorized by architectures including bundled, flexible, TTR, SCR, and hybrid risers (combination of steel and flexible pipes).

4.2.1.4 Export riser

Export risers are similar to production risers except with larger diameters and lower pressures. So export risers can also be categorized in architecture.

4.2.2 Categorization by architecture

4.2.2.1 Bundle riser

Bundled risers usually consist of a core riser and multiple satellite risers. The satellite risers are maintained in position by guides on the core riser. This kind of configuration was firstly deployed under the platform and then later placed near the platform.

4.2.2.2 Flexible riser

A flexible pipe consist of multiple layers in which each layer takes different responsibilities. Normally the inner metal carcass will resist the collapse, a plastic sheath will contain fluid, a steel vault will resist hoop stress, steel armors will resist axial tensile loads and a plastic outer sheath will prevent seawater penetration.

The configurations which can be seen on Figure 2 (Bai, Y. and Bai, Q. 2005) are determined based on various factors including riser global behavior and geometry, structural integrity, rigidity, and continuity, cross sectional properties, means of support, costs.

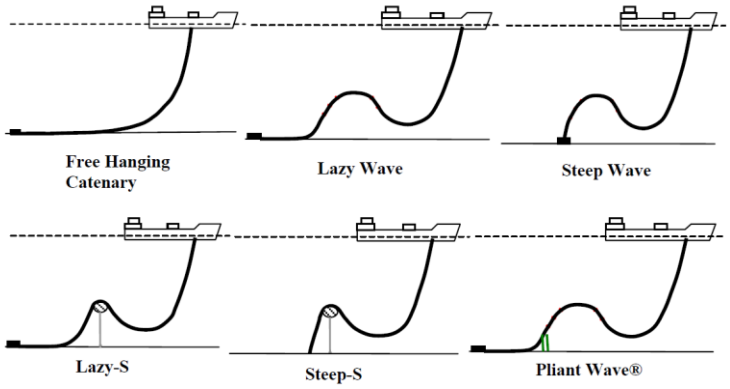

Figure 2 Flexible riser configurations

4.2.2.2.1 Free hanging catenary

This configuration is the simplest and cheapest scheme, which requires minimal subsea infrastructure and installation. In benign environments, flexible pipes could function in free-hanging mode. In severe environments, platform induced lateral offset could cause large variation of in riser tension and TDP position. Then compression buckling at the TDP and bird caging of the tensile armor tends to occur. A couple of configurations close to the lower end are developed to reduce the effects since.

4.2.2.2.2 Lazy wave and steep wave

This layout added a buoyance module at the lower part to provide positive apparent weight and thus prolonged the riser length compared to the free-hanging. Floater motion influence can be decoupled from the TDP. Lazy wave has less subsea configuration but steep wave are less prone to switch to other configurations when fluid density changes because of the subsea base and the bend stiffener.

Buoyance module requires firm clamping to the pipeline to avoid slippage and additional stress. In the meantime, the clamping should not damage the sheath to cause water leakage to the annulus. Buoyance modules tend to lose buoyance with time so that the configurations has 10% buoyance margin.

4.2.2.2.3 Lazy S and steep S

In the configurations, there is a subsea buoy either fixed to a seabed infrastructure or positioned by chains. In addition to the TDP riser moment decoupling, tension variation is absorbed by the buoy.

‘S’ type is only considered when ‘Lazy’ type is not available because ‘S’ type installation is more complicated. In case of large motions, lazy ‘S’ still might endure the compression issues leaving the Steep ‘S’ as the option.

4.2.2.2.4 Pliant wave

This layout is similar to steep wave where the tension is transferred to the anchor but not TDP. The pliant wave is tied back to the well beneath the floater which makes intervention accessible without additional vessels. This configuration can accommodate a wide range of bore fluid densities and vessel motions without causing significant configuration change and inducing high stresses. However, this layout is only considered if there other options are not feasible because of the complicated installation.

4.2.2.3 TTR

All the risers require top tension. The stability of the TTR are guaranteed by the excess of top tension over apparent weight. BOP of the TTR production (injection) lines are usually on the platform such the risers tubing should be able to sustain the leaking pressure. Seabed connection as the drilling risers are also equipped with a stress joint to overcome bending concentration. Because the rotations at top and bottom is limited, TTR is very sensitive to floater heavy motions due to wave and current loads. Therefore TTRs are normally used for shallow waters and the heave motions need to be compensated. Reduced top-tension will cause bending increase especially with strong current environment. Negative top-tension even leads to buckling.

For TTRs of the TLP, tensioners are usually adopted whereas spar uses air cans. Therefore for spars flexible joints are used on the keel level. Top-tension ratio (top tension over apparent weight) varies greatly from 1.2 to 1.8. There is another difference between the tensioners and air cans if the platform offset. For the tensioner condition, the top tension increases with offset because of tensioner stiffness. The air can condition is just the opposite because of the compressibility of the gas in the cans. Also, buoyancy cans decouple the vertical riser movement from the vessel. However, installation process requires heavy lift vessel and specially designed rig. For both TLPs and spars, the spacing of riser is small and the risers are not restricted by guides. Hence, interactions resulting from various factors should be taken care of.

4.2.2.4 SCR

Catenary risers self-compensate the heave motion compared with TTRs. The catenary riser is sensitive to environmental loads due to the low effective tension. Fatigue damage due to VIV can be fatal. Helical strakes and faring can be applied to reduce the vibration.

The word catenary used to describe a chain suspended between points in spaces. By definition the chain line is deemed with no bending stiffness. But in the scale of the ocean, the bending stiffness of the steel pipes have little significance on the shape of the spans. The shape is determined by weight buoyance and hydro forces and can be described by the traditional catenary equation. An illustration of comparison between a SCR and a TTR can be seen in Figure 3(Bai, Y. and Bai, Q. 2005).

SCRs shares similar problems with free-hanging flexible risers of tension and TDPs movement fluctuations, resulting in fatigue, resulting from induced upper end motions. The application of adding buoyance near the seabed like lazy-wave configuration solved the problem. The first installation was on a turret moored FPSO offshore Brazil (BC-10, Shell) in 2009 (Wajnikonis C.J. and Leverette 2009).

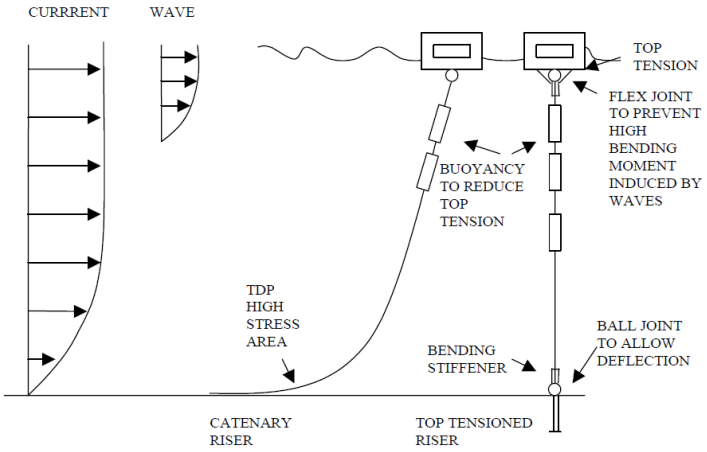

Figure 3 SCR and TTR components illustration

4.2.2.5 Mid-depth export lines

The middle range export lines are used to transport oils from an FPSO to a loading buoy which can be seen in Figure 4 (Sparks 2011). Middle part of the lines are usually equipped with buoyancy modules to maintain a W shape. The shape and depth is influenced by the density of the internal fluid. Both steel and flexible pipes can be used as this function.

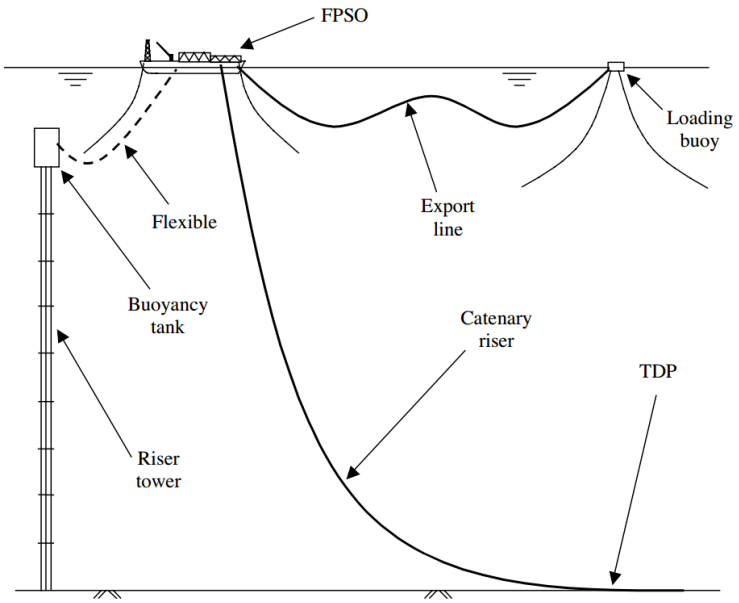

Figure 4 Riser towers, catenary risers, and mid-depth export lines

4.3 Top tension riser compensating system

Tensioning system is used to support the riser mainly compensating heave motions such as traditional hydraulic tensioners, air cans, RAM tensioners, tensioner deck and counterweights, wire line tensioners (Bai, Y. and Bai, Q. 2005).

The two types of tensioner system of concern are wire line tensioners and direct acting tensioners (DAT). Both systems despite the different dimensions and forms share almost the same working principles. In the two systems, there are cylinders which connect to the low pressure gas reservoir on one side and gas oil accumulator on the other side. To fully utilize the stroke, the pistons should be at the mid position at the calm sea.

In the wire line system, top tensioners are equipped with tensioner wires. The tensioner are positioned some degrees apart from the riser center line and normally higher than the ones in the direct acting system. Therefore the platform stability is more crucial in the wire line tensioner system. Even though the direct acting system is positioned lower the accompany equipment are more heavy and the maintenance are more complicated. The two systems are illustrated as below in Figure 5 (GRYTOYR et al. 2011).

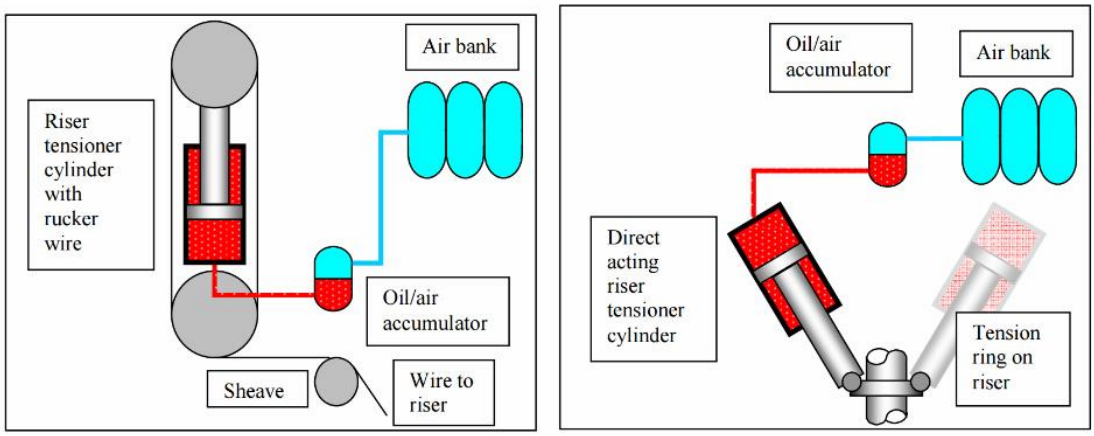

Figure 5 Wire line tensioning and direct acting tensioning

The tensioners are applied with constant force and thus non-linear springs are used for the tensioners themselves. The connection stiffness between tensioner and vessel are also needed to be modelled other than fixed connection to accommodate more reasonable results at the very beginning of the time when tensioners reaches the maximum stroke in the future reference (LARSEN Circa April 2015).

During normal drilling and operations like landing or lifting off the BOP from the sea floor, a compensating system is needed to make up for the relative displacements between the floating drilling platform and riser upper end. An illustration of components of tensioners can be seen from the Figure 5 (THORY 1998).

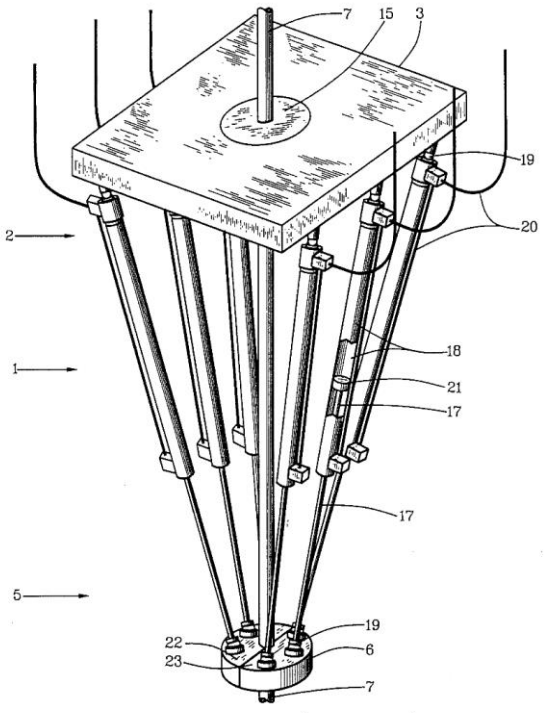

Figure 6 Tensioner heave compensator for drilling riser

The main components of the riser tension system are hydraulic cylinders, accumulators and, air pressure vessels. The rod side of the hydraulic cylinders are mechanically (see Figure above) connected with a tension ring which is on the upper end of the outer barrel. Connections are made of shackle-and-eye which allows for rotation. Accordingly the inclination of the cylinders accounts for the later roads which would have caused bending in the cylinders. The gravity and acceleration will lead to some extend of bending in the barrel and rod, especially when low tension force combine with large outgoing stroke. The hydraulic cylinders are single acting and only pull.

It is the stroke of the cylinders that compensate for the relative displacements between the floating drilling platform and riser upper end. To main the tension level, the cylinders are connected with Nitrogen pressure vessels (NPV). NPVs are preliminarily configured to a pressure. The pressure remains almost constant because of the large volume of the nitrogen. The large volume of air act like a soft spring which provides almost constant tension for the entire stroke of the hydraulic cylinder.

A schematic description of the riser tensioner system is given as in figure below. One of the several equal systems is illustrated. Little attention is needed to be paid for if well maintained. The oil/nitrogen accumulator is coupled in the bottom of the oil in the cylinder. The top manifold of high pressure nitrogen is connected to NPVs while the cylinder lower pressure side is connected to a LP NPV. The pressure in the LP NPV is kept nearly constant by using a common nitrogen vessel.

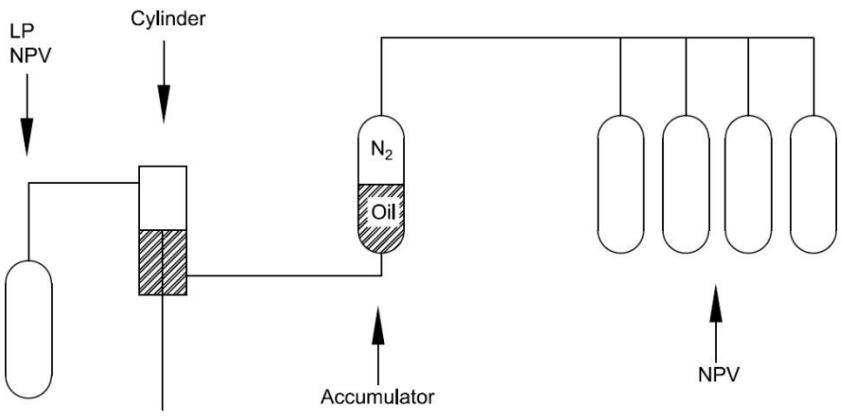

Figure 7 Riser tensioning system

The oil will run from cylinder to accumulator when the cylinder extends and run the opposite way when the cylinder retracts. When platform move upward of drifts off, the cylinders extend to account for the movement. The limited volume will make the pressure and hence tension rise. When platform move the opposite way, the cylinders will retract and, pressure and tension will decrease. When the retract speed is high, the small bore on LP NPV will act as a cushion with lower speed than the retract speed. The shut-off valve between the under manifold of the accumulator and cylinders will

also help by cutting the supply of oil. A brief view of the functions of the different NPVs are explained in Table below (STEN 2012).

Table 1NPV functions

Working NPVs	Pneumatic spring of the tensioner cylinders
Standby NPVs	Quick available nitrogen for pressure rise in working NPV's
Common NPVs	To make pressure nearly constant on piston side

4.4 Riser components

The riser components should be able to sustain high tension and bending moment and have enough flexibility to resist fatigue. The weight should be as low as possible to minimize the tension and accommodate floater motions. The normal components if a riser are conduit, interface with floater and wellhead, components, auxiliary.

4.4.1 Flexible joints

Flexible joints are used at the ends of the riser to account for the large rotations with minimum bending moment. Flexible joints usually exhibit non-linear behavior and then should be modelled with non-linear rotations spring or short beam with non-linear stiffness.

Generally flexible joints only accounted for rotations observed. However, for riser working in the deep water depth, large tension effect and tension fatigue should be considered.

4.4.2 Riser joints

A riser joint is a seamless rigid pipe with mechanical connectors welded on both ends. For drilling risers, choke and kill lines are attached to the riser by connector's flange on ends and guides in the middle. The joints is assembled the same way as pipes as stabbing one stalk at a time into the string.

The joints are made of steel, titanium, aluminum or composites in which steel is predominated used. The joints are linked by connectors as threaded, grooved, flanged, dogged, clip type, box and pin.

4.4.3 Buoyancy modules

Buoyance modules are used to reduce top tension. These modules can be thin-walled air cans or fabricated syntactic foams which strapped to the riser joints. Careful design and durable materials should be operated to resist water absorption in a long term. The syntactic foam will increase the drag diameter and accelerate the VIV fatigue.

4.4.4 Ancillary device

To prevent the upper part of the flexible risers from reaching out allowable radius before hang-off arrangement, two kinds of ancillary device bend stiffeners and bellmouths. Bend stiffeners provide a better performance under high motions a better moment transition between the connections. Bend stiffeners are used subsea sometimes at the end connection of steep S or steep wave to prevent over-bending. With the same purpose, bending restrictor are used for static pipelines at bottom and top connections. An illustration of both ancillary devices are showed below

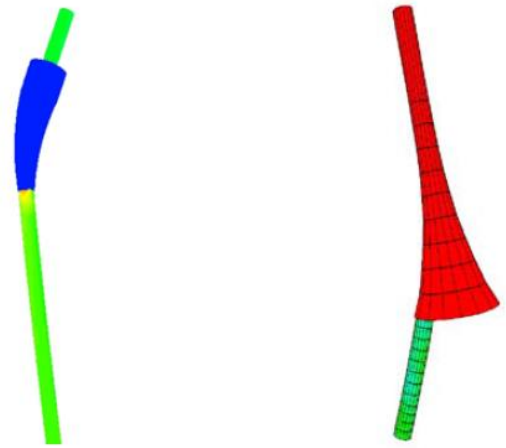

Figure 8 Bend stiffener (left) and bend mouth (right)

4.5 Effective tension

Effective tension is applied on the volume force model because the deformation caused by the effective tension won't influence the volume force. Volume force can only be changed by submerged weight to which the influence of effective tension is negligible.

4.5.1 Archimedes' Law

The buoyancy inflicted on a body equals the weight of the fluid it displaced. The body could be partially immersed or fully immersed. The buoyance will pass the center of gravity of the fluid displaced.

Superposition is then applied to derive another form of the Archimedes' Law for further reference. Both systems shown below in Figure 8 is in equilibrium condition. If forces in the displace fluid are subtracted from the submerged body, the resultant equivalent system will be left equal as well. In addition superposition don't require if the density is constant or the force pass the center of gravity (Sparks 2011).

$$T = W_a = W_t - W_f \ (4.5.1.1)$$

T: Tension
W_t: Body Weight
W_f: Displaced Fluid Weight
W_a: Apparent Weight

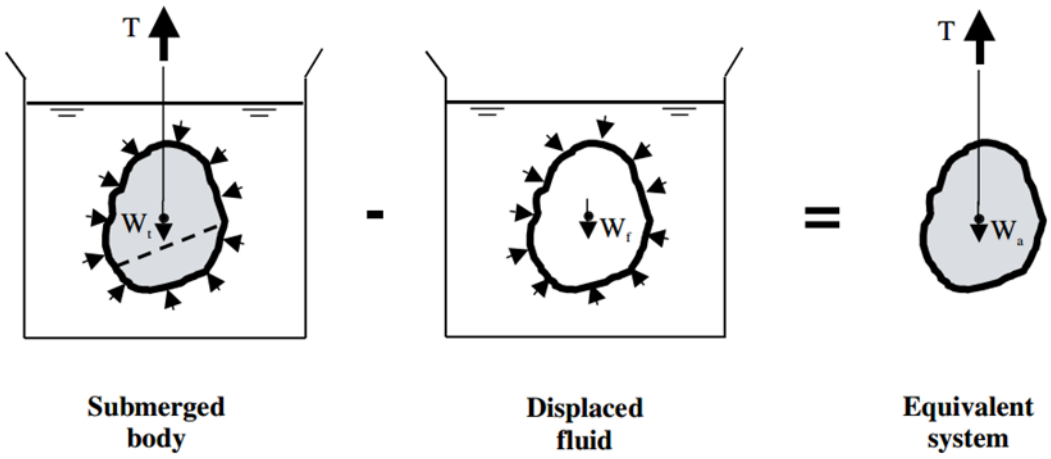

Figure 9 Archimedes' Law

4.5.2 Riser effective tension by superposition

Superposition can be adopted on the riser pipe section under internal and external pressures. Shear forces and moments are omitted for convenience. According to convention tensions and pressures are positive. See Figure 9 below.

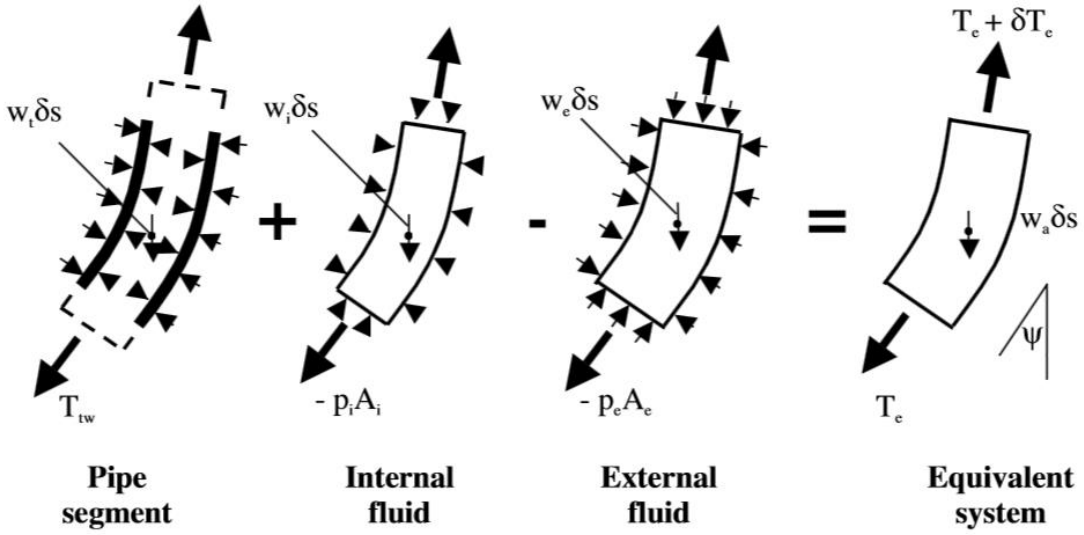

Figure 10 Pipe section equivalent system

The later pressures acting on the riser inner section in the pipe segment system are opposite to the ones on the internal fluid system while later pressures on outer section of the pipe segment system and external fluid system are the same. Hence, pipe segment system plus internal fluid system minus external fluid system will results in zero lateral forces in the equivalent system.

$$T_e = T_{tw} + (-p_i A_i) - (-p_e A_e) = w_a \delta s = (w_t + w_i - w_e)\delta s \quad (4.5.2.1)$$

T_{tw}: True Wall Tension
p_i: Internal Fluid Pressure
p_e: External Fluid Pressure
A_i: Internal Cross-sectional Area
A_e: External Cross-sectional Area
w_t: Tube Weight per Unit Length
w_i: Internal Fluid Column Weight per Unit Length
w_e: External Fluid Column Weight per Unit Length
w_a: Apparent Weight per Unit Length
δs: Segment Length

Top tension on one hand helps the low bending stiffness and on the other hand carry the weight of the riser. For a TTR, top tension can be approximated when lower end effective tension is given according to superposition. Bending moment and shear forces are omitted for simplicity. The figure above shows a whole riser above the wellhead in which both the left and middle system are in equilibrium. Subtracting the middle system from the left one, it can been seen as follows.

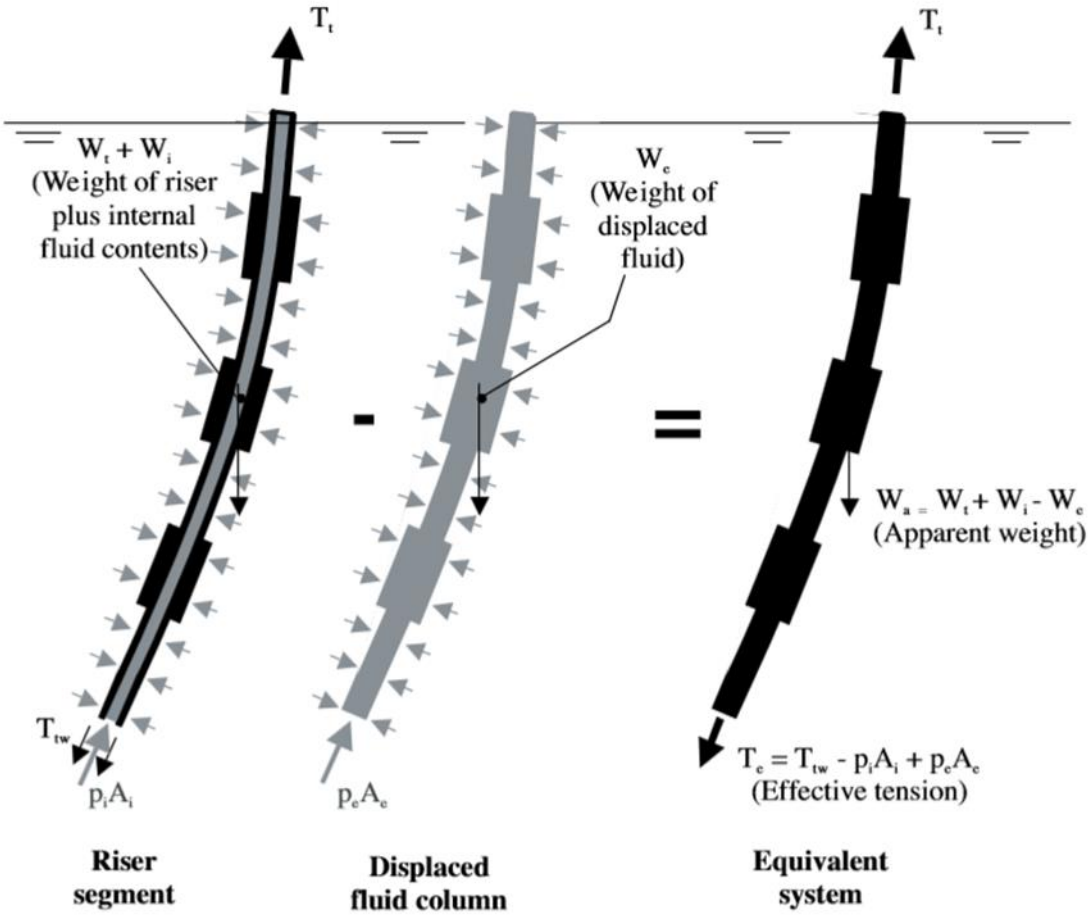

Figure 11 Long riser section equivalent system

$$T_e = T_{tw} - p_i A_i + p_e A_e = T_t - W_a = T_t - (W_t + W_i - W_e)\ (4.5.2.2) \rightarrow$$
$$T_t = T_e + (W_t + W_i - W_e)\ (4.5.2.3)$$

T_t: Top Tension
$W_a = W_t + W_i - W_e$
W_a: Riser Apparent Weight
W_t: Riser True Pipe Weight
W_i: Riser Internal Fluid Weight
W_e: Riser External Fluid Weight

4.5.3 Riser effective tension physical meaning

Assume a beam element with small deflection and uniform moment of inertia. The effective tension concept is expended to the strong form of the beam element which is derived as followed.

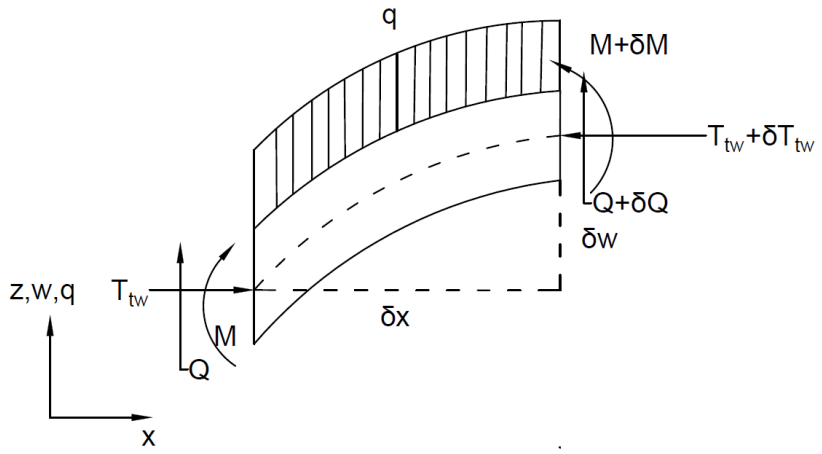

Figure 12 Incremental beam element under forces

For an incremental small beam element (Figure 11), due to the right hand side moment equilibrium (secondary forces omitted)

$$Q\delta x - T_{tw}\delta w = \delta M \rightarrow Q = \frac{\partial M}{\partial x} + T_{tw}\frac{\partial w}{\partial x} \quad (4.5.3.1)$$

Q: Element Shear Force
w: Beam Vertical displacement

Due to the vertical force equilibrium

$$\delta Q + q\delta x = 0 \rightarrow \frac{\partial Q}{\partial x} = -q \quad (4.5.3.2)$$

q: lateral loads per unit length

Combine the $(4.5.3.1)$ and $(4.5.3.2)$ above

$$\frac{\partial Q}{\partial x} = \frac{\partial^2 M}{\partial x^2} + T_{tw}\frac{\partial^2 w}{\partial x^2} = -q \quad (4.5.3.3)$$

Assuming cross sections remains plane and perpendicular to the beam axis, then
In one specific cross section displacement in the x direction

$$u = -z \cdot w_{/x} \quad (4.5.3.4)$$

Hence from (4.5.3.4) strain is

$$\varepsilon = \frac{\partial u}{\partial x} = -z \cdot w_{,xx} \ (4.5.3.5)$$

According to Hook's Law from (4.5.3.5)

$$\sigma = E \cdot \varepsilon = \frac{\partial u}{\partial x} = -z \cdot w_{,xx} \ (4.5.3.6)$$

E: Young's Modulus

The stress will cause the beam to bend in the vertical plane from (4.5.3.6)

$$M = \int_A z \cdot \sigma dA = \int_A -E \cdot z^2 \cdot w_{,xx} dA = -EIw_{,xx} \ (4.5.3.7)$$

In which

$$I = \int_A z^2 dA \ (4.5.3.8)$$

The differential equation for a beam under axial force then

$$EI \frac{d^4 w}{dx^4} + T_{tw} \frac{\partial^2 w}{\partial x^2} + q = 0 \ (4.5.3.9)$$

For pipe wall

$$EI \frac{\partial^4 w}{\partial x^4} + T_{tw} \frac{\partial^2 w}{\partial x^2} + q + q_{i21} + q_e = 0 \ (4.5.3.10)$$

For internal fluid column

$$-p_i A_i \frac{\partial^2 w}{\partial x^2} + q_{i12} = 0 \ (4.5.3.11)$$

q_i: The interactive force between the pipe wall and internal fluid column, $q_{i21} + q_{i12} = 0 \ (4.5.3.12)$
q_e: The external pressure force
Adding (4.5.3.10) and (4.5.3.11)above.

$$EI \frac{\partial^4 w}{\partial x^4} + (T_{tw} - p_i A_i) \frac{\partial^2 w}{\partial x^2} + q_{dyn} + q_e = 0 \ (4.5.3.13)$$

For displaced fluid column

$$-p_e A_e \frac{\partial^2 w}{\partial x^2} + q_e = 0 \ (4.5.3.14)$$

Substract $(4.5.3.14)$ from $(4.5.3.13)$ above.

$$EI \frac{\partial^4 w}{\partial x^4} + (T_{tw} - p_i A_i + p_e A_e) \frac{\partial^2 w}{\partial x^2} + q = 0 \ (4.5.3.15)$$

The riser segment can be seen as two column coupled together with same deflection: pipe wall, inner fluid column. Then the differential equation can be written separately but have to include the interaction forces. The displaced fluid column can be seen as a datum system. The internal fluid column and pipe wall are coupled together. Their interaction forces are opposite and deflections are same.

4.5.4 Elastic stiffness and geometric stiffness

The risers are usually one single line which means no branches. The stiffness is mainly used for limiting deflections caused by current and waves. The effective tension (axial force) is the governing stiffness parameter. The stiffness is composed of both elastic stiffness and geometric stiffness (Larsen 1990).

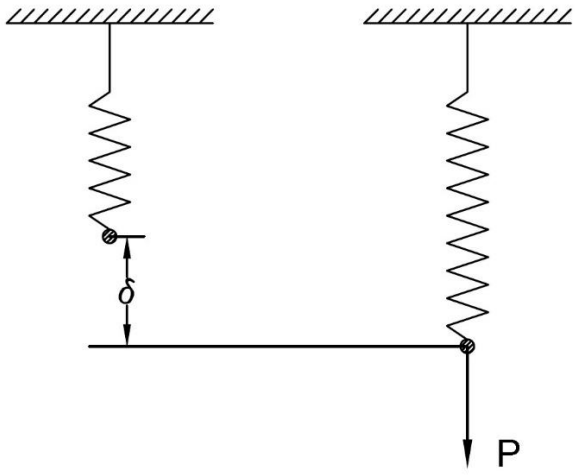

Figure 13 Elastic stiffness illustration

$$K = \frac{P}{\delta} \ (4.5.4.1)$$

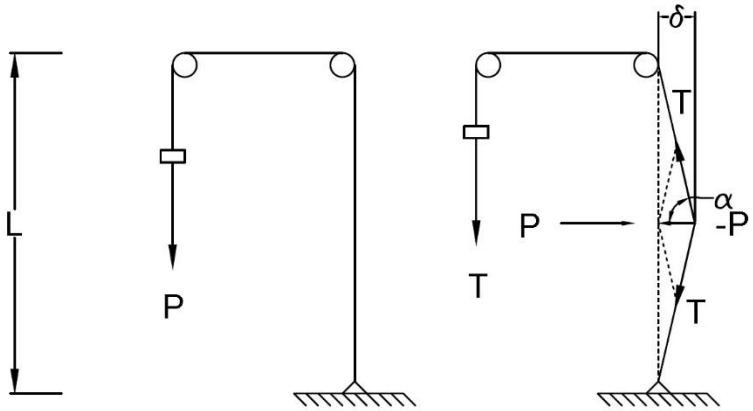

Figure 14 Geometric stiffness illustration

$$\text{For small } \delta,\ K = \frac{P}{\delta} = \frac{2T\cos\alpha}{\delta} = \frac{2T\cdot\frac{\delta}{L/2}}{\delta} = \frac{4T}{L} \quad (4.5.4.2)$$

The structural behavior of risers are characterized by large deformations and small elastic strains such that geometric stiffness (from lateral direction) is more important than elastic stiffness.

4.6 Subsea equipment and EDS

The LMRP is a crucial equipment in order to initiate the EDS in case needed. The LMRP is the upper section of a two-section BOP stack, which interfaces with the lower subsea BOP stack. The LMRP consists of the hydraulic connector, annular BOP(s), flex/ball joint, riser adapter, flexible choke and kill lines, and subsea control pods (API 2004).

Zero offset is the most efficient configuration for the riser in operation and other conditions. Largest value of effective tension can be achieved along the whole section of the riser. In the meanwhile, smaller elasticity and less tension are accounted for to straighten the riser when lockup occurs. Because zero offset provides larger geometrical stiffness. Accordingly the platform connected with the riser should be kept in an acceptable area to limit the offset to avoid unnecessary stresses. Anchors and mooring lines can be used for shallow waters but dynamic positioning (DP) are required for deep waters (Hermanrud 2014).

The EDS would securely disconnect the riser from the BOP. The initiation may be because of different scenarios but the main reason is to avoid damaging the well head when floater cannot maintain the position over the well. The EDS is needed for all the DP and moored drilling units (Kavanagh et al. 2002). Because of the characteristics of the thrusters' forces, large redundancy of the DP system are to be met. The support vessels for operation and maintenance need three times redundancy.

In case EDS fails to perform, a weak link on the riser can break at a pre-defined force which will not damage the well head. Thus the damage it may inflict on the environment is limited to the minimal. The capacity of the week link should be larger than the normal operation and lower than the next weakest joint. Any increase to the both ends are desired. The position of the weak link should be close to the well head such that the riser left part would not fall and damage the well head.

After the EDS is successfully performed, the mechanical energy will cause the riser to recoil upwards. The tensioning system should be tuned to minimize the recoil to avoid buckling. The system should also be adjusted that the LMRP would not come back and hit the well head. DAT system has an advantage over the wire line system because the recoil can be controlled directly by the oil flow in the DAT system.

4.6.1 Disconnecting reasons

Drift off is the main concern of the current thesis. It means DP is not functioning and the MODU cannot maintain the position above the wellhead. This could be caused by loss of power, system malfunction, engine breakdown and human errors.

Drive off is similar to drift off but is more serious. Because DP is malfunctioning which means other than the environmental loads, thrusters' forces have a chance in the same direction as environmental loads to drive the MODU away.

If storm forecast is larger than the MODU can handle, the MODU would need to disconnect beforehand for safety. This is called planned disconnection and would cause a long downtime for deep water depth (Grønevik 2013).

In case gas leak from the well head, it would endanger the buoyancy of the MODU. The carbon gas may cause fire or explosion when certain conditions are met.

4.6.2 EDS activation

There are three ways to initiate EDS: manually from the bridge or control room, automatic mode function and ROV intervention locally at the BOP (Grønevik 2013). There are hydraulic and electric communication between the BOP and floater. If both systems disconnect, BOP with its own battery would initiate the EDS.

5. Computer programs

5.1 FEM program Riflex

Analytical methods which only take the parts of the structure into consideration has always been a struggle until the time when the design through analysis method became widely used. The FEM method make the factors of interactions between different parts of the system observable and comparable with the lab and field tests. In addition, the realistic simulation are always project specific. Installation, maintenance, testing, geological environment and many other operations prescribe the specific load conditions, then the designers can identify the concern to modify their solutions.

With the development of computer science, finite element method was made available to analysis both global behavior and local strength of the risers. The traditional code design may involve uncertainties in parameters and application methods and thus conservatism will occur. Therefore the two methods can be compared to determine the margin of the optimization. The new approach is named design through analysis and can reduce redundant conservatism by the implementation through the local analysis, and capital expenditure (CAPEX) and operating expenditure (OPEX) will consequently be minimized. But rules and codes should cover the general design context as many uncertainties are involved in the input and analysis method. Because of the realistic simulation of FEM method, mitigation can be taken compared with the rules and design codes. The uncertainties can be modelled with statistics to determine the probability distribution for a variety of loads and effects.

5.1.1 Riflex structure

RIFLEX is a computational program specializing in slender structures, including flexible risers, conventional steel risers, pipelines, mooring lines, fish cage systems.

Important features are as follows.

*unlimited rotations and translations in 3D coordinates
*beam and bar elements based on small strain theory
*predefined nonlinear material properties
*stiffness contributions from geometry stiffness (axial force for transverse stiffness)

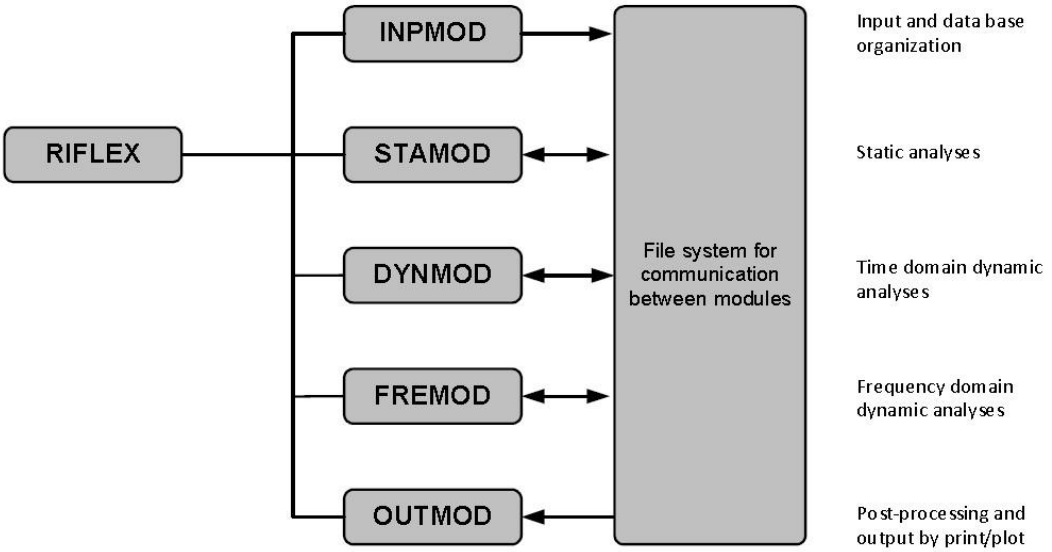

Figure 15 Riflex program components

The Riflex program contains five modules and the brief functions of the modules are illustrated in the figure 13 above. Users need to specify input files for INPMOD, STAMOD, DYNMOD, and OUTMOD modules (SINTEFF 2013).

5.1.1.1 Physical constants

In order to give the users freedom to define mass and force units, inconsistent units might occur. A constant GCONS is used as a specification of the difference of defined units.

$$\mathrm{GCONS} = (\mathrm{F}/\mathrm{M})/(\mathrm{L}/\mathrm{T}\text{^}2) \quad (5.1.1.1.1)$$

F: force unit
M: mass unit
L: length unit
T: time unit

5.1.1.2 Line and component description

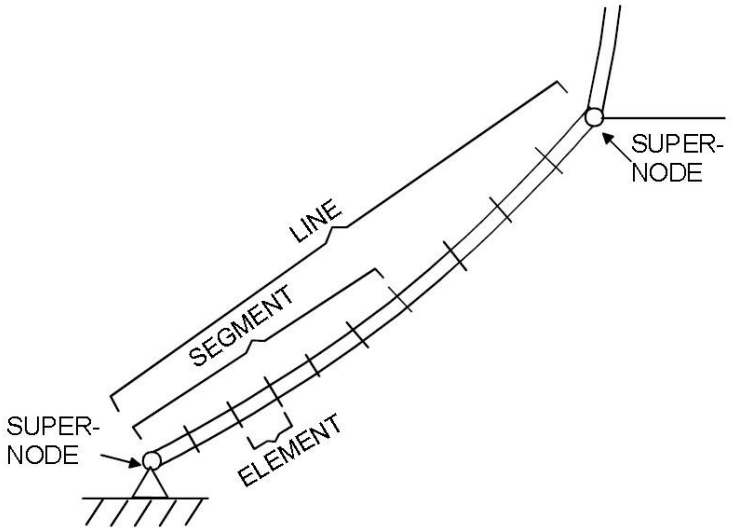

SUPERNODE	Branching points or nodes with specified boundary conditions
LINE	Suspended structure between two supernodes.
SEGMENT	(Part of) line with uniform cross section properties and element length
ELEMENT	Finite element unit

Figure 16 Riflex system terms

Branching points and terminal points are designated supernodes. The System topology is defined by supernodes and connectivity between them. Supernodes are classified as free, fixed or prescribed depending on the boundary condition.

The component is identified by component type number and describes the mechanical properties. External and internal area, mass and hydro dynamical coefficients must be specified. There are three types of components: cross sectional components, nodal components, and special components. Element mesh is calculated automatically depending on the topology, line, component types.

5.1.1.3 Stress free specification

Stress free configuration is the base of FEM calculations which define the status with no stress and deformations. The stress free parts with bending stiffness are always straight if there is no initial deformation. This initial configuration are specified by positions of super nodes and the intermediate FEM nodes positions are determined based on the positions of super nodes.

5.1.1.4 Mesh generation

The FEM mesh is generated automatically according to topology, line and component. Elements are of equal length within segments.

5.1.2 HDF5 data format

HDF5 is a data model, library, and file format for storing and managing data. All the varieties used in Sima is in the HDF5 formet.

There are two major objects in HDF5, a group and a dateset. Objects are categorized in group as a tree structure. Dateset contains the raw data values. In addition, affiliated information can be stored in attributes. Attributes can be attached to both group and dataset (Marintek 2015).

Varieties of data types are supported. No limitations are set for the file sizes and number of objects. Because of the virtual file layer, common used and customized drivers allow extremely flexible storage and data transfer capabilities. Parallel I/O is supported to allow the efficient data transfer. HDF5 can be ported to virtually all computing platforms and have C, C++, Java, and Fortran90 distributions interfaces (HDFGROUP 2011).

Via the grouping and linking mechanisms, complex data relationships and dependencies can be achieved. HDF5 accommodates common type and arbitrary user defined metadata.

6. FEM theory in Riflex

6.1 Lagrangian description

Basic continuum mechanics theory uses generalized stress/strain measures and this make large cross-sectional deformation possible. Lagrangian description is used to describe the particle motions in a global fixed coordinate with base vector $\mathrm{I_i}$.

$$\mathbf{x} = \mathbf{X} + \mathbf{u} \quad (6.1.1)$$

$\mathbf{X}$: particle original position
$\mathbf{u}$: particle displacement

6.2 Co-rotated ghost reference

In RIFLEX, beam elements is formulated by a co-rotated ghost reference description. It means the material particle motions are related to a local coordinate frame which translates and rotates with the average motions of the body. The total motion would be a combination of local position vector and local reference system.

Therefore there are four types of configuration involved for the beam elements non-linear analysis: body initial configuration C_0, body co-rotated ghost configuration C_{0n} at time t, body deformed configuration C_n at time t, body deformed configuration C_{n+1} at time $\mathrm{t} + \Delta\mathrm{t}$.

This method assumes that the initial configuration C_0 translates and rotates as a rigid body configuration C_{0n} so that it at any time is located close to the actual deformed configuration C_n and C_{n+1}. All the configurations can be seen in Figure 15 below.

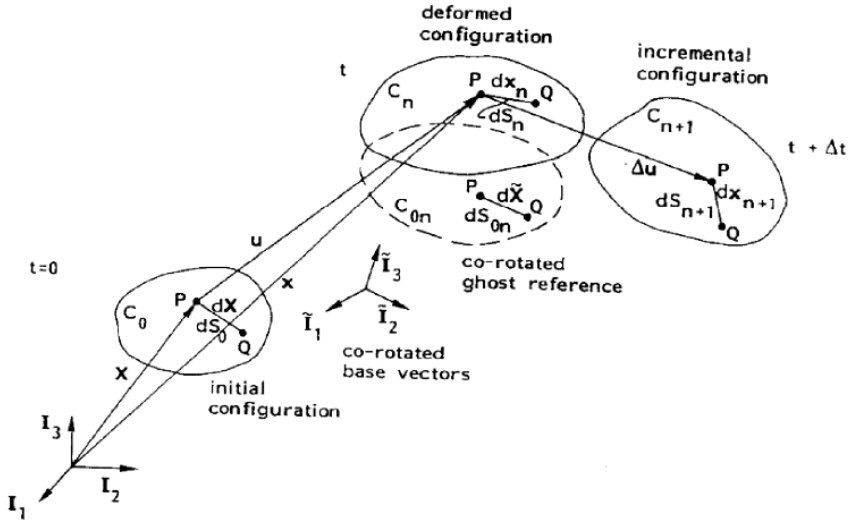

Figure 17 Various configurations of a body

6.3 Green strain tensor and 2nd Piola-Kirchhoff stress tensor

Green strain tensor is defined as

$$\mathbf{E} = \frac{1}{2}(\mathbf{F}^{\mathrm{T}} \cdot \mathbf{F}) - \mathbf{I} \quad (6.3.1)$$

Where

$$\mathbf{F} = \frac{\partial \mathbf{x}}{\partial \mathbf{X}} = \frac{\partial(\mathbf{X} + \mathbf{u})}{\partial \mathbf{X}} = \mathbf{R} \cdot \mathbf{U} \quad (6.3.2)$$

$$\mathbf{F}^{\mathrm{T}} \cdot \mathbf{F} = (\mathbf{R} \cdot \mathbf{U})^{\mathrm{T}} \cdot (\mathbf{R} \cdot \mathbf{U}) = \mathbf{U}^{\mathrm{T}} \cdot \mathbf{U} \quad (6.3.3)$$

Where

$\mathbf{U}$ is stretch tensor, $\mathbf{R}$ is rotation tensor, $\mathbf{F}$ is deformation gradient

Therefore rotation is eliminated in the green tensor.

$$\mathrm{E_{ij}} = \frac{1}{2}\left(\frac{\partial \mathrm{u_i}}{\partial \mathrm{X_j}} + \frac{\partial \mathrm{u_j}}{\partial \mathrm{X_i}} + \frac{\partial \mathrm{u_k}}{\partial \mathrm{X_i}}\frac{\partial \mathrm{u_k}}{\partial \mathrm{X_j}}\right) \quad (6.3.4)$$

Green Strain=Small Strain Terms+ Quadratic Terms

This feature makes green strain a bit higher then engineering strain. For small strains, the green tensor and pure stretch tensor $\mathbf{U}-\mathbf{I}$ are very close.

2nd Piola-Kirchhoff stress tensor can be defined as

$$\dot{\mathbf{F}}=\frac{\mathrm{d}}{\mathrm{dt}}\left(\frac{\partial \mathbf{x}}{\partial \mathbf{X}}\right)=\frac{\partial}{\partial \mathbf{X}}\left(\frac{\mathrm{d}\mathbf{x}}{\mathrm{dt}}\right)=\frac{\partial \mathbf{v}}{\partial \mathbf{X}}=\left(\frac{\partial \mathbf{v}}{\partial \mathbf{x}}\right)\left(\frac{\partial \mathbf{x}}{\partial \mathbf{X}}\right)=\mathbf{L}\cdot\mathbf{F}\ (6.3.5)$$

Therefore,

$$\dot{\mathbf{F}}^{\mathbf{T}}=\mathbf{F}^{\mathbf{T}}\cdot\mathbf{L}^{\mathbf{T}}\ (6.3.6)$$

From $(6.3.1)$ and $(6.3.6)$,

$$\dot{\mathbf{E}}=\frac{1}{2}\left(\mathbf{F}^{\mathrm{T}}\cdot\dot{\mathbf{F}}+\dot{\mathbf{F}}^{\mathrm{T}}\cdot\mathbf{F}\right)=\frac{1}{2}(\mathbf{F}^{\mathrm{T}}\cdot\mathbf{L}\cdot\mathbf{F}+\mathbf{F}^{\mathbf{T}}\cdot\mathbf{L}^{\mathbf{T}}\cdot\mathbf{F})=\mathbf{F}^{\mathrm{T}}\cdot\left(\frac{\mathbf{L}+\mathbf{L}^{\mathbf{T}}}{\mathbf{2}}\right)\cdot\mathbf{F}$$
$$=\mathbf{F}^{\mathrm{T}}\cdot\mathbf{D}\cdot\mathbf{F}\ (6.3.7)$$

Where $\mathbf{v}$ is velocity, $\mathbf{L}$ is velocity gradient as an Eulerian quantity, $\mathbf{D}$ is called rate of deformation and is symmetric.

The counterpart of $\mathbf{D}$ is $\mathbf{W}$ which is called spin and antisymmetric

$$\mathbf{W}=\frac{\mathbf{L}-\mathbf{L}^{\mathbf{T}}}{\mathbf{2}}\ (6.3.8)$$

Considering the power generation,

$$\mathrm{P}=\mathbf{F}\cdot\mathbf{v}=\int\left(\frac{\mathbf{F}}{\mathrm{A}}\right)\cdot\left(\frac{\mathrm{dv}}{\mathrm{dx}}\right)\mathrm{dV}=\int\boldsymbol{\sigma}\colon\mathbf{L}\,\mathrm{dV}=\int\boldsymbol{\sigma}\colon(\mathbf{W}+\mathbf{D})\,\mathrm{dV}=\int\boldsymbol{\sigma}\colon\mathbf{D}\,\mathrm{dV}=$$

$$\int\boldsymbol{\sigma}\colon\left(\mathbf{F}^{-\mathrm{T}}\cdot\dot{\mathbf{E}}\cdot\mathbf{F}^{-\mathbf{1}}\right)\mathrm{dV}=\int\sigma_{\mathrm{ij}}\mathrm{F}_{\mathrm{im}}^{-\mathrm{T}}\dot{\mathrm{E}}_{\mathrm{mn}}\,\mathrm{F}_{\mathrm{nj}}^{-1}\mathrm{JdV}_0=\int\mathrm{JF}_{\mathrm{mi}}^{-1}\sigma_{\mathrm{ij}}\mathrm{F}_{\mathrm{jn}}^{-1}\dot{\mathrm{E}}_{\mathrm{mn}}\,\mathrm{dV}_0=$$

$$\int\boldsymbol{\sigma}^{\boldsymbol{PK2}}\colon\dot{\mathbf{E}}\,\mathrm{dV}_0\ \ (6.3.9)$$

Where

$$\boldsymbol{\sigma}^{\boldsymbol{PK2}}=\mathrm{J}\mathbf{F}^{-\mathbf{1}}\cdot\boldsymbol{\sigma}\cdot\mathbf{F}^{-\mathrm{T}}\ (6.3.10)$$

Where $\boldsymbol{\sigma}$ is true stress, $\mathrm{dV}=\mathrm{Ad}\mathbf{x}$ is deformed differential volume, dV_0 is the initial differential volume.

This means $\boldsymbol{\sigma}^{\boldsymbol{PK2}}$ is conjugate to $\dot{\mathbf{E}}$ for power and $\mathbf{E}$ for energy. Therefore the pairing is used with the virtual work principle to derive the FEM equations (McGinty 2012).

6.4 Stress and strains in co-rotated ghost reference description

If initial configuration C_0 is used as reference,

$$\mathbf{E} = \mathrm{E}_{\mathrm{ij}}\mathbf{I}_{\mathrm{i}}\mathbf{I}_{\mathrm{j}} \ (6.4.1)$$

If ghost configuration C_{0n} is used as reference,

$$\mathbf{E} = \widetilde{\mathrm{E}}_{\mathrm{ij}}\tilde{\mathbf{I}}_{\mathrm{i}}\tilde{\mathbf{I}}_{\mathrm{j}} \ (6.4.2)$$

If both reference body and base vectors are rotated in the same way.

$$\mathrm{E}_{\mathrm{ij}} = \widetilde{\mathrm{E}}_{\mathrm{ij}} \ (6.4.3)$$

Similarly

$$\sigma_{\mathrm{ij}} = \widetilde{\sigma}_{\mathrm{ij}} \ (6.4.4)$$

Thus no transformations is needed for stress and strain tensor components if co-rotated ghost reference is used.

6.5 Virtual work principles

In static analysis,

$$\int_{\mathrm{V}_0} \boldsymbol{\sigma} : \delta\mathbf{E} \, \mathrm{dV}_0 = \int_{\mathrm{A}_0} \mathbf{t}_0 : \delta\mathbf{u} \, \mathrm{dA}_0 + \int_{\mathrm{V}_0} \mathbf{f}_0 : \delta\mathbf{u} \, \mathrm{dV}_0 \ (6.5.1)$$

Virtual quantities are prefixed with δ, $\mathbf{t}_0$ and $\mathbf{f}_0$ are unit surface traction and unit volume force respectively in the initial configuration.

Nonlinearity problems requires a linearized incremental form of equation which can be based on the configuration of C_n and C_{n+1} (Wang 1986).

$$\int_{V_0} (\boldsymbol{\sigma}: \delta\Delta\mathbf{E} + \Delta\boldsymbol{\sigma}: \delta\mathbf{E}) dV_0 = \int_{A_0} \Delta\mathbf{t_0}: \delta\mathbf{u}\, dA_0 + \int_{V_0} \Delta\mathbf{f_0}: \delta\mathbf{u}\, dV_0 \quad (6.5.2)$$

Small finite increments between C_n and C_{n+1} are prefixed with Δ.

In dynamic analysis,

$$\int_{V_0} \boldsymbol{\sigma}: \delta\mathbf{E}\, dV_0 + \int_{V_0} \rho_0\, \ddot{\mathbf{u}} \cdot \delta\mathbf{u} dV_0 + \int_{V_0} \tilde{c}\dot{\mathbf{u}} \cdot \delta\mathbf{u}\, dV_0 = \int_{A_0} \mathbf{t_0}: \delta\mathbf{u}\, dA_0 + \int_{V_0} \mathbf{f_0}: \delta\mathbf{u}\, dV_0 \quad (6.5.3)$$

ρ_0 is mass density, $\tilde{c}$ is viscous damping density function. The two additional components provides the inertia and damping matrix.

Similarly the incremental form is as (Rmseth 1978),

$$\int_{V_0} (\boldsymbol{\sigma}: \delta\Delta\mathbf{E} + \Delta\boldsymbol{\sigma}: \delta\mathbf{E}) dV_0 + \int_{V_0} \rho_0\, \Delta\ddot{\mathbf{u}} \cdot \delta\mathbf{u} dV_0 + \int_{V_0} \tilde{c}\Delta\dot{\mathbf{u}} \cdot \delta\mathbf{u}\, dV_0 = \int_{A_0} \Delta\mathbf{t_0}: \delta\mathbf{u}\, dA_0 + \int_{V_0} \Delta\mathbf{f_0}: \delta\mathbf{u}\, dV_0 \quad (6.5.4)$$

6.6 Finite element method implementation

6.6.1 Large rotations in space

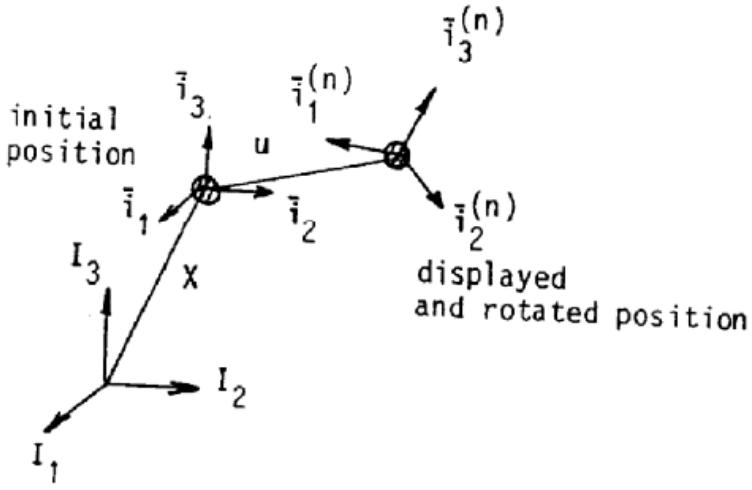

Figure 18 Translated and rotated nodal point

Rotations in space are designated by rotation matrix. Nodal point rotation in the initial configuration is denoted as $\bar{\mathbf{i}}_i$ and is parallel with global base vectors $\mathbf{I}_i$.

Then the nodal point position after rigid body translations and rotations can be represented as (See Figure 16),

$$\mathbf{X_p} = \mathbf{x} + \mathbf{e^0} = \left(\mathrm{X_i} + \mathrm{v_i} + \mathrm{e_j^0}\overline{\mathrm{T}}_{\mathrm{ij}}\right)\mathbf{I} \quad (6.6.1.1)$$

Where

$\mathrm{e_j^0}$ and $\overline{\mathrm{T}}_{\mathrm{ij}}$ are components of the initial eccentricity vector $\mathbf{e^0}$ and the rotation matrix $\overline{\mathbf{T}}_{\mathbf{ij}}$.

The nodal point rotation needs updating as the incremental steps increases in the nonlinearity numerical calculations in the following deformed configurations.

$$\bar{\mathbf{i}}_{\mathbf{i}}^{(\mathrm{n}+1)} = \overline{\mathbf{T}}_{\mathbf{ij}}^{(\mathrm{n}+1)}\mathbf{I}_{\mathbf{j}} \quad (6.6.1.2)$$

Assuming the incremental rotations from configuration C_n to C_{n+1} is small

$$\Delta\theta = \Delta\theta_i \mathbf{I_i} \quad (6.6.1.3)$$

$\Delta\theta_i$ is the rotational components about the global base vectors $\mathbf{I_i}$.

It is also shown that (Bergan et al. 1985; Mollestad 1983),

$$\bar{\mathbf{i}}_{\mathbf{i}}^{(n+1)} = \overline{\mathbf{T}}_{\mathbf{ij}}^{(n+1)} \mathbf{I_j} = \overline{\mathbf{T}}_{\mathbf{ik}}^{(n)} \widetilde{\mathbf{T}}_{\mathbf{kj}} \mathbf{I_j} \quad (6.6.1.4)$$

Where $\widetilde{\mathbf{T}}_{\mathbf{kj}}$ represents the incremental rotation matrix from configuration C_n to C_{n+1} with the$\Delta\theta_i$ in the order$\Delta\theta_1 \rightarrow \Delta\theta_2 \rightarrow \Delta\theta_3$.

$$\widetilde{\mathbf{T}}_{\mathbf{kj}} = \begin{bmatrix} C2 \cdot C3 & S3 \cdot C1 + S1 \cdot S2 \cdot S3 & S1 \cdot S3 - S2 \cdot C1 \cdot C3 \\ S3 \cdot C2 & C1 \cdot C3 - S1 \cdot S2 \cdot S3 & S1 \cdot C3 + S2 \cdot S3 \cdot C1 \\ S2 & -S1 \cdot C2 & C1 \cdot C2 \end{bmatrix} \quad (6.6.1.5)$$

Where

$$S1 = \sin\Delta\theta_1; S2 = \sin\Delta\theta_2; S3 = \sin\Delta\theta_3; C1 = \cos\Delta\theta_1; C2 = \cos\Delta\theta_2; C3 = \cos\Delta\theta_3$$

6.6.2 Beam element

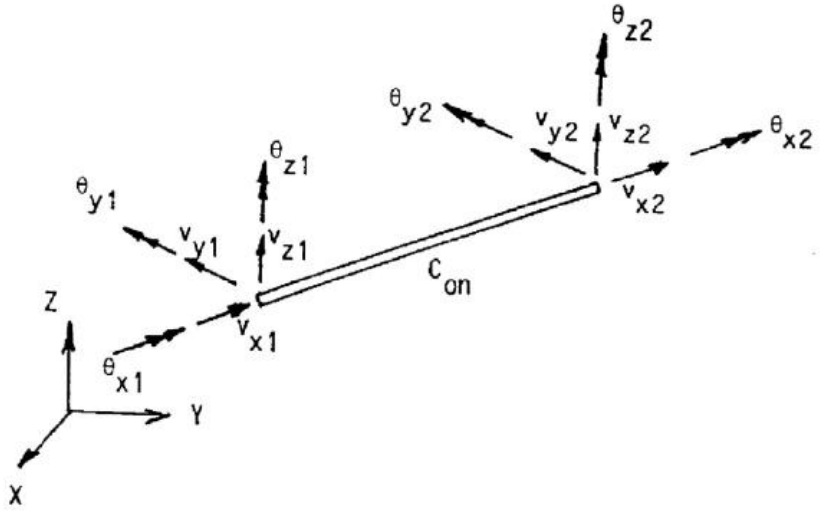

Figure 19 Beam element degrees of freedom (DOF)

Beam element degrees of freedom are defined as above, with three translations and three rotations on each node referred to the local system on the configuration C_{0n}. X-axis is along the secant direction through the cross section centroid. Y-axis is the average direction of the principle y-axes. Z-axis is perpendicular to the x-y plane.

The beam theory assumptions are as follows,

*a plane normal to the x-axis remains plane and normal after the deformation
*lateral contraction because of the axial elongation are neglected
*small strains
*later shear deformations because of lateral forces are neglected
*coupling between torsion and bending are neglected and therefore torsional stability and warping resistance are neglected

Displacement of arbitrary point is expressed as

$$\mathbf{u}(x,y,z) = \mathbf{u_0} - y\frac{d\mathbf{v_0}}{dx} - z\frac{d\mathbf{w_0}}{dx} \quad (6.6.2.1)$$

$$\mathbf{v}(x,y,z) = \mathbf{v_0} - z\theta \quad (6.6.2.2)$$

$$\mathbf{w}(x,y,z) = \mathbf{w_0} + y\theta \quad (6.6.2.3)$$

6.6.2.1 Interpolation function

Displacement within an element can be interpolated as,

$$\mathbf{u_0} = \mathbf{N_u v_u} \text{ with } \mathbf{v_u^T} = [v_{x1} \quad v_{x2}] \quad (6.6.2.1.1)$$

$$\mathbf{v_0} = \mathbf{N_v v_v} \text{ with } \mathbf{v_v^T} = [v_{y1} \quad \theta_{z1} \quad v_{y2} \quad \theta_{z2}] \quad (6.6.2.1.2)$$

$$\mathbf{w_0} = \mathbf{N_w v_w} \text{ with } \mathbf{v_w^T} = [v_{z1} \quad \theta_{y1} \quad v_{z2} \quad \theta_{y2}] \quad (6.6.2.1.3)$$

$$\boldsymbol{\theta_0} = \mathbf{N_\theta v_\theta} \text{ with } \mathbf{v_\theta^T} = [\theta_{x1} \quad \theta_{x2}] \quad (6.6.2.1.4)$$

The linear interpolation function is intuitively shown as,

$$\mathbf{N_u} = \mathbf{N_\theta} = \left[1 - \frac{x}{L} \quad \frac{x}{L}\right] \quad (6.6.2.1.5)$$

The cubic interpolation function is can be derived as

$$\mathbf{N_q} = [1 \quad x \quad x^2 \quad x^3] \quad (6.6.2.1.6)$$

$$v = \mathbf{N_q q} = \mathbf{N_q}\begin{bmatrix} q_1 \\ q_2 \\ q_3 \\ q_4 \end{bmatrix} \quad (6.6.2.1.7)$$

$$\mathrm{w} = \mathbf{N_q q} = \mathbf{N_q} \begin{bmatrix} q_1 \\ q_2 \\ q_3 \\ q_4 \end{bmatrix} \quad (6.6.2.1.8)$$

$$\mathbf{v_v} = \begin{bmatrix} \mathrm{v_{y1}} \\ \theta_{z1} \\ \mathrm{v_{y2}} \\ \theta_{z2} \end{bmatrix} = \begin{bmatrix} \mathrm{v}(0) \\ \mathrm{v}'(0) \\ \mathrm{v}(\mathrm{l}) \\ \mathrm{v}'(\mathrm{l}) \end{bmatrix} = \mathbf{A_v q} \quad (6.6.2.1.9)$$

$$\mathbf{v_w} = \begin{bmatrix} \mathrm{v_{y1}} \\ \theta_{z1} \\ \mathrm{v_{y2}} \\ \theta_{z2} \end{bmatrix} = \begin{bmatrix} \mathrm{w}(0) \\ -\mathrm{w}'(0) \\ \mathrm{w}(l) \\ -\mathrm{w}'(l) \end{bmatrix} = \mathbf{A_w q} \quad (6.6.2.1.10)$$

From (6.6.2.1.7) and (6.6.2.1.9)

$$\mathbf{N_v} = \mathbf{N_q A_v^{-1}} \quad (6.6.2.1.11)$$

From (6.6.2.1.8) and (6.6.2.1.10)

$$\mathbf{N_w} = \mathbf{N_q A_w^{-1}} \quad (6.6.2.1.12)$$

6.6.2.2 Internal reaction forces

By equations (6.5.1) and (6.6.2.1.1)~(6.6.2.1.4),

$$\boldsymbol{\sigma_u} = \int_{L_0} \mathbf{N_{u,x}} \mathrm{N_{xx}}\, \mathrm{dx} \quad (6.6.2.2.1)$$

$$\boldsymbol{\sigma_v} = \int_{L_0} \mathbf{N_{v,xx}} \mathrm{M_y}\, \mathrm{dx} \quad (6.6.2.2.2)$$

$$\boldsymbol{\sigma_w} = \int_{L_0} \mathbf{N_{w,xx}} \mathrm{M_z}\, \mathrm{dx} \quad (6.6.2.2.3)$$

$$\boldsymbol{\sigma_u} = \int_{L_0} \mathbf{N_{\theta,xx}} \mathrm{M}_{\boldsymbol{\theta}}\, \mathrm{dx}\ (6.6.2.2.4)$$

$\mathrm{N_{xx}}$, $\mathrm{M_y}$, $\mathrm{M_z}$, $\mathrm{M}_{\boldsymbol{\theta}}$ are cross sectional force resultant which is determined from predefined strain-force relationship. Because of the complexity of the marine slender structures (flexible pipes, umbilicals, wire, etc), it is more convenient to have this relationship which can be seen in Figure 18.

$$\mathrm{M} = \mathrm{M}(\mathrm{R}, \mathrm{p})(6.6.2.2.5)$$

$$\mathrm{N} = \mathrm{N}(\Delta \mathrm{x})\ (6.6.2.2.6)$$

$$\mathrm{M_T} = \mathrm{M_T}(\Delta\theta)\ (6.6.2.2.7)$$

Where
M: bending moment
R: radius of curvature
p: pressure difference
$\Delta \mathrm{x}$: axial elongation per unit length
$\Delta\theta$: axial rotation per unit length

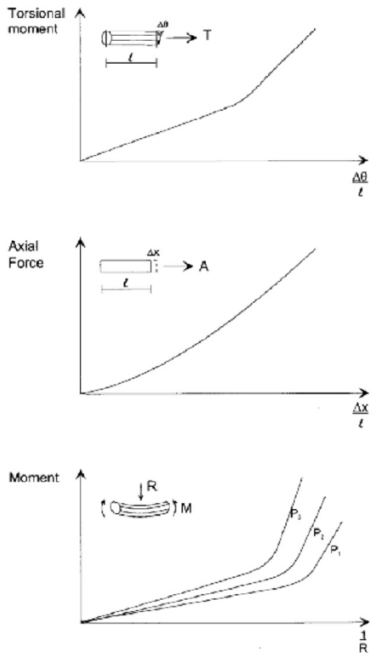

Figure 20 Nonlinear cross section properties

6.6.2.3 Stiffness matrix

By equation (6.5.2), the former term is used to derive geometric stiffness matrix, the latter material stiffness matrix.

The geometric stiffness is as,

$$\mathbf{k_G} = \begin{bmatrix} \mathbf{0} & \mathbf{0} & \mathbf{0} & \mathbf{0} \\ \mathbf{0} & \mathbf{k_{Gvv}} & \mathbf{0} & \mathbf{0} \\ \mathbf{0} & \mathbf{0} & \mathbf{k_{Gww}} & \mathbf{0} \\ \mathbf{0} & \mathbf{0} & \mathbf{0} & \mathbf{0} \end{bmatrix} \quad (6.6.2.3.1)$$

$$\mathbf{k_{Gvv}} = \int_{L_0} \mathrm{N_{xx}} \mathbf{N_{v,x}} \, \mathrm{dx} \quad (6.6.2.3.2)$$

$$\mathbf{k_{Gww}} = \int_{L_0} \mathrm{N_{xx}} \mathbf{N_{w,x}} \, \mathrm{dx} \quad (6.6.2.3.3)$$

It can be seen the axial force contributes to the transverse stiffness.

The material stiffness is as,

$$\mathbf{k_M} = \begin{bmatrix} \mathbf{k_{Muu}} & \mathbf{0} & \mathbf{0} & \mathbf{0} \\ \mathbf{0} & \mathbf{k_{Mvv}} & \mathbf{0} & \mathbf{0} \\ \mathbf{0} & \mathbf{0} & \mathbf{k_{Mww}} & \mathbf{0} \\ \mathbf{0} & \mathbf{0} & \mathbf{0} & \mathbf{k_{M\theta\theta}} \end{bmatrix} \quad (6.6.2.3.4)$$

$$\mathbf{k_{Muu}} = \int_{L_0} \mathrm{N_T} \mathbf{N_{u,x}^T} \mathbf{N_{u,x}} \, \mathrm{dx} \quad (6.6.2.3.5)$$

$$\mathbf{k_{Mvv}} = \int_{L_0} \mathrm{B_{yT}} \mathbf{N_{v,xx}^T} \mathbf{N_{v,xx}} \, \mathrm{dx} \quad (6.6.2.3.6)$$

$$\mathbf{k_{Mww}} = \int_{L_0} \mathrm{B_{zT}} \mathbf{N_{w,xx}^T} \mathbf{N_{w,xx}} \, \mathrm{dx} \quad (6.6.2.3.7)$$

$$\mathbf{k_{M\theta\theta}} = \int_{L_0} \mathrm{GI_\theta} \mathbf{N_{\theta,x}^T} \mathbf{N_{\theta,x}} \, \mathrm{dx} \quad (6.6.2.3.8)$$

N_T, B_{yT}, B_{zT}, GI_θ are axial stiffness, bending stiffness in y direction, bending stiffness in z direction, torsional stiffness. Because x axis passes the cross section centroid and y and z follow the average principles, there is no coupling.

So the tangential stiffness is

$$\mathbf{k_T} = \mathbf{k_G} + \mathbf{k_M} \quad (6.6.2.3.9)$$

6.6.2.4 Distributed external loads

Assuming the external loads are linear distributed

$$\mathbf{N} = \mathbf{N}_{\boldsymbol{u}} = \mathbf{N}_{\boldsymbol{\theta}} \quad (6.6.2.4.1)$$

$$\mathbf{S_u} = \int_{L_0} \mathbf{N_u^T} p_x(x)\, dx = \int_{L_0} \mathbf{N_u^T N}\, dx \cdot \mathbf{p_x} \quad (6.6.2.4.2)$$

$$\mathbf{S_v} = \int_{L_0} \mathbf{N_v^T} p_y(x)\, dx = \int_{L_0} \mathbf{N_v^T N}\, dx \cdot \mathbf{p_y} \quad (6.6.2.4.3)$$

$$\mathbf{S_u} = \int_{L_0} \mathbf{N_w^T} p_x(x)\, dx = \int_{L_0} \mathbf{N_w^T N}\, dx \cdot \mathbf{p_z} \quad (6.6.2.4.4)$$

$$\mathbf{S_u} = \int_{L_0} \mathbf{N_\theta^T} p_x(x)\, dx = \int_{L_0} \mathbf{N_\theta^T N}\, dx \cdot \mathbf{p_\theta} \quad (6.6.2.4.5)$$

$\mathbf{p}_x$, $\mathbf{p}_y$, $\mathbf{p}_z$, $\mathbf{p}_\theta$ are load intensities at nodes. External loads can alternatively use lumped formulation. For penetrating sea surface elements, linear distributions will be on the wetted length only which is from submerged element end to sea surface intersection point.

6.6.2.5 Mass terms

Mass terms includes structural mass and added mass which are contributions from hydrodynamic loads

$$\mathbf{m} = \mathbf{m^s} + \mathbf{m^h} \quad (6.6.2.5.1)$$

$$\mathbf{m_{uu}^{s}} = \mathrm{m}^{\mathrm{s}} \int_{L_0} \mathbf{N_u^T N_u}\, \mathrm{dx} \qquad \mathbf{m_{uu}^{h}} = \mathrm{m}_x^h \int_{L_0} \mathbf{N_u^T N_u}\, \mathrm{dx} \quad (6.6.2.5.2)$$

$$\mathbf{m_{vv}^{s}} = \mathrm{m}^{\mathrm{s}} \int_{L_0} \mathbf{N_v^T N_v}\, \mathrm{dx} \qquad \mathbf{m_{vv}^{h}} = \mathrm{m}_y^h \int_{L_0} \mathbf{N_v^T N_v}\, \mathrm{dx} \quad (6.6.2.5.3)$$

$$\mathbf{m_{ww}^{s}} = \mathrm{m}^{\mathrm{s}} \int_{L_0} \mathbf{N_w^T N_w}\, \mathrm{dx} \qquad \mathbf{m_{uu}^{h}} = \mathrm{m}_z^h \int_{L_0} \mathbf{N_w^T N_w}\, \mathrm{dx} \quad (6.6.2.5.4)$$

$$\mathbf{m_{uu}^{s}} = \mathrm{m}_\theta^{\mathrm{s}} \int_{L_0} \mathbf{N_\theta^T N_\theta}\, \mathrm{dx} \qquad \mathbf{m_{uu}^{h}} = \mathrm{m}_{\boldsymbol{\theta}}^h \int_{L_0} \mathbf{N_\theta^T N_\theta}\, \mathrm{dx} \quad (6.6.2.5.5)$$

m^{s} is structural mass per unit length, $\mathrm{m}_\theta^{\mathrm{s}}$ is gyration mass per unit length, m_x^h, m_y^h, m_z^h are local added mass per unit length, $\mathrm{m}_{\boldsymbol{\theta}}^h$ is local x-axis rotation added mass per unit length. For penetrating sea surface element, similar rules that only submerged parts contributes applies.

In above the interpolation, functions used are the same as the ones in the stiffness matrix which provides displacements within the element as a function of the nodal displacements. Therefore it suggests the correctness of application of the energy method since kinematic energy is in consistence with the potential energy. This consistent mass and kinematic matrix mean an equivalent Rayleigh-Ritz method. For conformal element, the Rayleigh-Ritz method is too rigid and provides upper bound eigenfrequencies.

Mass matrix can alternatively use lumped formulation too. There are several methods to retrieve the lumped formulation. The simplest method is based on equilibrium conditions by distributing the mass among the nodes which can be seen in Figure 21 (LANGEN and SIGBJØRNSSON 1986).

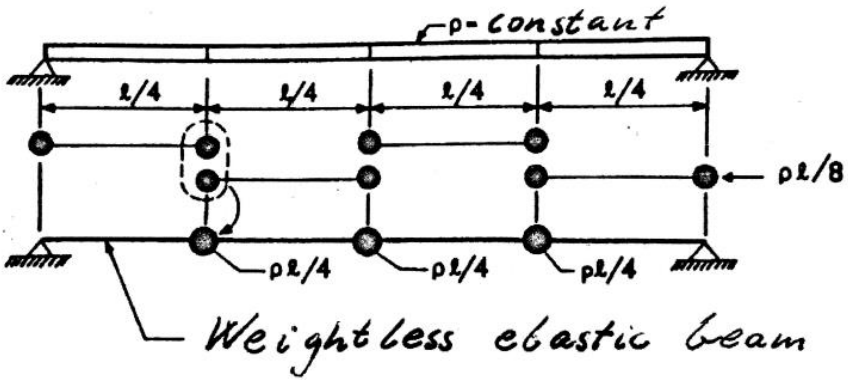

Figure 21 Lumped mass simple equilibrium distribution

The mass matrix can also be determined by unit acceleration. Imagine a unit acceleration and lumped mass would equal to the nodal force which is in equilibrium with the distributed inertia force.

For complex element shapes, virtual work principle can help to determine the mass matrix. By considering the virtual work equilibrium between the consistent load vector $\mathbf{P}$ and the imaged unit acceleration induced inertia force.

$$\delta\mathbf{v}^T\mathbf{P} = \int_V \delta\mathbf{u}^T\rho \cdot 1dV = \delta\mathbf{v}^T \int_V \mathbf{N}^T\rho dV \longrightarrow \mathbf{P} = \int_V \mathbf{N}^T\rho dV \quad (6.6.2.5.6)$$

Lumped mass matrix can also be derived from consistent mass matrix. In each row of the consistent matrix, translation diagonal term can be calculated by adding up the term corresponding to the same translation direction. The rotation term in addition need to be multiplied by factor α.

For higher order elements which there are notes at midsides, above methods may cause negative mass. If positive definite mass matrix is needed, then diagonal terms can be taken from the consistent mass and scaled to the degree that total mass equals the correct value.

Comparison between consistent and concentrated mass for beam elements can be seen in Figure 22. N is the number of elements. n is the frequency number. $\bar{\omega}$ is the computed frequency and ω is the exact frequency. It can be seen that concentrated mass will yield lower value than the exact frequency and consistent mass higher value. For beam element, consistent mass is behaving better than the concentrated one. However, consistent mass is not always behaving better. Hinton's diagonal mass matrix would be as same accurate as the corresponding consistent mass.

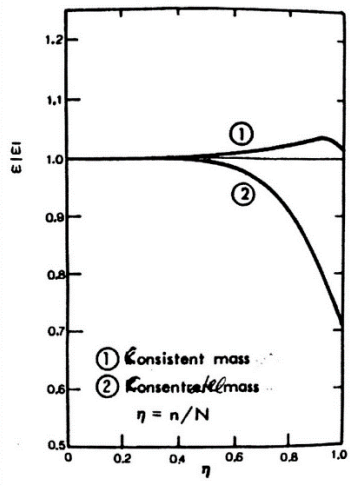

Figure 22 Beam element frequency comparison between lump mass and concentrated mass

6.6.2.6 Beam end deformational rotations

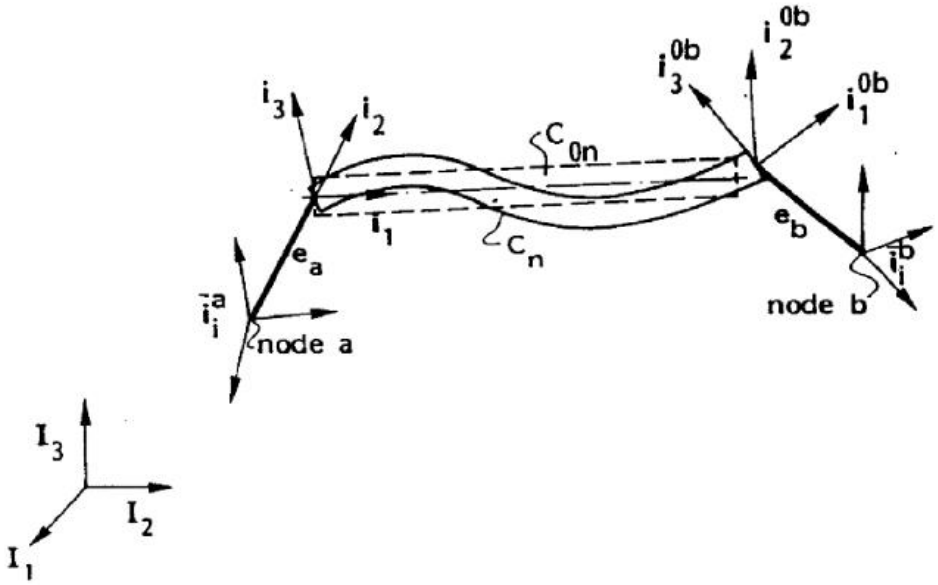

There are in total four system coordinate involved: Global base coordinate $\mathbf{I_i}$, nodal point coordinate $\bar{\mathbf{i}}_\mathbf{i}$ corresponding to the configuration C_{0n}, beam end coordinate $\mathbf{i_i}$ which is possibly eccentrically connected to $\bar{\mathbf{i}}_\mathbf{i}$, deformed beam end coordinate $\mathbf{i_i^0}$ corresponding to the configuration C_n. $\bar{\mathbf{i}}_\mathbf{i}$ and $\mathbf{i_i^0}$ are on both of the beam ends. The transformations between $\bar{\mathbf{i}}_\mathbf{i}$ and $\mathbf{i_i}$ don't change.

Transformation between $\mathbf{i_i}$ and $\mathbf{i_i^0}$ can be derived,

$$\mathbf{i_i^0} = \overline{\mathbf{T}}_{\mathbf{ik}}^{\mathbf{0}}\mathbf{I_k} \ (6.6.2.6.1)$$

$$\mathbf{i_i} = \overline{\mathbf{T}}_{\mathbf{ij}}\mathbf{I_j} \ (6.6.2.6.2)$$

Since $\overline{\mathbf{T}}_{\mathbf{ij}}$ is orthogonal, from $(6.6.2.6.1)$ and $(6.6.2.6.2)$,

$$\mathbf{i_i^0} = \overline{\mathbf{T}}_{\mathbf{ij}}^{\mathbf{0}}\overline{\mathbf{T}}_{\mathbf{kj}}\mathbf{i_k} \ (6.6.2.6.3)$$

From the equation $(6.6.1.5)$,

$$\Delta\theta_1 \approx \widetilde{T}_{23} = \overline{\mathbf{T}}_{\mathbf{2j}}^{\mathbf{0}}\overline{\mathbf{T}}_{\mathbf{3j}} \ (6.6.2.6.4)$$

$$\Delta\theta_2 \approx \widetilde{T}_{31} = \overline{\mathbf{T}}_{\mathbf{3j}}^{\mathbf{0}}\overline{\mathbf{T}}_{\mathbf{1j}} \ (6.6.2.6.5)$$

$$\Delta\theta_3 \approx \widetilde{T}_{12} = \overline{\mathbf{T}}_{\mathbf{1j}}^{\mathbf{0}}\overline{\mathbf{T}}_{\mathbf{2j}} \ (6.6.2.6.6)$$

6.6.2.7 Beam element modelling convention

Compressive loads are expected at the lower part of the riser. According to the guideline of the riflex manual, element length should be l.

$$\mathrm{l} \leq \frac{1}{2(\mathrm{EI}/\mathrm{q})^{\frac{1}{3}}} (6.6.2.7.1)$$

$$\mathrm{l} \leq \frac{1}{\pi(\mathrm{EI}/\mathrm{P}_c)^{\frac{1}{3}}} \ (6.6.2.7.2)$$

Where
EI: cross-sectional stiffness
q: largest lateral load intensity
P_c: largest compressive loads

6.7 System stiffness matrix storage

System stiffness matrix is very sparse which mean many values are zero. The system stiffness matrix features symmetry and band structure according to which the storage can be greatly reduced. Usually computers store the system stiffness matrix in two forms: band storage (constant bandwidth) and skyline storage (variable bandwidth). The two forms can be seen in figure 23 below (MATHISEN 2012).

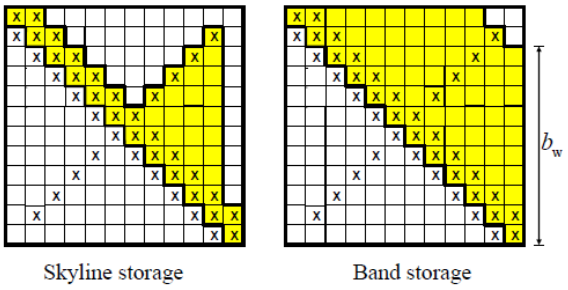

Figure 23 Skyline and band storage illustration

7. Static analysis

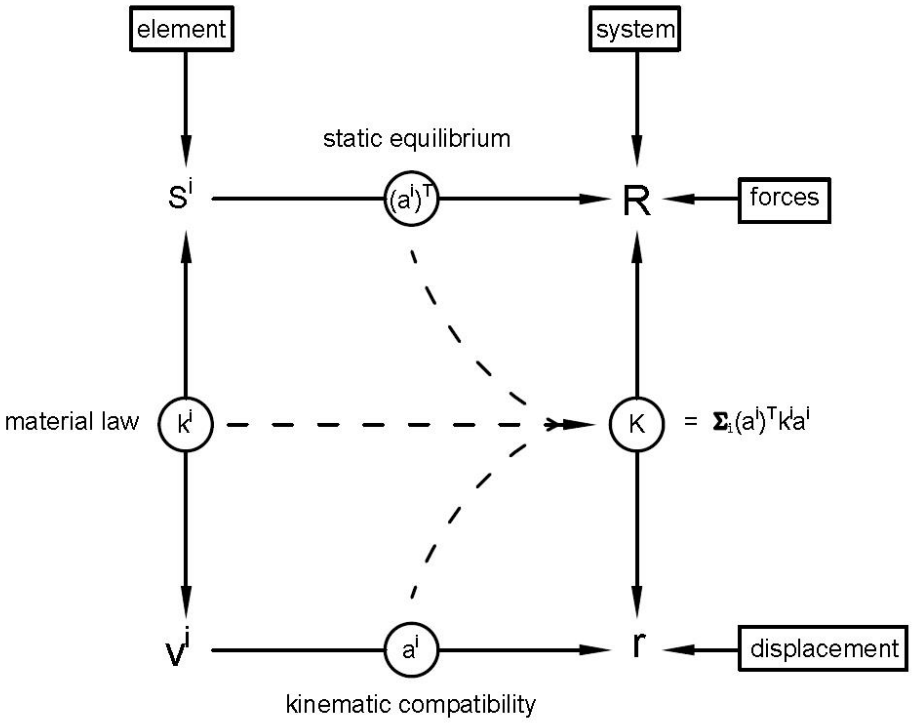

Figure 24 System formulation assembly

The static FEM analysis is to determine the nodal displacement vector which determine the state of the FEM model. By doing static FEM analysis, the complete system is in equilibrium condition. According to the Figure 23 (MATHISEN 2012), the system matrix is formulated by kinematic compatibility. Each element contribute to the whole system by the assembly. After the assembly, the static state of the FEM model can be solved with the formula below:

$$\mathbf{R^S}(\mathbf{r}) = \mathbf{R^E}(\mathbf{r}) \quad (7.1)$$

Where

$\mathbf{r}$ determines the stress-free configuration. E.g. for beams displacements and rotation.

$\mathbf{R^S}(\mathbf{r})$ is the internal structural reaction force assembled from individual elements.

$\mathbf{R^R}(\mathbf{r})$ is the external force matrix including specified forces, volume forces, and distributed forces.

7.1 Incremental equilibrium iterations

The solution is found by incremental-iterative method. In detail, the loads (denoted by k) are accumulating step by step and within each step the displacement vector is taken from the last step and iteration (step denoted by j) is processed until an acceptable

criterion is reached.

The imbalance load vector for each load step k is,

$$\mathbf{R_k(r)} = \mathbf{R_k^S(r)} - \mathbf{R_k^E(r)} \text{ (7.1.1)}$$

The start value of each load step k is,

$$\mathbf{\Delta r_k^0} = -\left[\frac{\mathbf{\partial R_{k-1}}}{\mathbf{\partial r}}\right]^{-1} (\mathbf{R_{k-1}^S} - \mathbf{R_k^E}) \text{ (7.1.2)}$$

$$\mathbf{r_k^0} = \mathbf{r_{k-1}} - \mathbf{\Delta r_k^0} \text{ (7.1.3)}$$

After start value in the specific load step k is determined, Newton-Raphson iteration is done within the load step,

$$\mathbf{\Delta r_k^j} = -\left[\frac{\mathbf{\partial R_{k-1}}}{\mathbf{\partial r}}\right]^{-1} \mathbf{R_k^{j-1}} \text{(7.1.4)}$$

$$\mathbf{r_k^j} = \mathbf{r_k^{j-1}} - \mathbf{\Delta r_k^j} \text{ (7.1.5)}$$

After each Iteration step j, imbalance load vector $\mathbf{R_k^{j-1}}$ is updated, and displacement vector $\mathbf{r_k^j}$ is updated until the max step j is reached or prescribed criterion is met.

The criterion is based on a modified Euclidean displacement norm,

$$\|\mathbf{r_k}\| = \frac{1}{\mathrm{N}} \sum_{\mathrm{i=1}}^{\mathrm{N}} \mathrm{r_{ki}^2} \text{ (7.1.6)}$$

Only translational displacements are accountable for the equation, N is number of active translational degrees of freedom.

The criterion will be as

$$\frac{\|\mathbf{\Delta r_k^j}\|}{\|\mathbf{r_k^j}\|} = \frac{\|\mathbf{r_k^j}\| - \|\mathbf{r_k^{j-1}}\|}{\|\mathbf{r_k^j}\|} < \varepsilon \text{ (7.1.7)}$$

Incremental rotations are processed according to the equation $(6.6.1.5)$. The incremental-iteration procedure can be illustrated as in Figure 24 (MOAN 2003).

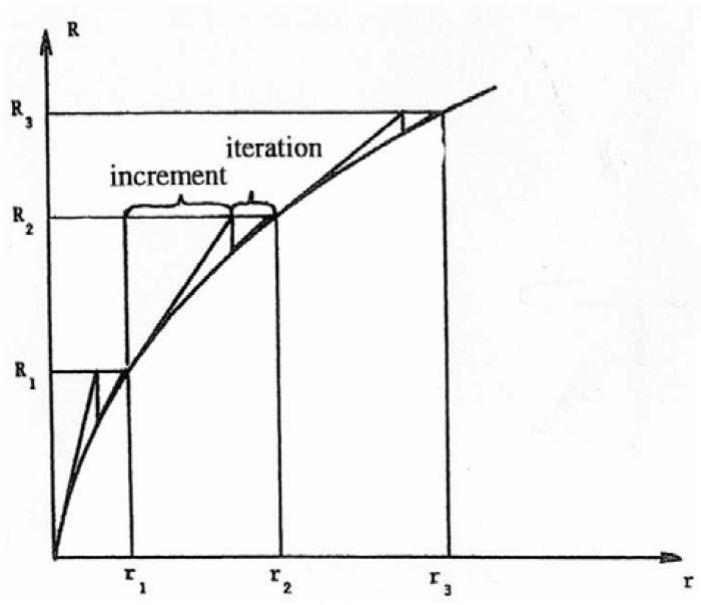

Figure 25 Combined incremental-iterative solution procedures

7.2 Improving numerical stability for static analysis

Generally, incremental load steps k are supposed to be kept small to maintain the stability. There are also some procedures taken to cope with the numerical instability.

The system stiffness for slender structures at first load steps are low because transverse stiffness is mainly governed by geometric stiffness which is zero starting from stress-free configurations. Artificial axial force of 0.01 axial strain is implemented in the RIFLEX program. In the meantime before the geometric stiffness is gradually finishing developing, load steps are scaled that steps are small at the beginning and gradually increasing. The scale function is as below,

$$f_p(i) = \frac{1 - e^{-(\frac{1}{N})}}{1 - e} \quad i = 1,2,3, \dots N \ (7.2.1)$$

N is total number of load increments, i is incremental load step.

The loads types of static analysis are arranged in the following sequence.

1. Volume forces: buoyancy and weight
2. Specified displacements with the nodal boundary conditions: top and bottom ends boundary conditions
3. Specified forces: top tension
4. Position dependent forces: current forces

The sequence of the analysis is done by default from 1 to 4 with 20 load steps k of each basic load type.

Volume forces if by default load sequence will cause instability because of the compression. Therefore volume forces, specified displacements, and specified force (top tension) are loaded simultaneously.

Similarly considering the influence of sensitivity to transverse stiffness, it should be that load sequence 2 and 4 needs more steps and load sequence 1 and 3 less.

The suggestion in the RIFLEX theory manual is as below.

Table 2 Recommended load steps for beam FEM analysis

Load Types	FEM beam element number of load steps
Volume forces	5-10
Prescribe displacements	50-200
Current	1-10

The criterion suggestion in the RIFLEX theory manual

$$\varepsilon = 10^{-4} - 10^{-6} \text{ for beam elements}$$

Maximum equilibrium iterations are suggested between 5 and 15.

8. Dynamic analysis

Wind, tide, wave, and current varies with time. Riser natural frequencies are in many cases found in the frequency range of wave forces and vortex shedding (hydro elastic phenomenon such as lock-in vibration can happen). This implies the importance of dynamic analysis. Then modelling the correct damping is important. Because of the environment risers being with, the load effects should be depicted in a right and efficient way. In many cases, stochastic analysis is wanted.

When dealing with the stochastic property it is common to describe the stationary sea states (short sea states). In a short sea state, only the sea elevation change with time and is regarded as stationary Gaussian process which provide for the mathematical bases. Load effect is considered in a similar way. Therefore, a dynamic analysis is normally performed during a short sea states which has constant statistical properties.

Load effects not only depends on wave height but also on wave period. There are two reasons. One is calculation process of the wave force need the period. The other is dynamic response are strongly relied on load frequency. In order to establish the response and load spectrum, dynamic analysis should be performed.

First order wave forces usually possess significant energy with the period 3-24s. But Wave forces also have differential frequencies and they are called wave drift forces. The long-period motions are usually caused by this differential loads and the period is around 1-3 minutes.

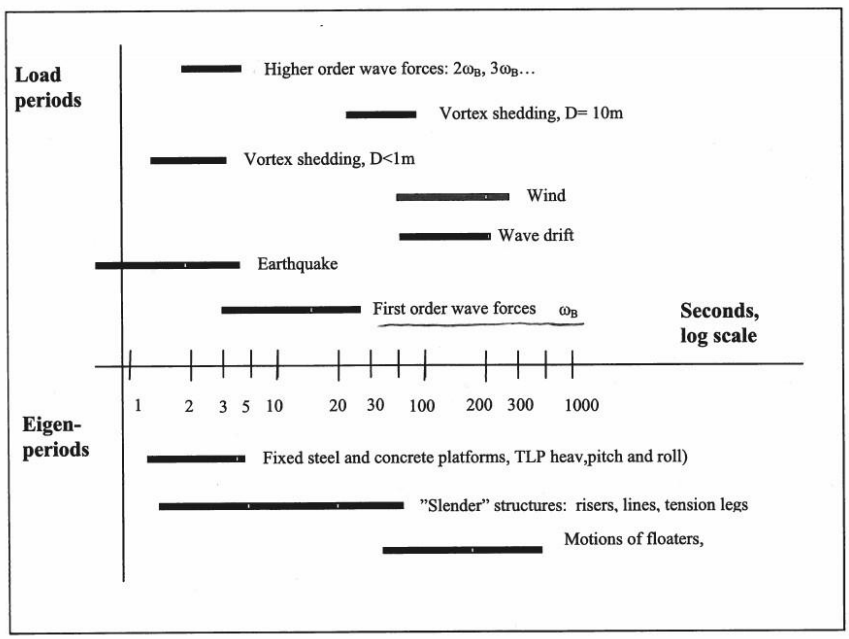

Figure 26 Summary of load perods and typical natural periods for marine structures

From figure above, the wind and wave drift loads periods is within the range of floater eignenpeirods.

8.1 Time and frequency domain

Two domains means two methods of describing processes and performing calculations. The purpose of the time and frequency domain analysis is to determine system response of the floater induced motions and hydrodynamic loads. The results of frequency domain analysis are the system Eigen-frequencies and Eigen-vectors. The results of time-domain analysis is a time series of selected response parameter such as stress, strain and shear forces.

8.2 Coupled analysis and separate analysis

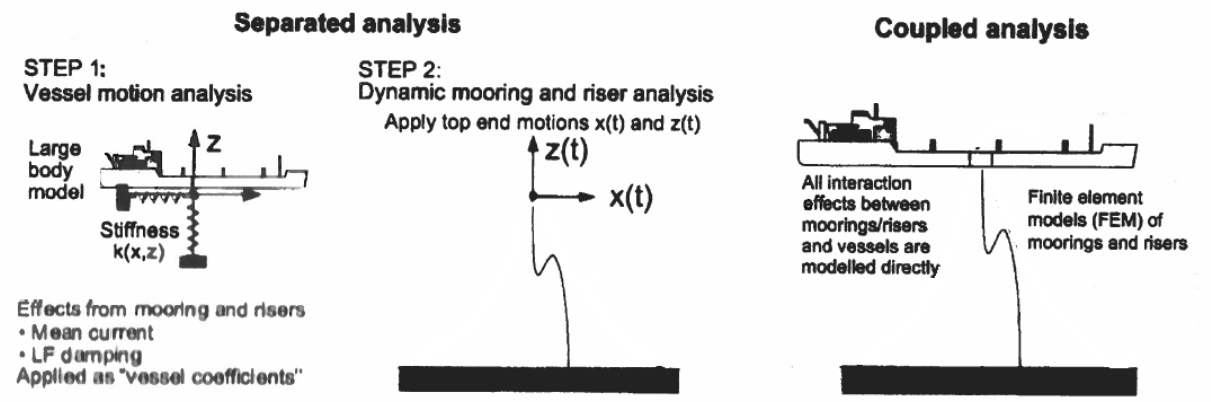

Figure 27 Coupled analysis of floter and riser

In a conventional separated analysis, mooring lines possess a great influence. Then the motions of floaters and the load effects from mooring lines and risers are analyzed separately. When calculating the motions of floaters, the load effects from mooring lines and risers are treated as position dependent nonlinear forces. The illustration can be seen from the figure above. Then the motions of floaters are used as excitation motions to obtain the dynamic loads for mooring lines and risers (ORMBERG and LARSEN 1997). In the current thesis, riser is the only influential factor and load effects from the riser on the floater are omitted.

Coupled analysis means simultaneous analysis of wave frequency and low-frequency responses and simultaneous analysis of vessel motion and riser dynamics.

8.3 Waves and transfer functions

8.3.1 Airy wave

Two models are used in Riflex for regular waves: airy linear wave theory, stoke's 5th order wave theory. The main difference between the two theories is that boundary condition pressure ($\mathrm{p} = 0$) is only approximately right at for Stroke's theory at sea surface but only valid at mean water level for airy linear wave theory. Thus the linear wave theory is only applicable for infinitesimal wave amplitudes. The main concern of the thesis is airy wave theory.

According to Airy linear theory the wave, wave potential is

$$\phi_0 = \frac{\zeta_a g}{\omega} C_1 \cos(-\omega t + kx\cos\beta + ky\sin\beta - \phi_\zeta) \quad (8.3.1.1)$$

Where
ζ_a: Wave Amplitude
g: Gravitational Acceleration
k: Wave Number
β: Wave Propagation Direction
ϕ_ζ: Wave Component Phase Angel

$$C_1 = \frac{\boldsymbol{cosh}k(z+d)}{\boldsymbol{cosh}kd} \quad (8.3.1.2)$$

In deep water, $C_1 \approx e^{kz}$ (8.3.1.3)

Where
d: Water Depth

Because the airy linear wave theory is only valid on the mean water level. The wave properties on the free surface is important and the wave potential needs to be adjusted to take that into consideration.

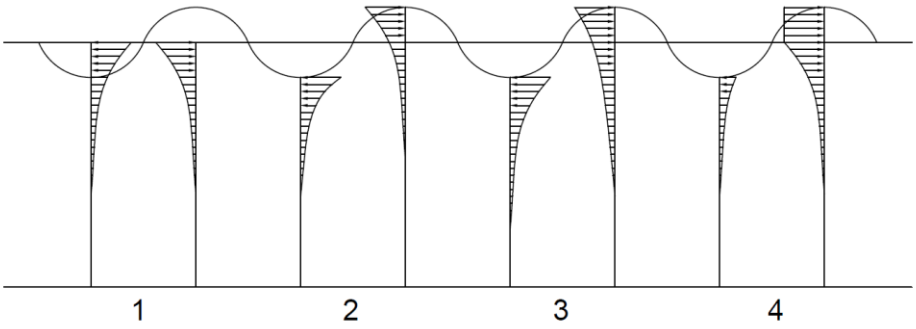

Figure 28 Different methods for wave potentials at sea surface

Method 1 is assuming the water level remains at the mean level and thus is integrated only to the mean level.

Method 2 is similar to method 2 but wave potential is moved parallel to the instantaneous sea surface.

Method 3 assumes that the linear theory is correct on the sea surface. The Potential is stretched or compressed based on the linear relationship between the modified z coordinate and the original z coordinate.

$$\text{When } \mathrm{Z}' = 0, \mathrm{Z} = \zeta; \text{When } \mathrm{Z}' = -\mathrm{D}, \mathrm{Z} = -\mathrm{D}$$

$$\mathrm{Z} - \zeta = \frac{-\mathrm{D} - \zeta}{-\mathrm{D} - 0}(\mathrm{Z}' - 0) (8.3.1.2)$$

Method 4 is called extrapolated airy theory. It is based on that the potential remains on the mean water level, and for troughs the potential is truncated till the instantaneous wave surface and for crests, wave potential is assumed to be constant equal to the mean water level. The condition that pressure at the boundary is equal to zero is satisfied at the wave crests but a high order error is introduced at the wave troughs.

For regular wave models, wave kinematics can be calculated either at the static position or at the structural instantaneous position (static+dynamic). If the motions are mainly due to the linear wave-induced floater motion, wave kinematics at static positions is recommended. Because forced super node motions can be inconsistent with the instantaneous wave kinematics.

Then wave particle velocities and accelerations in an undisturbed field can be derived accordingly

$$\text{by } \frac{\omega^2}{\mathrm{g}} = \mathrm{ktanhkh}, \mathrm{v_m} = \frac{\partial \phi_0}{\partial \mathrm{m}}, \mathrm{a_m} = \frac{\partial \mathrm{v_m}}{\partial \mathrm{m}}, \mathrm{k} = \mathrm{x}, \mathrm{y}, \mathrm{z}\ (8.3.1.3)$$

According to linearized free-surface dynamic condition, on $z = 0$

$$g\zeta + \frac{\partial \phi}{\partial t} = 0 \text{ (8.3.1.4)}$$

Thus $\zeta = \zeta_a \sin\alpha$

Where
ζ: Wave Elevation

$\alpha = \omega t - kx\cos\beta - ky\sin\beta + \phi_\zeta$

The linear dynamic pressure is written as

$$p_d = -\rho\frac{\partial \phi}{\partial t} = \rho g \zeta_a C_1 \sin\alpha \text{ (8.3.1.5)}$$

The wave particle vertical motions is

$$\zeta = \int_0^t (v_z dt + z_0) = \zeta_a C_3 \sin\alpha \text{ (8.3.1.6)}$$

Where
z_0 is chosen that the average is zero.

$C_3 = \frac{\boldsymbol{sinh} k(z+d)}{\boldsymbol{sinh} kd}$ (8.3.1.7)

$v_z = \frac{\partial \phi}{\partial z}$

Written in the complex form,

$$\zeta = \zeta_a C_3 \exp i\alpha \text{ (8.3.1.8)}$$

The responses to the wave

$$R = H_r\zeta = r_a C_3 \exp i(\alpha + \phi_r) \text{ (8.3.1.9)}$$

$$r = ImR \text{ (8.3.1.10)}$$

Where
$r_a = |H_r|\zeta_a$
$ArgH_r = \phi_r$

8.3.2 Irregular waves

The irregular sea state is a combination of a wind sea and a swell sea

For undisturbed airy wave field

$$S_{\zeta,TOT}(\beta,\omega) = S_{\zeta,1}(\omega)\phi_1(\beta-\beta_1) + S_{\zeta,2}(\omega)\phi_2(\beta-\beta_2) \quad (8.3.2.1)$$

Where

$S_{\zeta,1}$ and $S_{\zeta,2}$ represent the wind and swell frequency component respectively. Various spectra can be used. See chapter 8.3.3.

The variation condition is satisfied $\int_0^\infty S_{\zeta,1}(\omega)d\omega + \int_0^\infty S_{\zeta,2}(\omega)d\omega = \sigma_\zeta^2$ (8.3.2.2)

ϕ_1 and ϕ_2 represent wave directionality and satisfies

$$\int_{-\pi/2}^{\pi/2} \phi_j(\beta)d\beta = 1\,;\phi_j(\beta) = 0 \text{ for } \frac{\pi}{2} < \beta < \frac{3\pi}{2} \quad (8.3.2.3).$$

β is the direction of interest and β_1 and β_2 are illustrated as below.

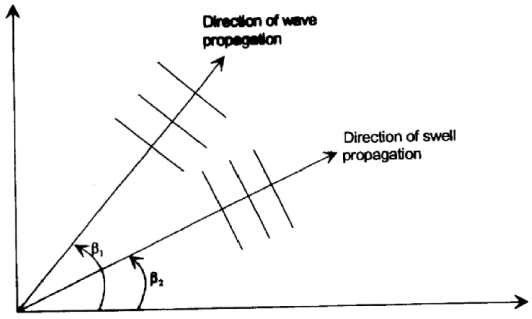

Figure 29 Wave travelling direction defination

The irregular sea is discretized into harmonic components and then wave elevation is realized by adding the harmonic components.

$$\zeta = I_m(Z_\zeta) = I_m\left(\sum_{j=1}^{N_\beta}\sum_{k=1}^{N_\infty} Z_{jk}\right) = I_m\left(\sum_{j=1}^{N_\beta}\sum_{k=1}^{N_\infty} A_{jk}\, e^{i(\omega_k t+\phi_{jk}^p+\phi_{jk})}\right)$$

$$= \sum_{j=1}^{N_\beta}\sum_{k=1}^{N_\infty} \sqrt{S_{\zeta,TOT}(\beta_j,\omega_k)\Delta\beta\Delta\omega}\,\sin(\omega_k t + \phi_{jk}^p + \phi_{jk}) \quad (8.3.2.4)$$

Where

$$\phi_{jk}^{p} = -k_k x \cos\beta_j - k_k y \sin\beta_j$$

$$\phi_{jk} \text{ is uniform distributed over} [-\pi, \pi]$$

8.3.3 Wave spectrum

Most Commonly used wave spectrums used on Norwegian Continental Shelf is (Haver 2007),

*Pierson-Moskowitz wave spectrum
*JONSWAP wave spectrum
*Torsethaugen wave spectrum

Sea states are defined as follows,

Wind Sea: a wind sea is the result of the local wind field. Because both wave field and wind field propagate in space, an observed sea at a given site could be the wind induced wave travelling over a long distance.

Swell Sea: frequencies and directions of a swell sea is narrower than the wind sea because it is not generated from local field. Waves with longer wave length and thus larger wave energy will survive after the long distance travel. It can be realized by the storms miles away where they break or by decaying wind sea after the wind is significantly reduced.

Combined Sea: Most sea states in practice is generally a combination of a pure wind sea and one or several swell sea processes. From a signal analysis point of view, swells can be regarded as a regular wave signal within the strong noise (Wikipedia 2015).

Fully developed wind sea: If the wind and wave field reach an equilibrium which means wind-wave interaction, wave-wave interaction and dissipation are in energy equilibrium. Practically, this situation hardly occurs in real ocean.

Growing Wind Sea: Assume a growing sea in space and in time with wind blowing from no wind to a strong wind. In the process the wind slowly grow in height, wave length (and thus wave period). The corresponding spectrum will more sharply peaked than the developed sea.

For fully developed nature, Person Moskowitz spectrum would be proper. If the relationship between significant wave height and peak period in the vicinity of the following relation, then a fully developed sea assumption could be reasonable.

$$t_p = 5\sqrt{h_s} \quad (8.3.3.1)$$

For growing seas, the JONSWAP spectrum proposed after the full scale measurements in the southern North Sea is suitable.

For general combined sea state, it will be a combination of approximate wave direction Wind Sea and one or several swell seas from random directions. It is conservative to assume that both seas will propagate in the same direction.

For an arbitrary combination of $\mathrm{h_s}$ and $\mathrm{t_p}$, the Torsethaugen spectral model is adopted for the frequency wave spectrum. The spectrum is a combination two JONSWAP like spectrum, one representing the wind sea and the other representing the swell sea.

The Torsethaugen model divide the $\mathrm{h_s}$ and $\mathrm{t_p}$ into a wind dominated region and a swell dominated region. The boundary is given by

$$\mathrm{t_{pb}} = 6.6\mathrm{h_s}^{0.333} \quad (8.3.3.2)$$

For a given $\mathrm{h_s}$, if $\mathrm{t_p}$ is lower than $\mathrm{t_{pb}}$, it indicates a growing wind sea. Otherwise it indicates a swell sea or decaying wind sea.

8.3.4 Wind and current

The wind field is 2-dimentional which means velocity is unidirectional in the horizontal plane and varies along the vertical direction.

Generally current configuration is constant with time. Quasi-static current variation can be included in a quasi-static analysis. In the dynamic analysis, current can varies with time.
Current is denoted in the global frame

$$\mathrm{U}_c = [\mathrm{U}_{cx}, \mathrm{U}_{cy}, \mathrm{U}_{cz}] \quad (8.3.4.1)$$

U_z^C is zero.

8.3.5 Transfer functions

Current, wave, and wind varies with time and such environmental status is observed in a short time and defined statistically with certain parameters to represent the short term. The sea elevation (also maxima) is assumed to be Gaussian which give the

mathematical basis for wave process. The corresponding response process is considered to be stationary with constant parameters in the short term.

In case the three conditions below are satisfied,

1. For a given frequency, the wave height is proportional to the responsible amplitude.
2. The frequency of the responsible will be the wave frequency.
3. The one response frequency is indifferent to the simultaneous another frequency response.

Then the response process is considered to be Gaussian so the system is called linear system and superposition principle can be applied.

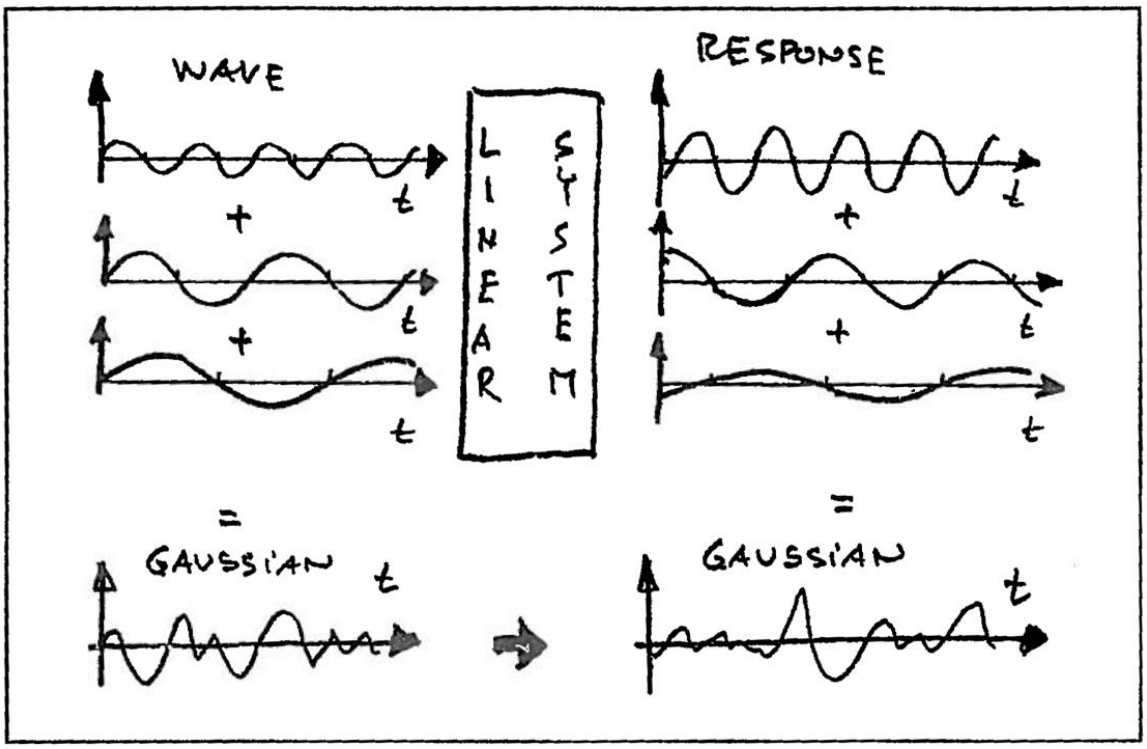

Figure 30 Linear system transfer

This is a proper assumption for the large volume floaters because not too many nonlinearities are introduced.

From wave to load, $\mathrm{F_0}(\omega) = \mathrm{H_H}(\omega) \cdot \eta_0(\omega)$ (8.3.5.1)

From load to response, $\mathrm{x_0}(\omega) = \mathrm{H_M}(\omega) \cdot \mathrm{F_0}(\omega) = \mathrm{H_M}(\omega) \cdot \mathrm{H_H}(\omega) \cdot \eta_0(\omega)$ (8.3.5.2)

$\mathrm{H_X}(\omega) = \mathrm{H_M}(\omega) \cdot \mathrm{H_H}(\omega)$ (8.3.5.3)

Where
F_0: Load Amplitude
η_0: Wave Amplitude
x_0: Response Amplitude
H_H : Hydrodynamic transfer function linearizing the load amplitude and wave amplitude for a give frequency.
H_M : Mechanical transfer function linearizing the load amplitude and response amplitude for a give frequency.
H_X: Transfer function linearizing the wave amplitude and response amplitude for a give frequency.

8.4 Morison Equation

8.4.1 Force domain

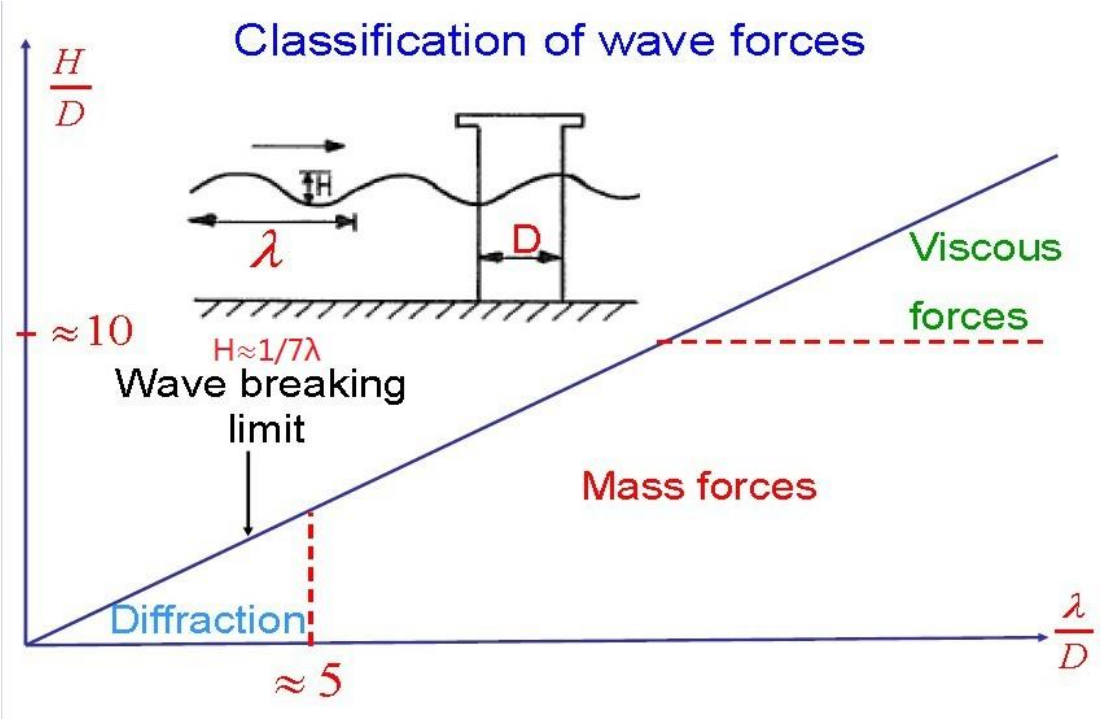

Figure 31 Force domain

According to the figure above (GRECO 2012), for small volume structures ($\lambda/D > 5$) the wave will not be affected by the structure and consequently long-wave approximation are available. Then the corresponding loads will originate from acceleration and velocity which are mass loads and viscous loads respectively. The predominant are for the two forces will depend on the steepness H/D. If $H/D < 10$, mass loads which is proportional to acceleration will dominate. Otherwise viscous loads which are proportional to squared power of velocity dominate. The viscous effects are connected with viscosity, flow separation, and wake. If $H/D \to \infty$ the

wave will be similar to slow-varying current. Therefore, $\lambda/D > 5$ is the area of interested with riser when Morison equation can be implemented.

For ambient oscillatory flow velocity equals to $U_M \sin(\omega t + \varepsilon)$

$$KC = \frac{U_M T}{D} \quad (8.4.1)$$

For incident wave case, $U_M = \omega\zeta$.

$$\text{Relative current number} = \frac{U_c}{U_M} \quad (8.4.2)$$

8.4.2 Force model

Morison equation are used where viscous forces matter and wave scattering is secondary which is omitted and can be applied to various cross sections. The equation is a semi-empirical formula for in-line forces which take effects normal to the cylinder and along the wave direction. Morison's equation is a long wave approximation if $C_M = 2$. Because the excitation force and Morison's equation would coincide for elongated cylindrical cross section. C_D is asymptotic value for large KC numbers and C_M is asymptotic for small KC numbers without viscous boundary layer effects. Roughness number has more influence on drag force in small KC numbers than large KC numbers. Usually the C_D and C_M are tuned by measured in-line forces.

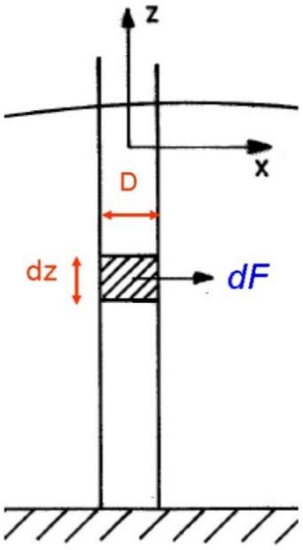

Figure 32 Morrison equation differential force model

According to Morrison equation,

$$dF(t) = \frac{1}{2}\rho C_D D dl(u(t) - \dot{r})|u(t) - \dot{r}| + \frac{1}{2}\rho C_M \frac{\pi D^2}{4} dl \cdot \dot{u}(t) - \rho(C_M - 1)\frac{\pi D^2}{4} dl \cdot \ddot{r} \quad (8.4.3)$$

The direction of positive force is the incident-wave propagation direction. Assuming the cross flow principle, $u(t)$ and $\dot{u(t)}$ are horizontal incident wave velocity and accelerations and the center of the cylinder. Therefore there is no contributions from tangential fluid velocity and acceleration. The term with C_D is called drag force and C_M mass force. No vortex shedding is included in the Morison's equation.

The relative velocity between the cylinder and wave should be accounted for when $\dot{r}$ is large enough. And the same applies for Diffraction force affected by relative acceleration $\ddot{r}$. But the FK force is not affected by the relative acceleration $\ddot{r}$ because FK force only rely on incident wave acceleration. Usually for practical application the velocity $u(t)$ is usually the vector sum of current and wave speed.

For linear deep wave, mass and drag force decrease with the e^{kz} and e^{2kz}. Therefore the drag force is concentrated on the sea surface. Linear wave kinematics will introduce an error as on sea surface, velocity and acceleration are not zero. In principle it should not be applied but in practice it is just used directly. The velocity term is usually the sum of current and wave if current exist. The velocity difference can be seen in Figure 33.

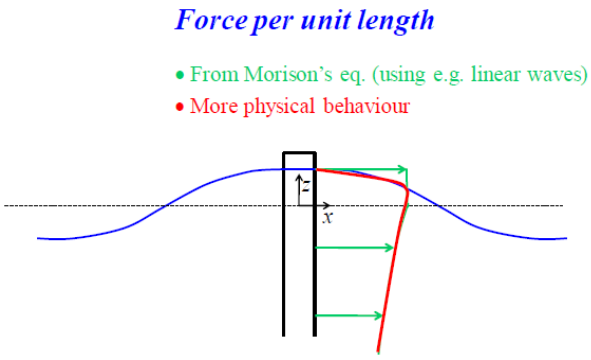

Figure 33 Force difference between model and reality

8.4.3 Flow separation

Oscillatory ambient flow make it hard for flow to separate because the periodicity make flow remain attached to the body more easily. Oscillatory ambient flow at low KC numbers don't separate because of the low periods. The flow always separate in a steady current. However for combined steady current and oscillatory flow, it depends on the relative current number. If $U_C/U_M > 1$, separation always occur (see Figure 34). Otherwise the flow may not separate because the flow will return to the body.

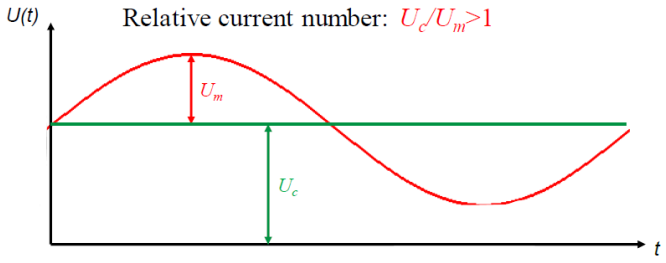

Figure 34 Flow separation condition for current and oscillatory flow condition

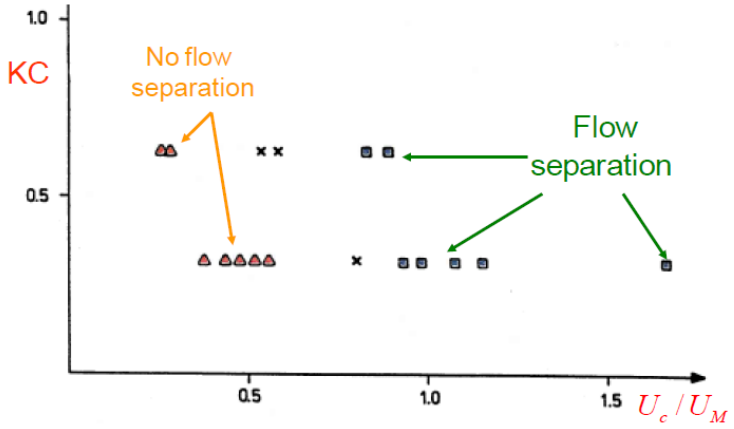

Figure 35 Flow separation for small KC number

Figure 35 above shows the flow separation occurs for small KC numbers. Thus it is important to quantify the flow separation.

Small KC numbers are relevant for many different conditions including the slow-drift motions of moored structures and ships/barges roll damping. Graham (1980) proposed a flow separation empirical equation for the C_D which is strongly dependent on the local flow.

$$C_D \propto KC^{\eta}, \eta = \frac{2\delta - \pi}{3\pi - 2\delta} \quad (8.4.3.1)$$

δ: body internal angle at the separation point.

For cylindrical cylinder ($\delta = \pi$), an experimental result is illustrated below.

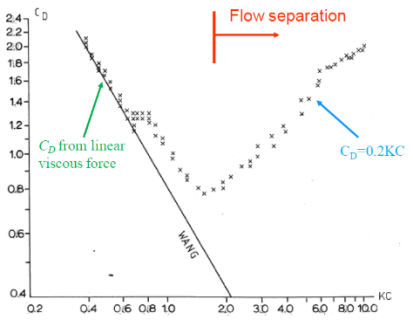

Figure 36 Cylindrical cylinder drag coefficient dependence on KC number

When there is no flow separation ($\mathrm{KC} \leq 1$), the $\mathrm{C_D}$ decrease as KC increase due to the viscous force which is in agreement with the unseparated laminar high Reynolds number flow by Wang (1986). When Flow began to separate, the KC will increase linearly in agreement with Graham and it will stay valid till $\mathrm{KC} \approx 10$.

For large KC numbers, oscillatory ambient flow will like steady current changing direction in large time. The induced vortex at the back stream will increase the $\mathrm{C_D}$ when the direction change. The effect will reach an asymptotic value when $\mathrm{KC} \to \infty$.

$$\mathrm{C_D} \approx \mathrm{C_{D|KC=\infty}}(1 + 0.58\mathrm{e}^{-0.064\mathrm{KC}})^2 \quad (8.4.3.2)$$

8.5 Structural damping

To introduce the structural damping for convenience, Global Rayleigh Damping is usually introduced for the tangential damping.

$$\mathbf{C} = \alpha_1\mathbf{M} + \alpha_2\mathbf{K}$$

For linear dynamic system,

$$\mathbf{\Phi_i^T C \Phi_j} = \alpha_1\mathbf{\Phi_i^T M \Phi_j} + \alpha_2\mathbf{\Phi_i^T K \Phi_j} = \mathbf{0}, \text{for } \mathbf{i} \neq \mathbf{j} \quad (8.5.1)$$

$$\bar{\mathrm{c}}_\mathrm{i} = \mathbf{\Phi_i^T C \Phi_i} = \alpha_1\bar{\mathrm{m}}_\mathrm{i} + \alpha_1\bar{\mathrm{k}}_\mathrm{i} \quad (8.5.2)$$

Where

$$\bar{\mathrm{m}}_\mathrm{i} = \mathbf{\Phi_i^T M \Phi_i} \quad (8.5.3)$$
$$\bar{\mathrm{k}}_\mathrm{i} = \mathbf{\Phi_i^T K \Phi_i} \quad (8.5.4)$$

Then

$$\boldsymbol{\lambda_i} = \frac{\bar{c}_i}{2\bar{m}_i\omega_i} = \frac{1}{2}\left(\frac{\alpha_1}{\omega_i} + \alpha_2\omega_i\right) \text{ (8.5.5)}$$

Which can be seen that α_1 damps the lower frequency mode, and α_2 damps the higher frequency mode. This can be seen as a reference for the nonlinear dynamic systems. The Rayleigh damping can be based on instantaneous tangential mass and stiffness matrices, but it will become numerically unstable as updating the mass and stiffness matrices which means it is mainly suitable for the moderate damping level. On the order hand, Rayleigh damping can be assembled at the instantaneous position of the elements by the local Rayleigh damping which is based on static equilibrium position of the elements. The shortcomings of the updated Rayleigh damping is then eliminated. Local damping can also be specified for the tension, bending and torsion for the element respectively.

8.6 Dynamic FEM inplementation

8.6.1 Load types

There are four types of loads

1. Weight and inertia forces, including the piping itself, internal fluid, and external wrapping.
2. Hydrostatic forces, based on water depth
3. Hydrodynamic forces, based on current, wave, and structural motions
4. Forced motion of line, based on vessel motions

The beam model cross sectional property is independent from pressure thus the equilibrium condition will not be affected. Pressure gradients will suffice. Loads are modelled as distributed line loads or point loads.

8.6.2 Dynamic equilibrium

From the virtual work dynamic equilibrium equation, the dynamic FEM can be expressed as,

$$\mathbf{R^I}(\boldsymbol{r}, \ddot{\boldsymbol{r}}, t) + \mathbf{R^D}(\boldsymbol{r}, \ddot{\boldsymbol{r}}, t) + \mathbf{R^S}(\boldsymbol{r}, \ddot{\boldsymbol{r}}, t) = \mathbf{R^E}(\boldsymbol{r}, \ddot{\boldsymbol{r}}, t) \text{ (8.6.2.1)}$$

$\mathbf{R^I}$ is inertia force vector, $\mathbf{R^D}$ is force vector, $\mathbf{R^S}$ is internal structural reaction force which is described in the static finite element chapter, $\mathbf{R^E}$ is the external vector.

$$\mathbf{R^I}(\boldsymbol{r}, \ddot{\boldsymbol{r}}, t) = [\mathbf{M^S} + \mathbf{M^F}(\boldsymbol{r}) + \mathbf{M^H}(\boldsymbol{r})]\ddot{\boldsymbol{r}} \text{ (8.6.2.2)}$$

$\mathbf{M^S}$ is structural mass matrix, $\mathbf{M^F}(\mathrm{r})$ is internal flow mass matrix and is time dependent if slug flow is considered, $\mathbf{M^H}(\boldsymbol{r})$ is hydrodynamic mass matrix from the from the Morrison's structural acceleration term.

$$\mathbf{R^D}(\boldsymbol{r}, \ddot{\boldsymbol{r}}, t) = [\mathbf{C^S}(\boldsymbol{r}) + \mathbf{C^H}(\boldsymbol{r}) + \mathbf{C^D}(\boldsymbol{r})]\ddot{\boldsymbol{r}} \ (8.6.2.3)$$

$\mathbf{C^S}(\boldsymbol{r})$ is internal structural damping matrix, $\mathbf{C^H}(\boldsymbol{r})$ is hydrodynamic damping matrix from diffraction effects of floating partly submerged elements, $\mathbf{C^D}(\boldsymbol{r})$ is specified discrete dashpot dampers.

In dynamic finite element time domain analysis, most important nonlinear effects included in the dynamic analyses are,

*geometric stiffness which is axial force contribution to the transverse stiffness
*nonlinear cross sectional stress-strain relationship
*structural velocity dependent Morrison equation terms
*integration loading to actual surface elevation
*contact issues

8.6.3 Dynamic equilibrium instability and accuracy

Newmark β family Method

$$\dot{\mathrm{r}}_{\mathrm{k+1}} = \dot{\mathrm{r}}_{\mathrm{k}} + (1-\lambda)\mathrm{h}\ddot{\mathrm{r}}_{\mathrm{k}} + \lambda\mathrm{h}\ddot{\mathrm{r}}_{\mathrm{k+1}} \ (8.6.2.4)$$

$$\mathrm{r}_{\mathrm{k+1}} = \mathrm{r}_{\mathrm{k}} + \mathrm{h}\dot{\mathrm{r}}_{\mathrm{k}} + \left(\frac{1}{2} - \beta\right)\mathrm{h}^2\ddot{\mathrm{r}}_{\mathrm{k}} + \beta\mathrm{h}^2\ddot{\mathrm{r}}_{\mathrm{k+1}} \ (8.6.2.5)$$

$$\mathrm{m}\ddot{\mathrm{r}}_{\mathrm{k+1}} + \mathrm{c}\dot{\mathrm{r}}_{\mathrm{k+1}} + \mathrm{k}\mathrm{r}_{\mathrm{k+1}} = \mathrm{Q}_{\mathrm{k+1}} \ (8.6.2.6)$$

k is time step, h is time length, r is component of displacement vector, λ and β are free parameters.
Put in matrix form, above equations can be as,

$$\begin{bmatrix} 0 & 1 & \lambda\mathrm{h} \\ 1 & 0 & \beta\mathrm{h}^2 \\ \mathrm{k} & \mathrm{c} & \mathrm{m} \end{bmatrix} \begin{bmatrix} \mathrm{r}_{\mathrm{k+1}} \\ \dot{\mathrm{r}}_{\mathrm{k+1}} \\ \ddot{\mathrm{r}}_{\mathrm{k+1}} \end{bmatrix} = \begin{bmatrix} 0 & 1 & (1-\lambda)\mathrm{h} \\ 1 & \mathrm{h} & (\frac{1}{2} - \beta)\,\mathrm{h}^2 \\ 0 & 0 & 0 \end{bmatrix} \begin{bmatrix} \mathrm{r}_{\mathrm{k}} \\ \dot{\mathrm{r}}_{\mathrm{k}} \\ \ddot{\mathrm{r}}_{\mathrm{k}} \end{bmatrix} + \begin{bmatrix} 0 \\ 0 \\ \mathrm{Q}_{\mathrm{k+1}} \end{bmatrix} \ (8.6.2.7a)$$

$$\mathbf{B_1 u_{k+1}} = \mathbf{B_0 u_k} + \mathbf{Q_k} \ (8.6.2.7b)$$

Introducing amplification matrix $\mathbf{A}$

$$\mathbf{A} = \mathbf{B_1^{-1} B_0} \ (8.6.2.8)$$

$$\mathbf{u_{k+1}} = \mathbf{A u_k} + \mathbf{B_1^{-1} Q_{k+1}} = \mathbf{A u_k} + \mathbf{F_k} = \mathbf{A^k u_1} + \sum_{\mathbf{i=1}}^{\mathbf{k}} \mathbf{A^{k-i} F_i} \quad (8.6.2.9)$$

To be stable, free vibrations should be limited for arbitrary start values which means $\mathbf{A^k}$ should be kept limited.

Amplification matrix $\mathbf{A}$ can be written as

$$\mathbf{A} = \mathbf{X \Lambda X^{-1}} \quad (8.6.2.10)$$

$$\mathbf{A^k} = \mathbf{X \Lambda^k X^{-1}} \quad (8.6.2.11)$$

$\mathbf{\Lambda}$ is a diagonal matrix containing eigenvalues λ_i

To meet the condition of stable

$$\rho(\mathbf{A}) = \max|\lambda_i| \leq 1 \quad (8.6.2.12)$$

There are two typical errors: period error and decreasing amplitude. The parameter that influence the accuracy are free parameters (λ and β) and time step length h. Damping will increase with $\mathrm{h/T}$ increasing which means higher frequency mode can be smoothed by the artificial damping. Therefore artificial damping can only be applied when false high frequency components exist. Generally for $\mathrm{h/T} \leq 0.01$ accuracy will suffice for all the methods.

Wilson's method is a modification of linear acceleration ($\beta = 1/6$) of the Newmark β family Method.

In the interval $0 < \tau < \theta \mathrm{h}$

$$\ddot{\mathrm{r}}(\tau) = \ddot{\mathrm{r}}_k + (\ddot{\mathrm{r}}_{k+1} - \ddot{\mathrm{r}}_k)\frac{\tau}{\mathrm{h}} \quad (8.6.2.13)$$

After integration

$$\dot{\mathrm{r}}(\tau) = \dot{\mathrm{r}}_k + \ddot{\mathrm{r}}_k \tau + (\ddot{\mathrm{r}}_{k+1} - \ddot{\mathrm{r}}_k)\frac{\tau^2}{2\mathrm{h}} \quad (8.6.2.14)$$

$$r(\tau) = r_k + \dot{r}_k\tau + \ddot{r}_k\frac{\tau^2}{2} + (\ddot{r}_{k+1} - \ddot{r}_k)\frac{\tau^3}{6}h \quad (8.6.2.15)$$

At time $\tau = \theta h$

$$\ddot{r}_{k+\theta} = (1-\theta)\ddot{r}_k + \theta\ddot{r}_{k+1} \quad (8.6.2.16)$$

$$\dot{r}_{k+\theta} = \dot{r}_k + \frac{\theta h}{2}(\ddot{r}_k + \theta\ddot{r}_{k+\theta}) \quad (8.6.2.17)$$

$$r_{k+\theta} = r_k + \theta h\dot{r}_k + (\theta h)^2(\frac{\ddot{r}_k}{3} + \frac{\ddot{r}_{k+\theta}}{6}) \quad (8.6.2.18)$$

Then the values at step $k+1$ can be calculated by setting $\theta = 1$

Then the stability of Wilson's method and Newman's method can be generalized in the table 3 below.

Table 3 Stability parameter dependence

Method	γ	β	θ	Stability
Second central difference	$1/2$	0	1	$h < 0.318T$
Fox-Goodwin's method	$1/2$	$1/12$	1	$h < 0.389T$
N.A.	$1/2$	$1/8$	1	$h < 0.450T$
Linear acceleration	$1/2$	$1/6$	1	$h < 0.551T$
N.A.	$1/2$	$1/5$	1	$h < 0.712T$
Constant average acceleration	$1/2$	$1/4$	1	Unconditional
Wilson's Method	$1/2$	$1/6$	$\theta > 1.37$	Unconditional

Wilson's method is unconditionally stable for $\theta > 1.37$. For non-linear analysis, the condition would rise to $\theta > 1.5$. However an artificial damping is involved. Therefore Wilson's method should not be used in nonlinear problems.

Unconditionally stable criteria of the Newmark's method is

$$\lambda \geq \frac{1}{2} \quad (8.6.2.19)$$

$$\beta \geq \frac{1}{4}(\lambda + \frac{1}{2})^2 \text{ (8.6.2.19)}$$

Among the unconditionally stable methods, constant average acceleration method has the smallest period error. Newmark's method with $\lambda \neq 1/2$ will give rise to article damping (λ larger than $1/2$ positive artificial damping, smaller than $1/2$ negative). Fox-Goodwin's method is conditionally stable but has the best smallest period error.

8.6.4 Non-linear dynamic analysis procedures

The two step dynamic equilibrium equation can be written as

$$(\mathbf{R}^{\mathbf{I}}_{\mathbf{k+\theta}} - \mathbf{R}^{\mathbf{I}}_{\mathbf{k}}) + (\mathbf{R}^{\mathbf{D}}_{\mathbf{k+\theta}} - \mathbf{R}^{\mathbf{D}}_{\mathbf{k}}) + (\mathbf{R}^{\mathbf{S}}_{\mathbf{k+\theta}} - \mathbf{R}^{\mathbf{S}}_{\mathbf{k}}) = (\mathbf{R}^{\mathbf{E}}_{\mathbf{k+\theta}} - \mathbf{R}^{\mathbf{E}}_{\mathbf{k}}) \text{ (8.6.4.1)}$$

The incremental form will be linearized by the tangential mass, damping, and internal structural stiffness matrix at the start of the increment

$$\mathbf{M_k}\Delta\ddot{\mathbf{r}}_\mathbf{k} + \mathbf{C_k}\Delta\dot{\mathbf{r}}_\mathbf{k} + \mathbf{K_k}\Delta\mathbf{r_k} = \mathbf{R}^{\mathbf{E}}_{\mathbf{k+\theta}} - \mathbf{R}^{\mathbf{E}}_{\mathbf{k}} \text{ (8.6.4.2)}$$

Where

$$\Delta\ddot{\mathbf{r}}_\mathbf{k} = \ddot{\mathbf{r}}_{\mathbf{k+\theta}} - \ddot{\mathbf{r}}_\mathbf{k} \text{ (8.6.4.3)}$$

$$\Delta\dot{\mathbf{r}}_\mathbf{k} = \dot{\mathbf{r}}_{\mathbf{k+\theta}} - \dot{\mathbf{r}}_\mathbf{k} \text{ (8.6.4.4)}$$

$$\Delta\mathbf{r}_\mathbf{k} = \mathbf{r}_{\mathbf{k+\theta}} - \mathbf{r}_\mathbf{k} \text{ (8.6.4.5)}$$

Residual forces at each step is added to balance equation of next step. Then incremental dynamic equilibrium equation is modified as,

$$\mathbf{M_k}\Delta\ddot{\mathbf{r}}_\mathbf{k} + \mathbf{C_k}\Delta\dot{\mathbf{r}}_\mathbf{k} + \mathbf{K_k}\Delta\mathbf{r_k} = (\mathbf{R}^{\mathbf{E}}_{\mathbf{k+\theta}} - \mathbf{R}^{\mathbf{E}}_{\mathbf{k}}) + [\mathbf{R}^{\mathbf{E}}_{\mathbf{k}} - (\mathbf{R}^{\mathbf{I}}_{\mathbf{k}} + \mathbf{R}^{\mathbf{D}}_{\mathbf{k}} + \mathbf{R}^{\mathbf{S}}_{\mathbf{k}})]$$
$$= \mathbf{R}^{\mathbf{E}}_{\mathbf{k+\theta}} - (\mathbf{R}^{\mathbf{I}}_{\mathbf{k}} + \mathbf{R}^{\mathbf{D}}_{\mathbf{k}} + \mathbf{R}^{\mathbf{S}}_{\mathbf{k}}) \text{ (8.6.4.6)}$$

The effective tension is proportional to the geometric stiffness so axial force must be updated each step of the incremental load.

From Newmark β family Method, the general form of the Newmark's method can be written as

$$\dot{\mathrm{r}}_{\mathrm{k+\theta}} = \dot{\mathrm{r}}_\mathrm{k} + (1-\lambda)\tau\ddot{\mathrm{r}}_\mathrm{k} + \lambda\tau\ddot{\mathrm{r}}_{\mathrm{k+\theta}} \text{ (8.6.4.7)}$$

$$\mathrm{r}_{\mathrm{k+\theta}} = \mathrm{r}_\mathrm{k} + \tau\dot{\mathrm{r}}_\mathrm{k} + \left(\frac{1}{2} - \beta\right)\tau^2\ddot{\mathrm{r}}_\mathrm{k} + \beta\tau^2\ddot{\mathrm{r}}_{\mathrm{k+\theta}} \text{ (8.6.4.8)}$$

Incremental values can be derived

$$\Delta\ddot{\mathbf{r}}_{\mathbf{k}} = \ddot{\mathbf{r}}_{\mathbf{k+\theta}} - \ddot{\mathbf{r}}_{\mathbf{k}} = \frac{1}{\beta\tau^2}\Delta\mathbf{r}_{\mathbf{k}} - \frac{1}{\beta\tau}\dot{\mathbf{r}}_{\boldsymbol{k}} - \frac{1}{2\beta}\ddot{\mathbf{r}}_{\mathbf{k}} \quad (8.6.4.9)$$

$$\Delta\dot{\mathbf{r}}_{\mathbf{k}} = \dot{\mathbf{r}}_{\mathbf{k+\theta}} - \dot{\mathbf{r}}_{\mathbf{k}} = \frac{\lambda}{\beta\tau}\Delta\mathbf{r}_{\boldsymbol{k}} - \frac{\lambda}{\beta\tau}\dot{\mathbf{r}}_{\boldsymbol{k}} - (\frac{\lambda}{2\beta} - 1)\tau\ddot{\mathbf{r}}_{\mathbf{k}} \quad (8.6.4.10)$$

Inserted (8.6.4.6) and (8.6.4.7) into (8.6.4.3) incremental form

$$\widehat{\mathbf{K}}_{\mathbf{k}}\Delta\mathbf{r}_{\mathbf{k}} = \Delta\widehat{\mathbf{R}}_{\mathbf{k}} \quad (8.6.4.11)$$

Where

$$\widehat{\mathbf{K}}_{\mathbf{k}} = \frac{1}{\beta\tau^2}\mathbf{M}_{\mathbf{k}} + \frac{\lambda}{\beta\tau}\mathbf{C}_{\mathbf{k}} + \mathbf{K}_{\mathbf{k}} \quad (8.6.4.12)$$

$$\Delta\widehat{\mathbf{R}}_{\mathbf{k}} = \mathbf{R}^{\mathbf{E}}_{\mathbf{k+\theta}} - \left(\mathbf{R}^{\mathbf{I}}_{\mathbf{k}} + \mathbf{R}^{\mathbf{D}}_{\mathbf{k}} + \mathbf{R}^{\mathbf{S}}_{\mathbf{k}}\right) + \left(\frac{1}{\beta\tau}\dot{\mathbf{r}}_{\boldsymbol{k}} + \frac{1}{2\beta}\ddot{\mathbf{r}}_{\mathbf{k}}\right)\mathbf{M}_{\mathbf{k}} + \left[\frac{\lambda}{\beta\tau}\dot{\mathbf{r}}_{\boldsymbol{k}} - \left(\frac{\lambda}{2\beta} - 1\right)\tau\ddot{\mathbf{r}}_{\mathbf{k}}\right] + \mathbf{C}_{\mathbf{k}} \quad (8.6.4.13)$$

After$\Delta\mathbf{r}_{\mathbf{k}}$ is solved from above, $\Delta\ddot{\mathbf{r}}_{\mathbf{k}}$ and $\Delta\dot{\mathbf{r}}_{\mathbf{k}}$ can be derived from (8.6.4.9) and (8.6.4.10) . Then $\mathbf{r}_{\mathbf{k+\theta}}$, $\dot{\mathbf{r}}_{\mathbf{k+\theta}}$, and $\ddot{\mathbf{r}}_{\mathbf{k+\theta}}$ can be achieved by equations (8.6.4.3)~(8.6.4.5).

$\mathbf{R}^{\mathbf{S}}_{\mathbf{k+\theta}}$, $\mathbf{R}^{\mathbf{D}}_{\mathbf{k+\theta}}$ and $\mathbf{R}^{\mathbf{I}}_{\mathbf{k+\theta}}$ can be solved, then tangential value $\mathbf{C}_{\mathbf{k+\theta}}$, $\mathbf{K}_{\mathbf{k+\theta}}$, and $\mathbf{M}_{\mathbf{k+\theta}}$ can be achieved.

Then equilibrium is obtained by iteration at each end of the time step in the similar way as static analysis. The right hand side of the incremental equation is replaced by the residual force.

$$^{\boldsymbol{i-1}}\mathbf{M}_{\mathbf{k+\theta}}\,{}^{i}\ddot{\Delta}_r + {}^{\boldsymbol{i-1}}\mathbf{C}_{\mathbf{k+\theta}}\,{}^{i}\dot{\Delta}_r + {}^{\boldsymbol{i-1}}\mathbf{K}_{\mathbf{k+\theta}}\,{}^{i}\Delta_r = \mathbf{R}^{\mathbf{E}}_{\mathbf{k+\theta}} - ({}^{\boldsymbol{i-1}}\mathbf{R}^{\mathbf{I}}_{\mathbf{k+\theta}} + {}^{\boldsymbol{i-1}}\mathbf{R}^{\mathbf{D}}_{\mathbf{k+\theta}} + {}^{\boldsymbol{i-1}}\mathbf{R}^{\mathbf{S}}_{\mathbf{k+\theta}}) \quad (8.6.4.14)$$

$${}^{i}\Delta\mathbf{r}_{\mathbf{k+\theta}} = {}^{i-1}\Delta\mathbf{r}_{\mathbf{k+\theta}} + {}^{i}\Delta_r \quad (8.6.4.15)$$

$${}^{i}\ddot{\Delta}_r = \frac{1}{\beta\tau^2}\,{}^{i}\Delta_r \quad (8.6.4.16)$$

$${}^{i}\dot{\Delta}_r = \frac{\lambda}{\beta\tau}\,{}^{i}\Delta_r \quad (8.6.4.17)$$

Then the iteration will be

$$\left(\frac{1}{\beta\tau^2}\,{}^{\mathbf{i-1}}\mathbf{M_{k+\theta}} + \frac{\lambda}{\beta\tau}\,{}^{\mathbf{i-1}}\mathbf{C_{k+\theta}} + {}^{\mathbf{i-1}}\mathbf{K_{k+\theta}}\right){}^{\mathrm{i}}\Delta_{\mathrm{r}} = \mathbf{R^{E}_{k+\theta}} - ({}^{\mathbf{i-1}}\mathbf{R^{I}_{k+\theta}} + {}^{\mathbf{i-1}}\mathbf{R^{D}_{k+\theta}} + {}^{\mathbf{i-1}}\mathbf{R^{S}_{k+\theta}}) \quad (8.6.4.18)$$

$\mathbf{C_{k+\theta}}$ and $\mathbf{K_{k+\theta}}$ are assumed to be updated each iteration, which is called Newton-Raphson iteration procedure. If they are kept constant instead, it would be called modified Newton-Raphson iteration.

From equation (8.6.4.9) and (8.6.4.16),

$${}^{\mathrm{i-1}}\Delta\ddot{\mathbf{r}}_{\mathbf{k}} = {}^{\mathrm{i-2}}\Delta\ddot{\mathbf{r}}_{\mathbf{k}} + {}^{\mathrm{i-1}}\ddot{\Delta}_{\mathrm{r}} = {}^{\mathbf{i-1}}\ddot{\mathbf{r}}_{\mathbf{k+\theta}} - \ddot{\mathbf{r}}_{\mathbf{k}} = \frac{1}{\beta\tau^2}\left({}^{\mathrm{i-2}}\Delta\mathbf{r_k} + {}^{\mathrm{i-1}}\Delta_{\mathrm{r}}\right) - \frac{1}{\beta\tau}\dot{\mathbf{r}}_{\mathbf{k}} - \frac{1}{2\beta}\ddot{\mathbf{r}}_{\mathbf{k}} \quad (8.6.4.19) \rightarrow$$

$${}^{\mathbf{i-1}}\ddot{\mathbf{r}}_{\mathbf{k+\theta}} = \frac{1}{\beta\tau^2}\left({}^{\mathrm{i-2}}\Delta\mathbf{r_k} + {}^{\mathrm{i-1}}\Delta_{\mathrm{r}}\right) - \frac{1}{\beta\tau}\dot{\mathbf{r}}_{\mathbf{k}} + \left(1 - \frac{1}{2\beta}\right)\ddot{\mathbf{r}}_{\mathbf{k}} \quad (8.6.4.20)$$

Similarly

$${}^{\mathrm{i-1}}\Delta\dot{\mathbf{r}}_{\mathbf{k}} = {}^{\mathrm{i-2}}\Delta\dot{\mathbf{r}}_{\mathbf{k}} + {}^{\mathrm{i-1}}\dot{\Delta}_{\mathrm{r}} = {}^{\mathbf{i-1}}\dot{\mathbf{r}}_{\mathbf{k+\theta}} - \dot{\mathbf{r}}_{\mathbf{k}} = \frac{\lambda}{\beta\tau^2}\left({}^{\mathrm{i-2}}\Delta\mathbf{r_k} + {}^{\mathrm{i-1}}\Delta_{\mathrm{r}}\right) - \frac{\lambda}{\beta\tau}\dot{\mathbf{r}}_{\mathbf{k}} - \left(\frac{\lambda}{2\beta} - 1\right)\tau\ddot{\mathbf{r}}_{\mathbf{k}} \quad (8.6.4.21) \rightarrow$$

$${}^{\mathbf{i-1}}\dot{\mathbf{r}}_{\mathbf{k+\theta}} = \frac{\lambda}{\beta\tau^2}\left({}^{\mathrm{i-2}}\Delta\mathbf{r_k} + {}^{\mathrm{i-1}}\ddot{\Delta}_{\mathrm{r}}\right) + \left(1 - \frac{\lambda}{\beta\tau}\right)\dot{\mathbf{r}}_{\mathbf{k}} - \left(\frac{\lambda}{2\beta} - 1\right)\tau\ddot{\mathbf{r}}_{\mathbf{k}} \quad (8.6.4.22)$$

The ${}^{\mathbf{i-1}}\mathbf{R^{S}_{k+\theta}}$ will updated by inserting ${}^{\mathrm{i-1}}\Delta\mathbf{r_k}$, the ${}^{\mathbf{i-1}}\mathbf{R^{I}_{k+\theta}}$ and ${}^{\mathbf{i-1}}\mathbf{R^{D}_{k+\theta}}$ will be updated based on ${}^{\mathbf{i-1}}\ddot{\mathbf{r}}_{\mathbf{k+\theta}}$ and ${}^{\mathbf{i-1}}\dot{\mathbf{r}}_{\mathbf{k+\theta}}$.

$${}^{\mathbf{i-1}}\mathbf{R^{I}_{k+\theta}} = \mathbf{M_{k+\theta}}\,{}^{\mathbf{i-1}}\ddot{\mathbf{r}}_{\mathbf{k+\theta}} \quad (8.6.4.23)$$

$${}^{\mathbf{i-1}}\mathbf{R^{D}_{k+\theta}} = \mathbf{C_{k+\theta}}\,{}^{\mathbf{i-1}}\dot{\mathbf{r}}_{\mathbf{k+\theta}} \quad (8.6.4.24)$$

The criterion to stop the analysis is also a modified Euclidian norm which is similar to the one used in static analysis.

8.6.5 Dynamic analysis guidelines

Constant average acceleration is recommended for the nonlinear analysis. Furthermore, the true Newton-Raphson iteration is suggested.

Constant Rayleigh damping formulation can lead to more well behaved system and thus should be used.

The time step which is strongly system and excitation dependent and thus should be small enough to represent the external loads and the discretized eigenpeirods.

For moderate nonlinearity, 70-200 time steps per load period should suffice. More steps are for more nonlinearities.

9. Analysis modelling

9.1 General properties

Acceleration of gravity: 9.80665 $\mathrm{m/s^2}$
Water density: 1025 $\mathrm{kg/m^3}$
Air density: 1.25 $\mathrm{kg/m^3}$
Mud density: 1600 $\mathrm{kg/m^3}$
Steel density: 7850 $\mathrm{kg/m^3}$
Buoyancy syntactic foam density: 680 $\mathrm{kg/m^3}$
Water kinematic viscosity: 1.1880×10^{-6} $\mathrm{kg/(m \cdot s)}$
Air kinematic viscosity: 1.8240×10^{-5} $\mathrm{kg/(m \cdot s)}$

9.2 Floater modelling

The MODU model is provided with the help of the Senior Research Scientist Knut Mo of MARINTEK. The name, dimensions and operational data are not achievable. The parameters needed for hydrodynamic calculation are valid but should not be disclosed. The valid data are summarized on the Figure 37. It can been seen that first order and second order effects are all considered which is sufficient for a drift off modelling.

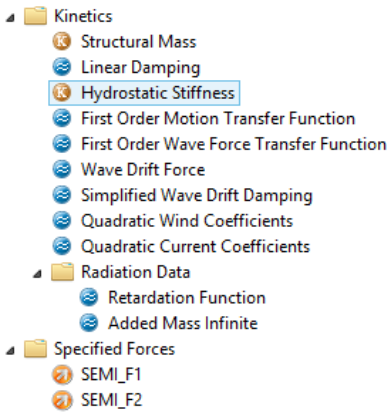

Figure 37 MODU parameters

9.3 Riser modelling

9.3.1 Riser components

The model data provided by Konsberg have contradictory statements. The buoyance provided by dimensions of the annular beam elements is not compatible with the values calculated by the prescribed dry weight of steel and submerged weight of steel. Thus an alternative simplified modelling is proposed. However, the components description can still be informative.

Name	Description
Diverter	Fixed to the vessel at a distance below drill floor.
Upper Flex Joint	The upper flex joint is used at the top of the riser and is designed to allow for the motion of the rig. This allows angular misalignment between the riser and the rig, thereby reducing the bending moment on the riser and rig equipment.
Spacer Joint	The riser spacer joint bridges the distance between the telescopic joint and the upper flex joint diverter adapter spool. This ensures proper access to the riser telescopic joint in its mid-stroke position during installation. This joint is only used for risers with DAT system.
Telescopic Joint	The telescopic joint expands and contracts adjusting the riser length and orientation to compensate for vertical displacement of the drilling unit.
Pup Joint	Pup joints are shorter versions of the regular riser joints. They are added to the riser make-up to achieve a suitable riser length.
Riser Joint w/buoyancy	Regular riser joint with additional buoyancy elements.
Riser Joint	Regular riser joint.
Lower Flex Joint	The lower flex joint is used to allow angular misalignment between the riser and the BOP stack, thereby reducing the bending moment on the riser.

9.3.2 Cross-sectional properties

The beam element inputs into Riflex for the riser steel piping part are as,

Mass/length: 242.25 $\mathrm{kg/m}$
External cross-sectional area: 0.2235 $\mathrm{m^2}$
Internal cross-sectional area: 0.1926 $\mathrm{m^2}$
Gyration radius: 0.182 m
No thermal/pressure expansion

Constant axial stiffness: 6.4807×10^9 N
Constant bending stiffness: 2.1457×10^8 $\mathrm{N \cdot m^2}$
Constant torsion stiffness: 4.905×10^8 $\mathrm{(N \cdot m^2)/rad}$

The inputs into Riflex for the riser syntactic buoyance foam part are as,

Mass/length: 242.25 $\mathrm{kg/m}$
Buoyancy volume/length: 0.3779 $\mathrm{m^2}$
Gyration radius: 0.2562 m
Covered fraction: 1.0

9.3.3 Global configuration

Global dimension distribution proportion for $300\ \mathrm{m}$, $1000\ \mathrm{m}$, $3000\ \mathrm{m}$ water depth are almost same, which are illustrated in the figure below. The top tension for three configurations are tuned that the bottom tension is $400\ \mathrm{KN}$.

For $1000\ \mathrm{m}$ water depth configuration (Figure 38), by equation $(4.5.2.1)$ and $(4.5.2.3)$,

$$\begin{aligned} T_{t\,1000} = T_{e\,1000} + 400 = w_a \delta s + 400 = w_{a1} * 10 + w_{a2} * 250 + w_{a3} * 750 + 400 \\ = 5.3977 * 10 + 3.1515 * 250 + 1.8731 * 750 + 400 \\ = 2646.677\ \mathrm{KN} \end{aligned}$$

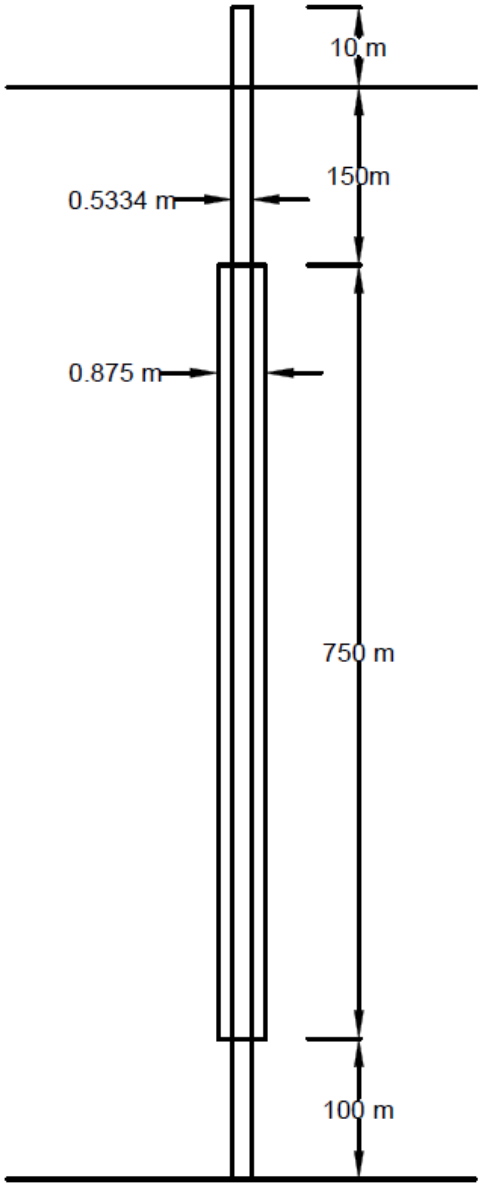

Figure 38 1000 m water depth configuration

For $300\ \mathrm{m}$ water depth configuration (Figure 39), similarly.

$$T_{t\,300} = T_{e\,300} + 400 = w_a \delta s = w_{a1} * 10 + w_{a2} * 75 + w_{a3} * 225 + 400$$
$$= 5.3977 * 10 + 3.1515 * 75 + 1.8731 * 225 + 400$$
$$= 1111.787\ \mathrm{KN}$$

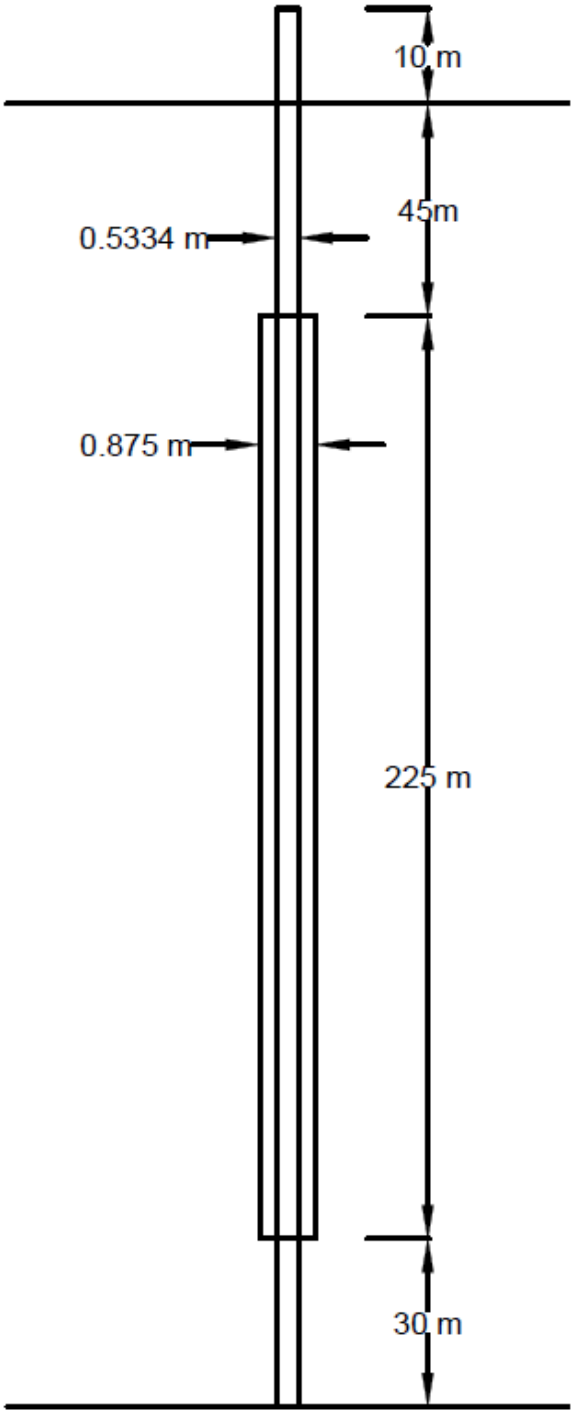

Figure 39 300 m water depth configuration

For $3000\ \mathrm{m}$ water depth configuration (Figure 39), similarly.

$$T_{t\,3000} = T_{e\,3000} + 400 = w_a \delta s = w_{a1} * 10 + w_{a2} * 750 + w_{a3} * 2250 + 400$$
$$= 5.3977 * 10 + 3.1515 * 750 + 1.8731 * 2250 + 400$$
$$= 7032.077\ \mathrm{KN}$$

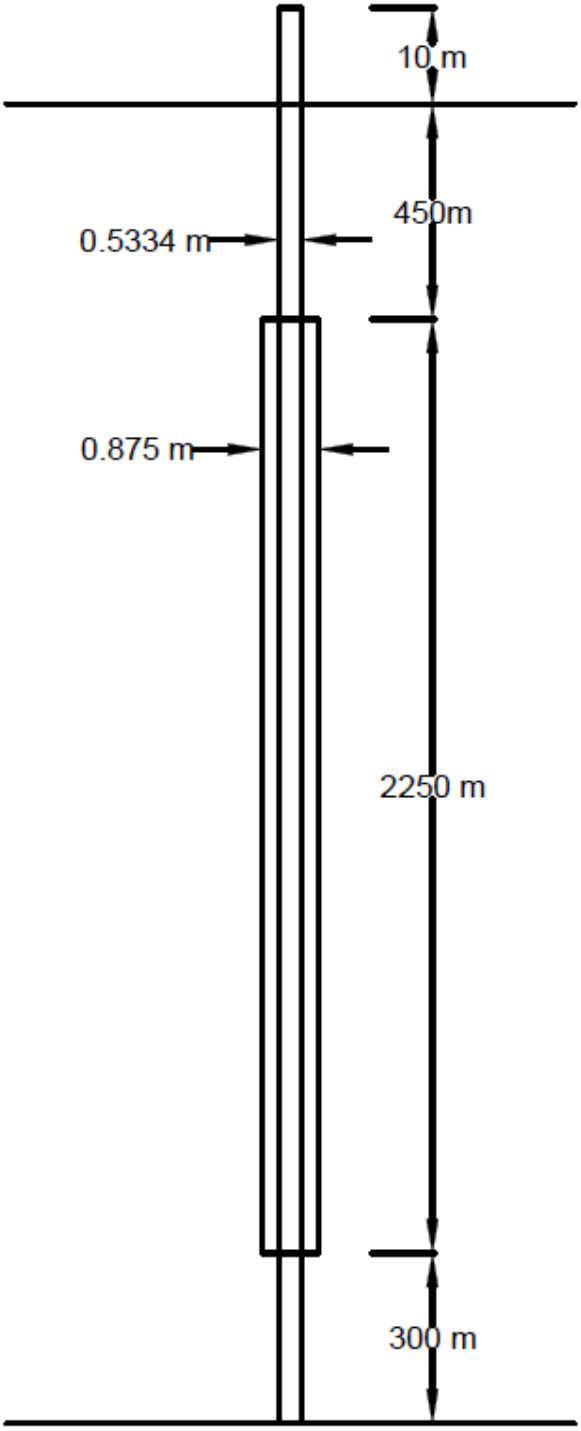

Figure 40 3000 m water depth configuration

9.4 Current and wind data

According to Ormberg and Larsen (1997), current have minimal influence on the tension but great influence on the riser curve. The top end angle will be greatly influenced and hence the horizontal component of the top tension which have a noticeable effect on the MODU motions will be highly dependent on the current profile. Therefore two profiles are proposed for each water depth which are illustrated in the figures below.

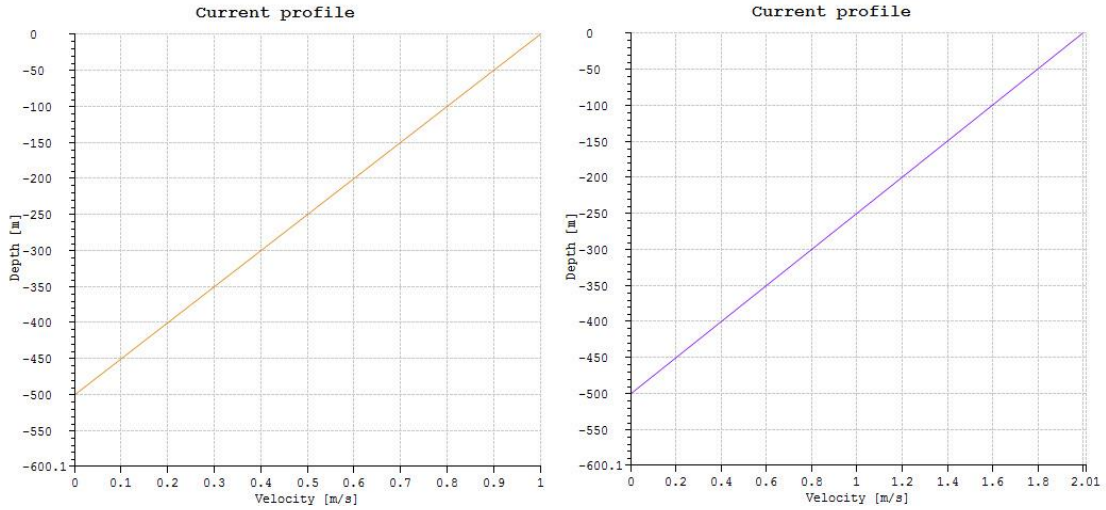

Figure 41 Current profiles for 1000 m water depth

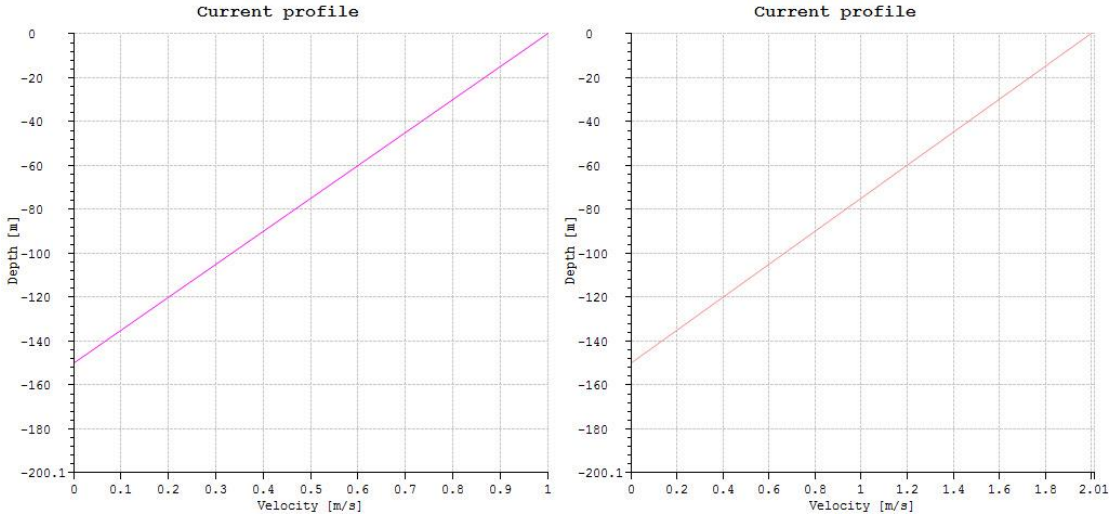

Figure 42 Current profiles for 300 m water depth

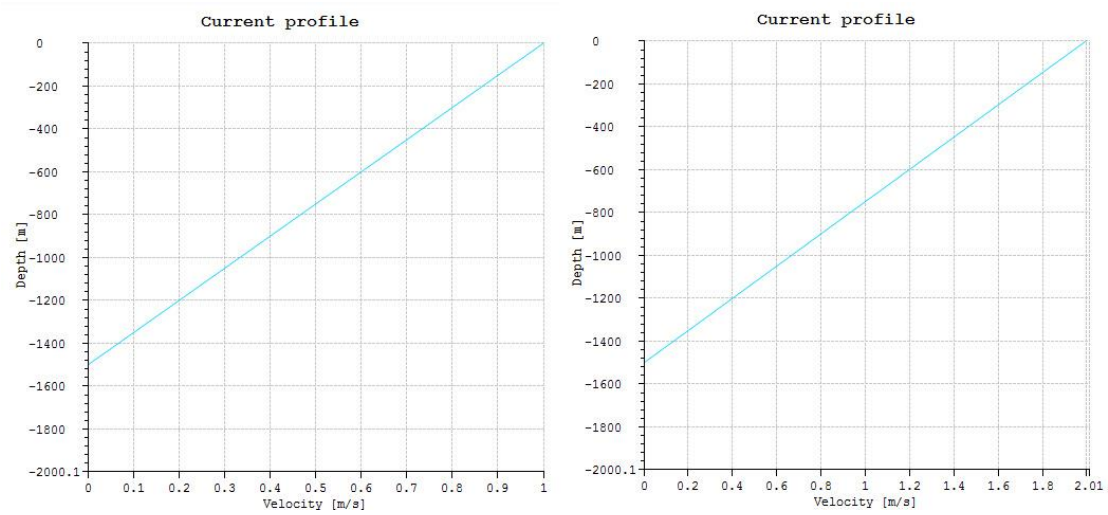

Figure 43 Current profiles for3000 m water depth

Wind parameters are described in the figure 44 below.

Direction: 0.0

Wind velocity:

Longitudinal Velocity	Lateral Velocity	Vertical Velocity
10.0	0.0	0.0

Shear profile levels:

Vertical Coordinate	Longitudinal Velocity Factor	Lateral Velocity Factor	Vertical Velocity Factor
0.0	0.5	0.0	0.0
20.0	1.0	0.0	0.0

Domain properties:

Lower Edge Z	Num Grid Points	Domain Resolution
0.0	20	0.1

Figure 44 Wind parameters

9.5 Calculation parameters

For static analysis,

According to chapter 6.7, Skyline configuration is adopted for matrix storage instead of sparse configuration to achieve a smaller storage data space.

According to chapter 6.6.2.5, consistent load and mass formulation is adopted to achieve a more accurate frequency response.

According to chapter 6.6.2.5, consistent load and mass formulation is adopted to achieve a more accurate frequency response.

According to chapter 7.2, consistent load and mass formulation is adopted to achieve a more accurate frequency response. Load sequence and steps also need some consideration (Figure 44). To avoid buckling problem, load number 1,2,3 are loaded simultaneously. To avoid snap-through issue, load number 2,4 are loaded simultaneously. Geometric stiffness is very sensitive to load number 2 and 4, thus load steps are relatively more.

No	Load Type	Run With Previous	N Step	Max Iterations	Accuracy
1	Volume Forces	☐	5	15	1.0e-06
2	Specified Displacements	☑	50	15	1.0e-06
3	Specified Forces	☑	20	15	1.0e-06
4	Current Forces	☑	10	15	1.0e-06

Figure 45 Load sequences, steps, and accuracy criteria

Nonlinear analysis is performed considering the many nonlinearities involved. Accordingly, constant Newmark's method whose parameters can be seen in table 3 is adopted for stability insurance, thus no artificial damping is involed. According to chapter 8.6.5, global Rayleigh damping (both coefficient equal to 0.01) is adopted for better behaved system. in figure 45.

9.6 Wave data

The Torsethaugen model is used for the current thesis analysis. Significant wave height $h_s = 5\ \mathrm{m}$ is proposed. According to equation (8.3.3.2),

$$t_{pb} = 6.6{h_s}^{0.333} = 6.6 * 5^{0.333} = 11.28\ \mathrm{s}$$

Then it is proposed

For wind wave, $t_{pw} = 7\ \mathrm{s}$; For Swell wave $t_{ps} = 15\ \mathrm{s}$.

Taking the peak period and significant wave height as a reference, by equation (8.4.1),

$$KC = \frac{U_M T}{D} = \frac{\frac{h_s}{2}\frac{2\pi}{t_{ps}}t_{ps}}{D} = \frac{5 * 3.14}{0.5334} = 29.43$$

$$U_M = \frac{h_s}{2}\frac{2\pi}{t_{ps}} = \frac{5}{2}\frac{2 * 3.14}{11.28} = 1.38\ \mathrm{m/s}$$

By equation (8.4.2),

$$\text{Relative current number} = \frac{U_c}{U_M} = \frac{1}{1.38} = 0.72, \text{for } U_c = 1 \text{ at the surface}$$

$$\text{Relative current number} = \frac{U_c}{U_M} = \frac{2}{1.38} = 1.45, \text{for } U_c = 2 \text{ at the surface}$$

$$\text{For } U_c = 1 \text{ at the surface}, C_D = 0.85 \text{ taken as the suggested value}$$

$$\text{For } U_c = 2 \text{ at the surface}, C_D \approx C_{D|KC=\infty}(1 + 0.58e^{-0.064KC})^2$$
$$= 1 * (1 + 0.58 * e^{-0.064*29.43}) = 1.18$$

Where U_c is taken as the surface value as drag force is concentrated on the surface.

9.7 Calculation operation procedure

For separate analysis, floater will drift off by wave, wind, and current forces which analyzed by program Simo. The position of floater center of gravity (COG) is recorded. Then the COG motion is input into the program Riflex to calculate the riser responses. Then the relative distance between the upper end vertical position of the riser and the floater COG vertical is calculated. Then Matlab is used to find the time moment that the relative distance reaches 5 m. The Riflex analysis is run-through again with the condition that by the time moment found in Matlab the boundary condition of the riser is changed that the upper end of the riser is changed from free to fixed to the floater.

For coupled analysis, the riser upper end and the floater will be linked together from the beginning of the time in the Simo-Riflex coupled analysis due to the limitation of the program scope. The interaction between the riser and floater will be accounted for during the analysis.

9.8 Load cases

For the situation of drilling floater losing power, normally the floater will drift away under the influence of current, wind and wave. The drilling riser will drift along with the platform tensioned by the tensioning system on the upper end.

With floater drifting along, the stroke of the tensioner would decrease until a certain moment that piston reach the cylinder bottom mainly because of offset. No more stroke available will not keep the tension relatively constant and thus the tension in

the riser will increase dramatically. To avoid the dramatic upsurge, more pressure might be applied to the cylinder to sustain a higher relatively constant tension.

As the floater drift by, the angle of the upper and bottom angle will increase, in the meantime the drilling strings within the riser will collide with the riser inner layer. If the angle exceed certain limit, the riser piping would be damaged and leakage may occur. A higher tension then may be applied to straighten the riser to reduce the angle.

On the other hand, the larger angle and tension, the larger the moment generated on the BOP which may damage the BOP leading to leakage. Therefore the applied tension need to be adjusted to reach a proper balance between the not-damaging riser inner layer angle and not-damaging BOP moment.

In the following load cases, all environmental forces are applied in the same direction. Angles, tensions, and BOP bending moment are recorded.

Load case number	1.1	1.2	2.1	2.2	3.1	3.2	4.1	4.2	5.1	5.2	6.1	6.2
Current speed at surface (M/S)	1	1	2	2	1	1	2	2	1	1	2	2
Coupling	No	Yes	No	Yes	No	Yes	No	Yes	No	Yes	No	Yes
Water depth (KM)	1	1	1	1	0.3	0.3	0.3	0.3	3	3	3	3
Drag coefficient	0.85	0.85	1.18	1.18	0.85	0.85	1.18	1.18	0.85	0.85	1.18	1.18

10. Analytical analysis

Sparks (2011) derived analytical solutions to near-vertical riser from cables. Curvature, displacement, end angles,, top-end set-down and the horizontal end reactions can be derived consequently.

Riser curvature can be approximated from cable results which is f_x/T_e.

He demonstrated that other than zones close to support, curvatures of beams and cables are almost equivalent. kL is called flexibility factor which indicates that higher the factor the less length the support will influence the curvature.

In which

$$k = \sqrt{\frac{T_e}{EI}} \quad (10.1)$$

The equivalence implies that the change of bending stiffness in areas far from supports will results in moment change and the corresponding stresses.

10.1 End rotation stiffness of constant tension beam

Governing equation for a constant tension beam is

$$EI\frac{\partial^4 w}{\partial x^4} - T_e\frac{\partial^2 w}{\partial x^2} - q = 0 \quad (10.1.1)$$

When only an end moment M_0 is applied,

$$-\frac{\partial^2 w}{\partial x^2} = \frac{M_0}{EI}\frac{\sinh k(L-x)}{\sinh kL} \quad (10.1.2)$$

$$\frac{\partial w}{\partial x} = \frac{kM_0}{T_e}\left[\frac{\cosh k(L-x)}{\sinh kL} - \frac{1}{kL}\right] \quad (10.1.3)$$

Then end bending stiffness is

$$M_0 \Big/ \left(\frac{\partial w}{\partial x}\right)_0 = \sqrt{T_e EI}\left(\frac{1}{\tanh kL} - \frac{1}{kL}\right)^{-1} \quad (10.1.4)$$

For kL much larger than 3,

$$M_0 \Big/ \left(\frac{\partial w}{\partial x}\right)_0 \approx \sqrt{T_e EI} \quad (10.1.5)$$

10.2 Riser angles derived from cable angles

Accounting for weight induced curvature at both top and bottom ends, cable curvature are as follows (can be derived from equation 10.3.1)

$$\left(\frac{\partial^2 w}{\partial x^2}\right)_t = \left(\frac{-q - w_a \frac{\partial w}{\partial x}}{T_e}\right)_t \quad (10.2.1)$$

$$\left(\frac{\partial^2 w}{\partial x^2}\right)_b = \left(\frac{-q - w_a \frac{\partial w}{\partial x}}{T_e}\right)_b \quad (10.2.2)$$

To obtain the same curvature, riser ends bending moment are applied as

$$M_t = EI_t \left(\frac{\partial^2 w}{\partial x^2}\right)_t \quad (10.2.3)$$

$$M_b = EI_b \left(\frac{\partial^2 w}{\partial x^2}\right)_b \quad (10.2.4)$$

Sparks (2011) proposed a semi-empirical equation based on equation $(10.1.5)$

$$\sqrt{(1 + 2q)^2 T_e EI} \quad (10.2.5)$$

Where

$$q = \frac{w_a}{kT_e} \quad (10.2.7)$$

For top-end,

$$q_t = -\frac{w_a}{k_t T_{te}}, k_t = \sqrt{\frac{T_{te}}{EI_t}}$$

For bottom-end,

$$q_b = \frac{w_a}{k_b T_{be}}, k_b = \sqrt{\frac{T_{be}}{EI_b}}$$

The angle correction after moment release

$$\delta\theta_t = \frac{M_t}{\sqrt{(1+2q_t)^2 T_{te} EI_b}} = \left[\frac{\left(-q - w_a \frac{\partial w}{\partial x}\right) EI}{T_e(1+2q)\sqrt{T_e EI}}\right]_t = \left[\frac{\left(-q - w_a \frac{\partial w}{\partial x}\right)}{kT_e(1+2q)}\right]_t \quad (10.2.8)$$

$$\delta\theta_b = \frac{-M_b}{\sqrt{(1+2q_b)^2 T_{be} EI_b}} = -\left[\frac{\left(-q - w_a \frac{\partial w}{\partial x}\right) EI}{T_e(1+2q)\sqrt{T_e EI}}\right]_b$$

$$= -\left[\frac{\left(-q - w_a \frac{\partial w}{\partial x}\right)}{kT_e(1+2q)}\right]_b \quad (10.2.9)$$

Then

$$\theta_{t\,riser} = \left(\frac{\partial w}{\partial x}\right)_t + \left[\frac{\left(-q - w_a \frac{\partial w}{\partial x}\right)}{kT_e(1+2q)}\right]_t \quad (10.2.10)$$

$$\theta_{t\,riser} = \left(\frac{\partial w}{\partial x}\right)_b - \left[\frac{\left(-q - w_a \frac{\partial w}{\partial x}\right)}{kT_e(1+2q)}\right]_b \quad (10.2.11)$$

10.3 Riser setdown

The governing differential equation of a tensioned beam with constant bending stiffness is

$$EI\frac{\partial^4 w}{\partial x^4} - \frac{\partial}{\partial x}(T_e\frac{\partial w}{\partial x}) - q = 0 \ (10.3.1)$$

The governing differential equation of static near-vertical cable (bending stiffness neglected) is

$$\frac{\partial}{\partial x}(T_e\frac{\partial w}{\partial x}) + q = 0 \ (10.3.2)$$

After integration

$$\frac{\partial w}{\partial x} = \frac{H_b - \int_0^x q dx}{T_e} \ (10.3.3)$$

H_b: horizontal component of the effective tension at the bottom end

Integrated again

$$w = \frac{H_b}{w_a}\ln\left(\frac{T_e}{T_{be}}\right) - \int_0^x \frac{\int_0^x q dx}{T_e} dx \ (10.3.4)$$

T_{be}: effective tension at the bottom end
$T_e = xw_a + T_{be}$
w_a: apparent weight per meter

When top-end offset w_t is known,

$$H_b = \frac{w_t + \int_0^L \frac{\int_0^x q dx}{T_e} dx}{\frac{1}{w_a}\ln\left(\frac{T_t}{T_{be}}\right)} \ (10.3.5)$$

Setdown is as follows

$$\text{setdown} = \frac{1}{2}\int_0^L \left(\frac{\partial w}{\partial x}\right)^2 dx = \frac{1}{2}\int_0^L \left(\frac{H_b - \int_0^x q dx}{T_e}\right)^2 dx \ (10.3.6)$$

10.4 Riser tension due to offset

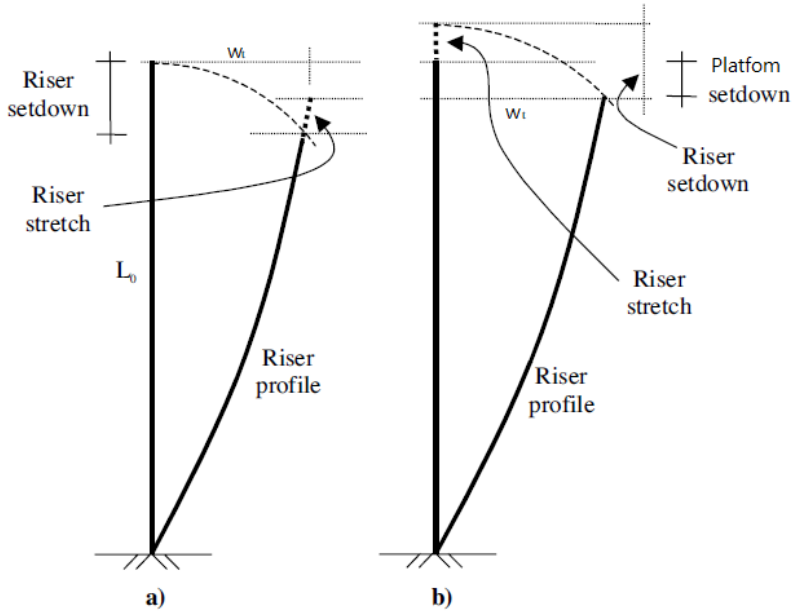

Figure 46 Top-end offset influence on profile

The effect of platform offset and set-down on the riser can be explained in two ways. Firstly from figure 47 a) under the constant initial top-tension $T_{t\ initial}$, the riser swing sideway w_t like a pendulum, then because riser set-down and platform set-down is different resulting from riser sag, the riser is stretched(or compressed). The final tension $T_{t\ final}$ is found by iteration. Secondly from figure 47 b), tension is increased to the final value $T_{t\ final}$, then move laterally w_t. The riser will set down to the exact platform level. $T_{t\ final}$ has to be found by iteration either but the two ways explained above give an clear relationship.

$$\text{riser setdown} - \text{riser strech} = \text{platform setdown} \quad (10.4.1)$$

$$\text{riser strech} = \frac{T_t - T_{t\ \text{inital}}}{k_{r+t}} \quad (10.4.2)$$

Where $k_{r+t} = \left(\frac{1}{k_{riser}} + \frac{1}{k_{tens}}\right)^{-1} = \frac{k_{riser} k_{tens}}{k_{riser} + k_{tens}}$

11. Results analysis

11.1.1 Comparison sequence and responses of interest

The comparisons in table 4 are performed in a sequence that first in row and in column, which means 1.1 and 1.2, 1.1 and 2.1, 1.1 and 3.1, 1.1 and 5.1, and so on.

The green grids in the table 4 are used for exclude the repeated comparisons. Load cases that are paired to be compared are colored in the orange and yellow in table 4. The orange ones are key results and the yellow ones are for verification and reference.

Comparison between 1.1 and 1.2 are used to see the coupling influence.
Comparison between 1.1 and 2.1 are used to see the current influence under uncoupled circumstance.
Comparison between 1.1 and 3.1 are used to see the water depth influence under uncoupled circumstance.
Comparison between 1.2 and 2.2 are used to see the current influence under coupled circumstance.
Comparison between 1.2 and 3.2 are used to see the water depth influence under coupled circumstance.

Table 4 Load cases comparison sequence

	1.1	1.2	2.1	2.2	3.1	3.2	4.1	4.2	5.1	5.2	6.1	6.2
1.1												
1.2												
2.1												
2.2												
3.1												
3.2												
4.1												
4.2												
5.1												
5.2												
6.1												
6.2												

The tension in the riser is of mainly concern because it is highly connected with coupling effects, end angles, and so on. The heave motion of the riser upper end is an indicator of the sudden tension increase so it is included when comparing the tensions.

To see the coupling effects on the floater, the floater translational displacement, velocity, and vertical displacement are shown.

Upper flex joint angle is the angle of the flex joint component located between the diverter and the telescopic joint as part of the top assembly. Lower flex joint angle is the angle of the flex joint component located between the LMRP and the riser as part of the bottom assembly. Both angles are noteworthy because they are usually used as the design criteria indicator. No specified flex joint modelling is performed so that the angles are calculated by nodal displacements of 5 M long beam elements at upper and lower ends.

Lower end moments are of interest because it may damage the BOP.

Therefore in each case-to-case comparison, the parameters are compared in the following sequence. Only results of interest from the orange key grids are commented and the rest are in appendix (uploaded in DAIM zip file).

1. upper end tension and vertical displacement time series
2. upper end tension and vertical displacement with translational displacement as x-axis
3. floater translational displacement
4. floater translational velocity
5. floater vertical displacement
6. upper and lower angles time series
7. upper and lower angles with translational displacement as x-axis
8. lower end bending moment time series
9. lower end bending moment with translational displacement as x-axis

11.1.2 Load case 1.1

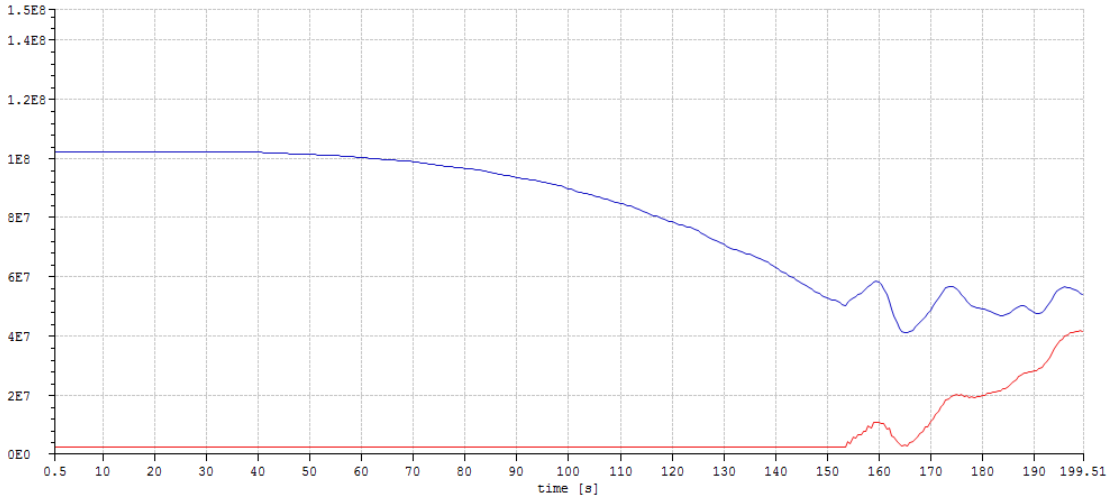

Figure 47 Riser upper end tension (N) (red) and vertical displacement (M) (scaled by 10^7 blue) time series for case 1.1

From figure 47, the tension before the locking moment varies within 10 KN and thus variation is almost indistinguishable. Therefore the waves, current and wind have effects on the riser have very limited influence on the tension.

From figure 47, stroke locking have a great influence on the riser tension. 6.5 S after the locking at 160 s, the tension increase from 2600 KN to 10900 KN.

From figure 47, the locking and riser tension increase happens exactly the same time. The tension fluctuate with the vertical displacement at the same trend after the locking. It can be seen that vertical displacement have a great influence on the tension fluctuation.

From figure 47 as floater drifts off, the riser goes from slack to stiff and the tension level increases because of the offset.

From figure 47 after locking, the floater moves upward and tension increases. Then the floater moves downwards and tension decreases but no noticeable lower than the tension level before locking.

11.1.3 Load case 1.2

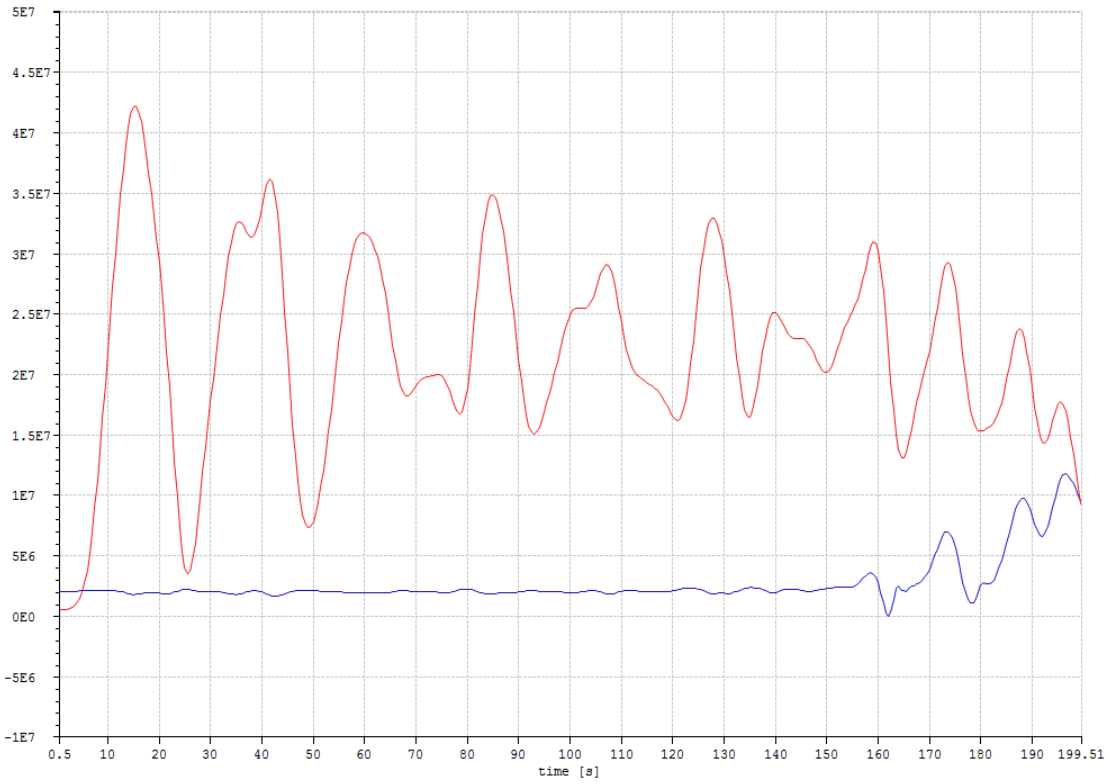

Figure 48 Riser upper end tension (N) (blue) and vertical displacement (M) (scaled by 10^7 red) time series for case 1.2

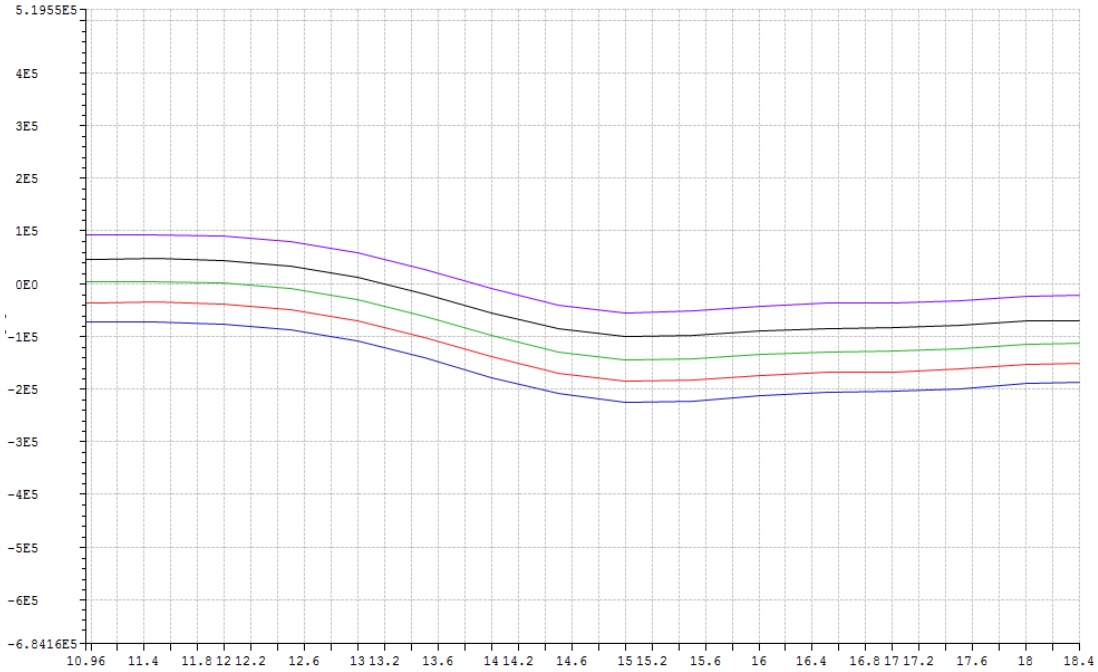

Figure 49 Riser axial force (N) at the lower parts of the riser time series case 1.2 from around 10 s to 18 s

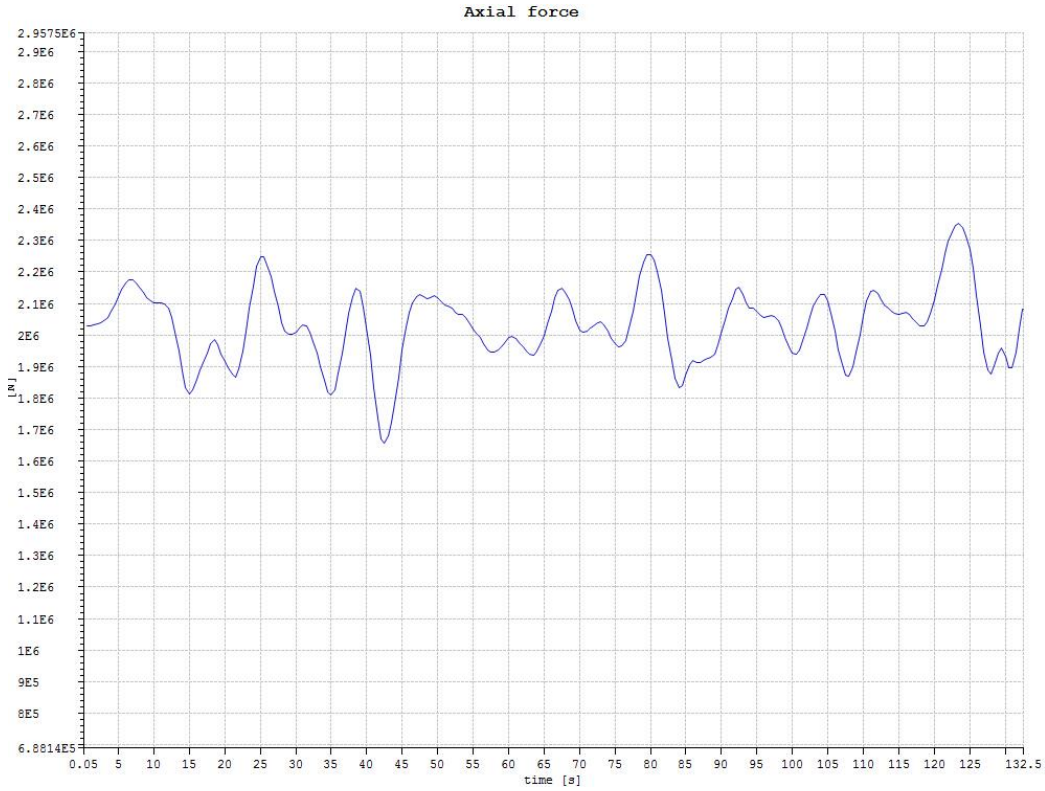

Figure 50 Riser upper end tension (N) time series for case 1.2 from around 0 s to 132 s

From figure 48 it can be seen that even the coupling effects are considered, the environmental loads effects on the tension are very limited.

From figure 48 because of the limitation of the program, the coupling condition is included at the beginning of the time cannot be changed in the middle. Therefore the top tension will decrease from two aspects. On one hand, top tension only support the apparent weight and no tension is left between the BOP and riser lower part. On the other hand, the lower part compression because of the own weight would reduce the top tension more. Hence it is deduced that the top tension would lower than $\mathrm{T_{e\,1000}} = 2247\ \mathrm{KN}$. This can be verified from figure 49 that lower part axial force (element number 1,4,7,10,13 from the sea bottom, each element 5 m long) experiences compression at an early time clip. This can also be confirmed from figure 50 that top tension varies from around 1650 KN to 2250 KN before around 120 S.

From figure 48 after 155 s, the top tension breaches $\mathrm{T_{t\,1000}} = 2647\ \mathrm{KN}$, and average top tension would increase because of the offset.

From figure 48, the insufficient effective tension can cause even negative force at the lower ends after the locking (around 162 s).

In principle this low top tension is not correct. On one hand it may cause numerical instability because of buckling of the riser lower part. On the other hand, the coupling effects is weakened and the results would be conservative for the locking time.

From figure 48 after locking, the amplitude fluctuation of the vertical displacement and top tension increase to a peak at around 175 S and decreases later on.

From figure 48 after 155 S, the vertical displacement and tension fluctuate at the same trend. The average displacement decrease and average tension increase because offset leads to the riser to be stiff and the riser drag the floater downwards. Comparing with the more conservative separate analysis that locking occurs at 153.5 s, the conservative weakened coupled analysis locking occurs at around 155 s. This locking time results shows not much difference.

11.1.4 Load case comparison between case 1.1 and 1.2

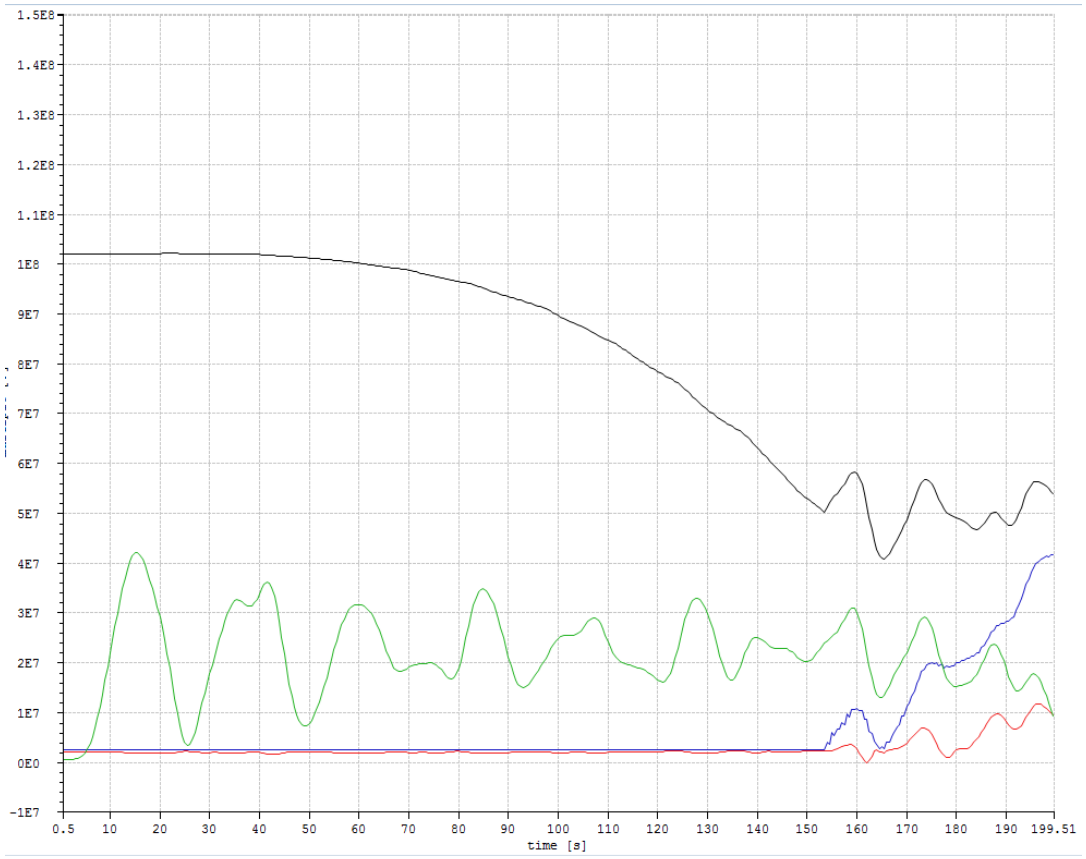

Figure 51 Riser upper end tension (N) and vertical displacement (M) time series for case 1.1 (displacement scaled by 10^7 green and tension blue) and case 1.2 (displacement scaled by 10^7 green and tension red)

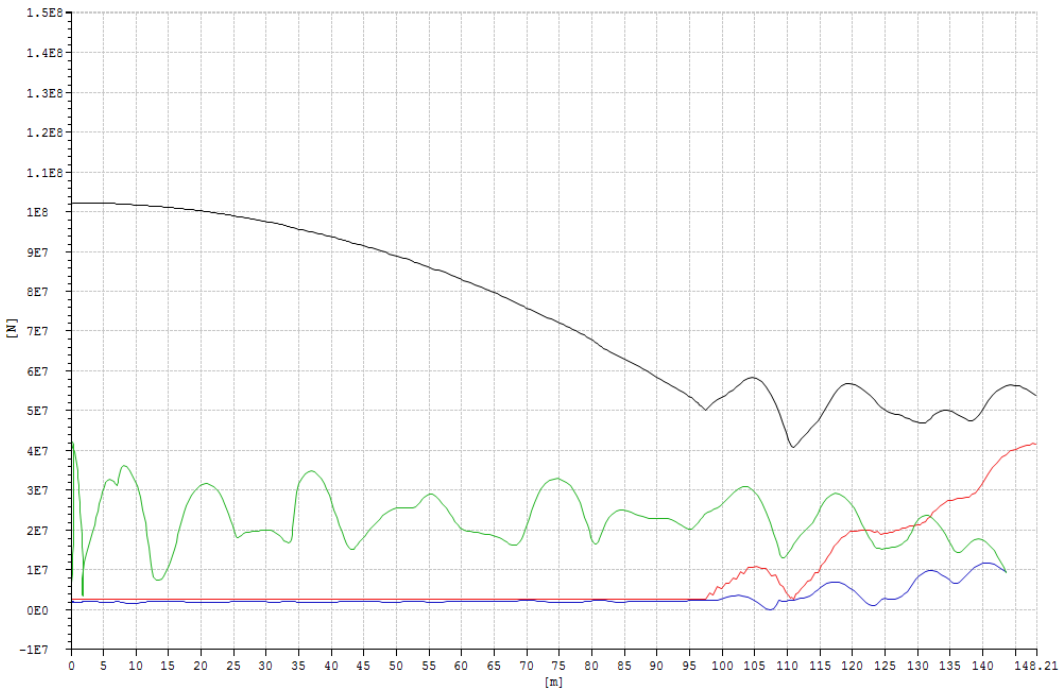

Figure 52 Riser upper end tension (N) and vertical displacement (M) with translational displcament as x-axis for case 1.1 (displacement scaled by 10^7 black and tension red) and case case 1.2 (displacement scaled by 10^7 green and tension red)

When riser upper end tension and vertical displacement are handled as a function of floater translational displacement, the results can be seen in figure 52. It can be seen that the locking for uncoupled analysis occurs at a shorter translational displacement (around 98m) than coupled analysis (around 100m). The other features are similar to the figure 51.

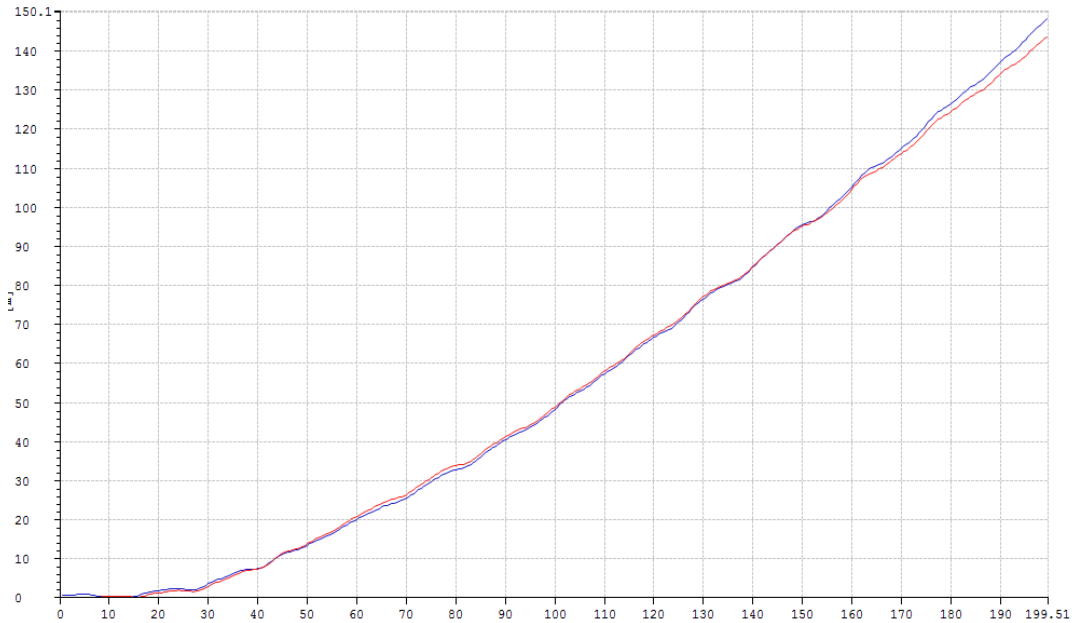

Figure 53 Floater translational displacement (M) time series for case 1.1 (blue) and case 1.2 (red)

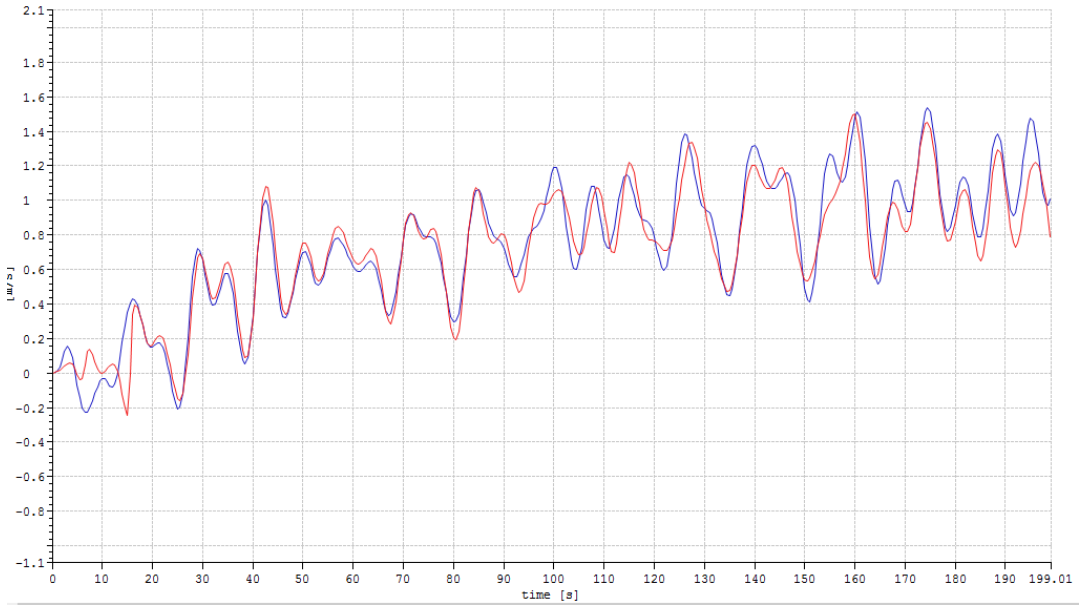

Figure 54 Floater translational velocity (M/S) time series for case 1.1 (blue) and case 1.2 (red)

From figure 51, the tension before locking in coupled analysis is a bit lower than uncoupled analysis as stated before. After locking, the tension develops faster in the uncoupled analysis. This resulted from 3 aspects. Firstly after the locking the floater moves downwards due to coupling effects (mainly tension) and riser would not extend as much as coupled analysis. Secondly, floater translational displacement is smaller in coupled analysis from figure 53 after locking. Thirdly, the floater moves slower in the translational direction after the locking from figure 54.

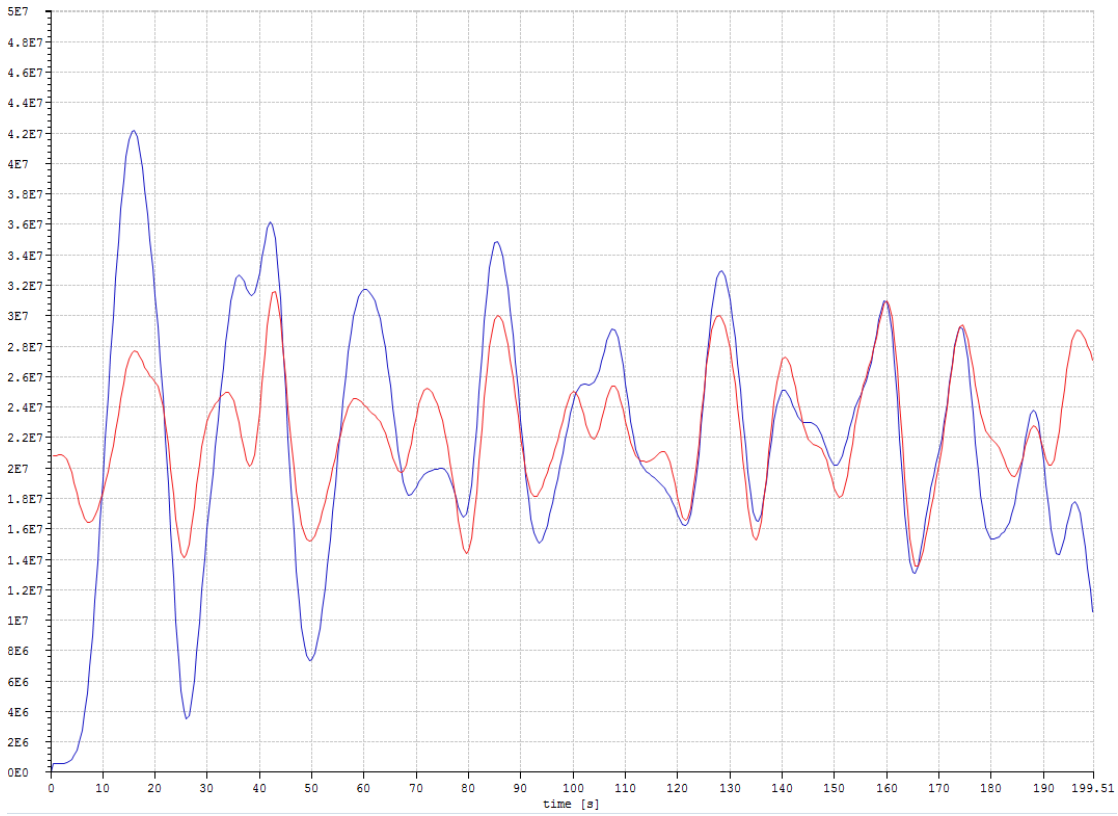

Figure 55 Floater vertical displacement (M) (scaled by 10^7) time series for case 4.1 (red) and case 4.2 (blue)

From figure 55 before locking, case 1.2 have larger vertical fluctuation amplitude than case 1.1 which should result from coupling effects.

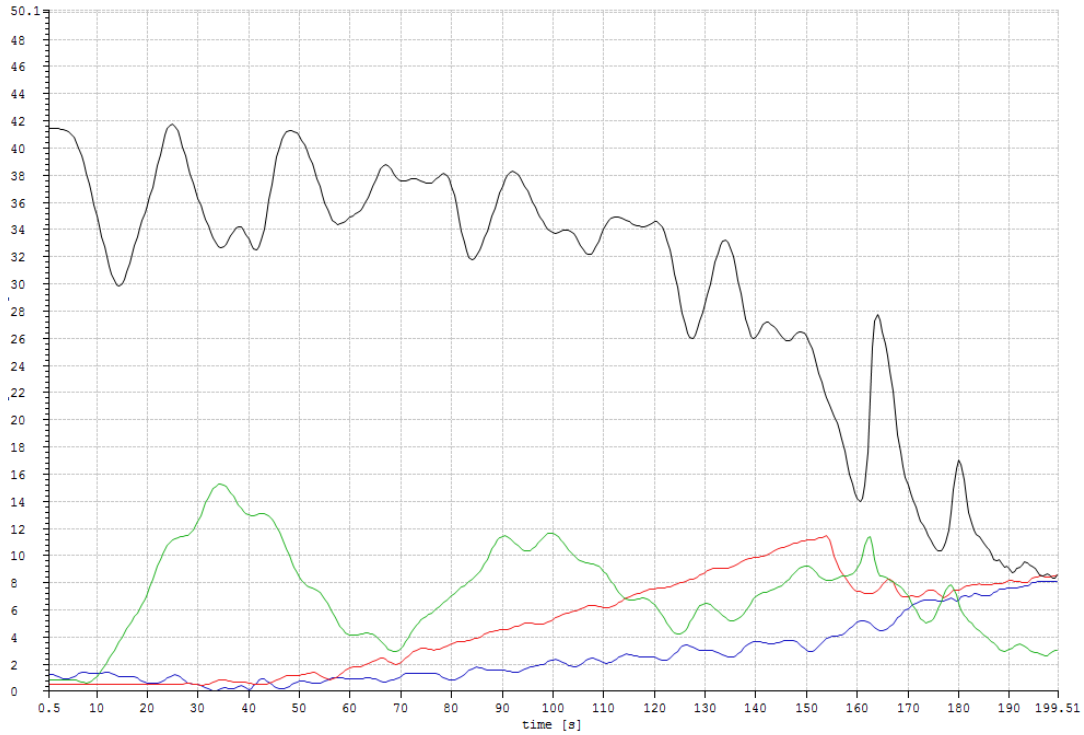

Figure 56 Upper and lower end angels (DEG) time series for case 1.1 (lower red and upper blue) and case 1.2 (lower black and upper green)

From figure 56 because the coupled analysis cannot provide enough effective tension, the angles are much larger than the uncoupled analysis and cannot be used as a reference.

From figure 56 for coupled analysis before locking (around 155 S), both angles decrease slowly because of the offset. For coupled analysis after locking (around 155 S), both angles decrease dramatically mainly because of the tension increase.

From figure 56 for uncoupled analysis, the lower angle experience a dramatic decrease when locking occurs. Then after the drop it will slowly increase and approach the upper angle as the riser is becoming stiffer and looks like a straight line. The reason for upper end does not experience a dramatic angle change is that upper end is dominated by floater motions.

11.1.5 Load case comparison between case 1.1 and 2.1

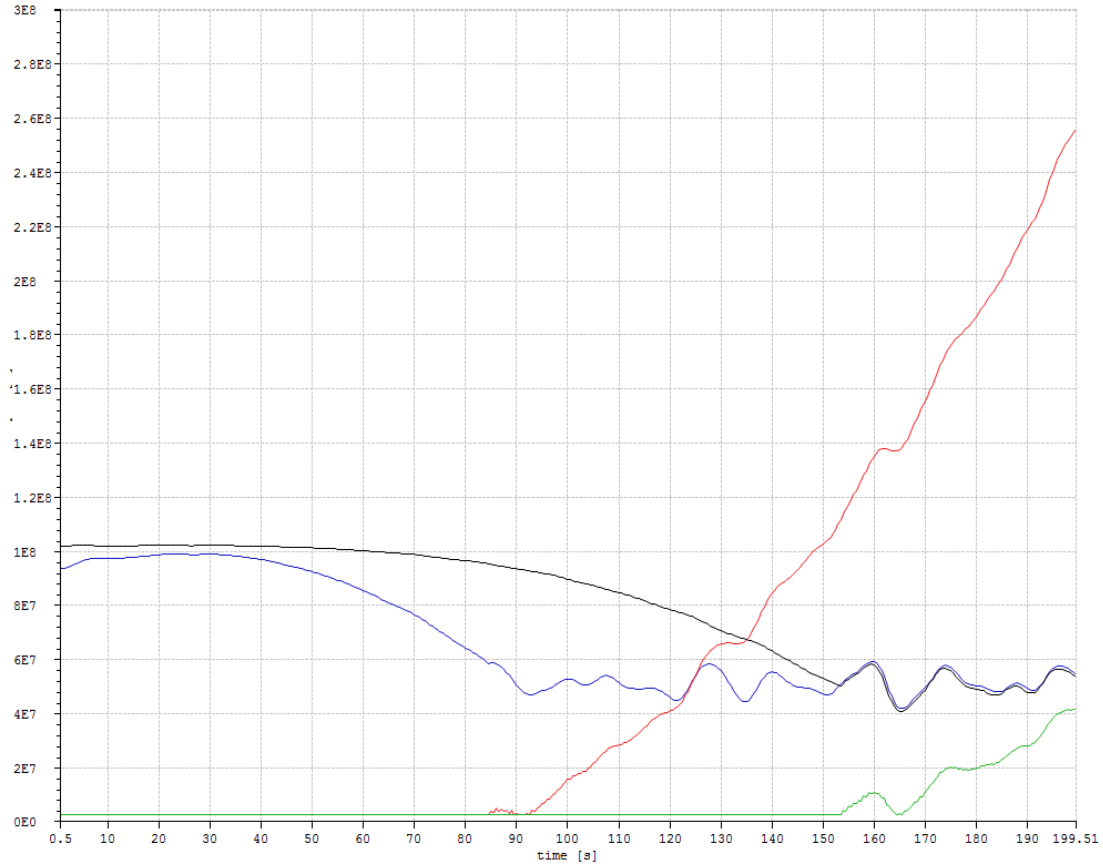

Figure 57 Riser upper end tension (N) and vertical displacement (M) time series for case 1.1 (displacement scaled by 10^7 black and tension green) and case 2.1 (displacement scaled by 10^7 blue and tension red)

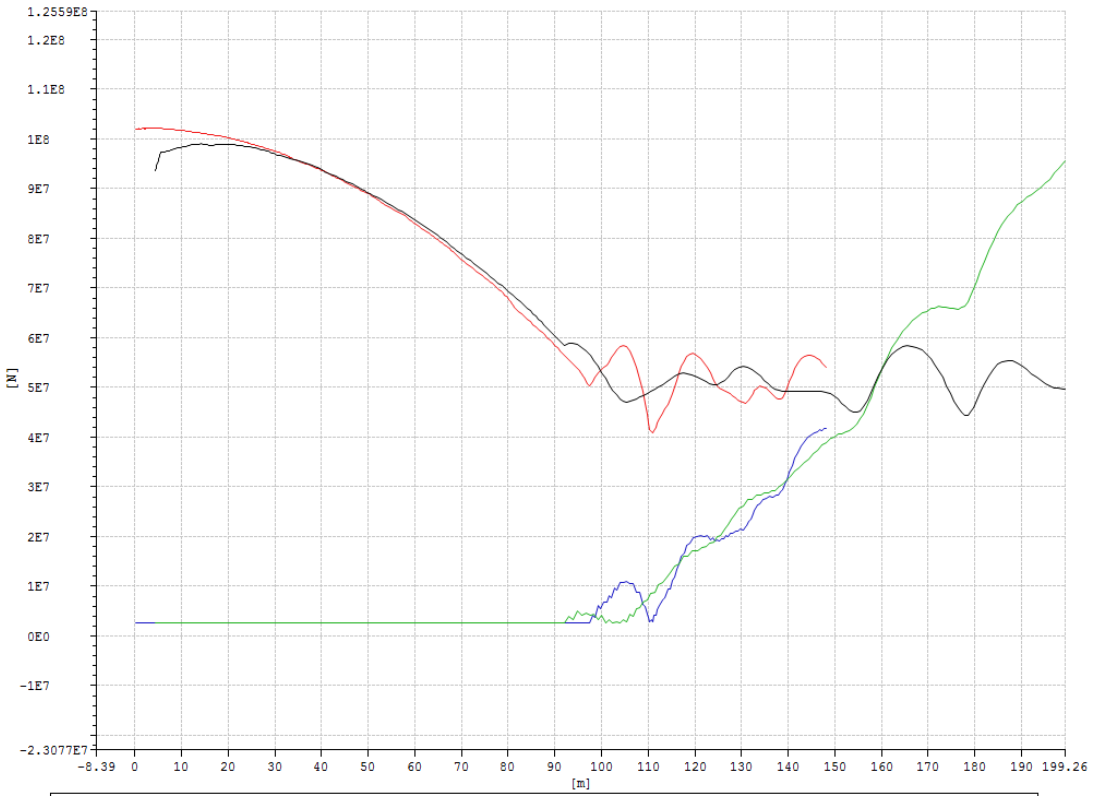

Figure 58 Riser upper end tension (N) and vertical displacement (M) with translational displacement as x-axis for case 1.1 (displacement scaled by 10^7 black and tension green) and case 2.1 (displacement scaled by 10^7 blue and tension red)

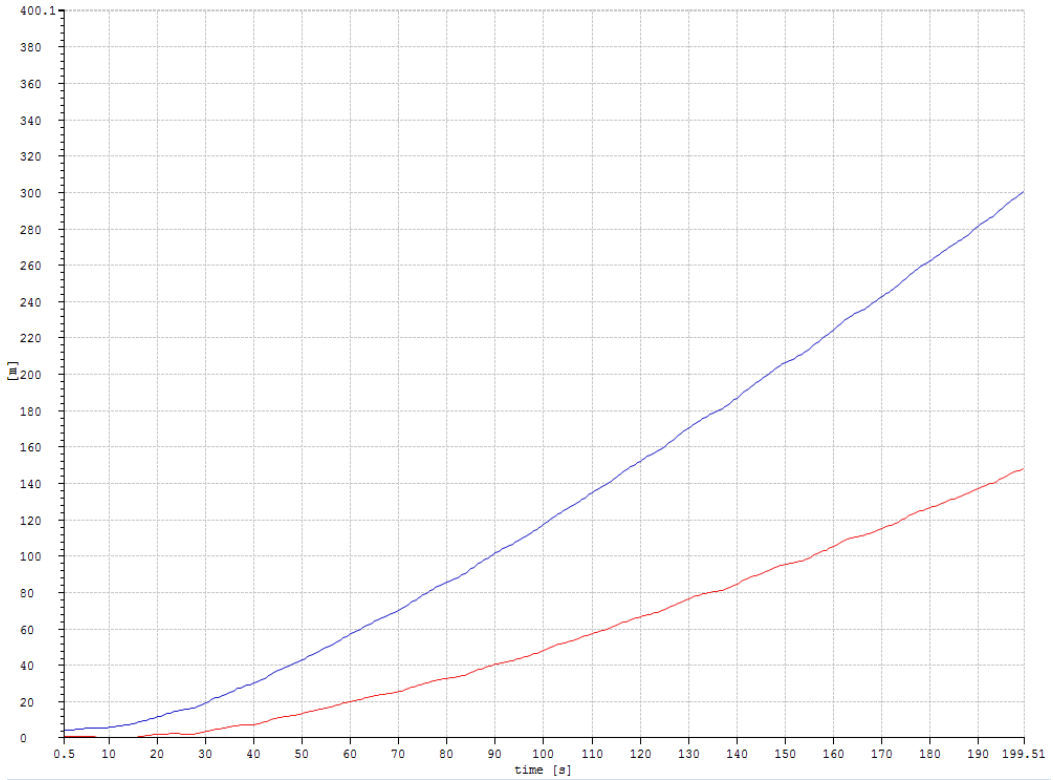

Figure 59 Floater translational displacement (M) time series for case 1.1 (red) and case 2.1 (blue)

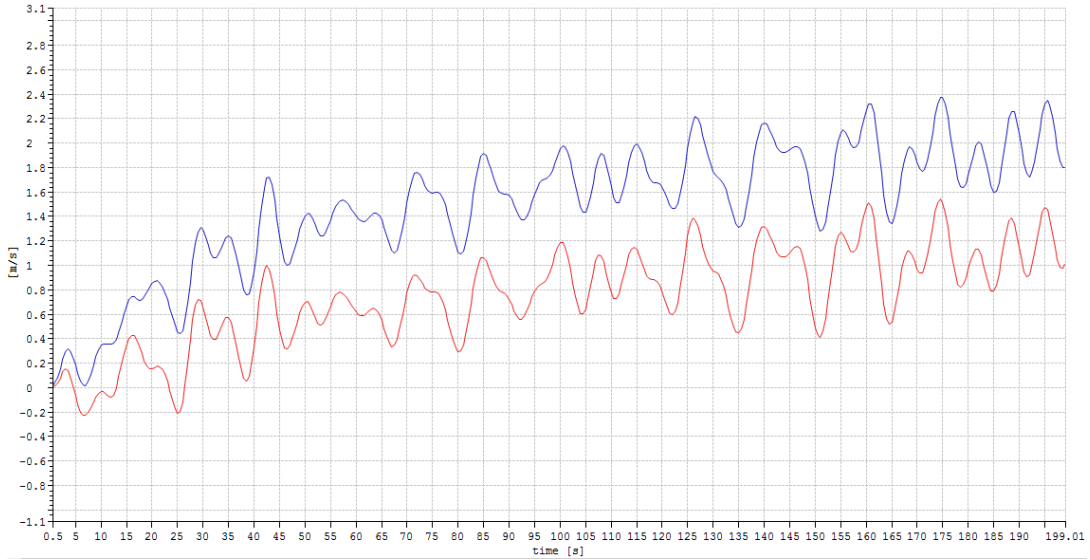

Figure 60 Floater translational velocity (M/S) time series for case 1.1 (red) and case 2.1 (blue)

From figure 57 for case 2.1 because of much higher current speed attack, the riser upper end is a bit lower than the case 1.1 at the very beginning. .

From figure 57 for case 2.1, because case 2.1 floater travels faster from figure 60 and more offset at the same time from figure 59. Hence the tension increase velocity in case 2.1 would be higher than the case 1.1.

From figure 57, current very minimal effects on the floater heave motion as the difference after both cases are locked is very minimal.

From figure 57 after the locking for both cases, it is confirmed as in chapter 10.1.2 that the effects of heave motion on the tension are the mainly the amplitude of the fluctuation. In the small period just after locking for case 1.1, the floater motion is mild and hence the tension fluctuation is mild. And for case 2.1 it is wilder.

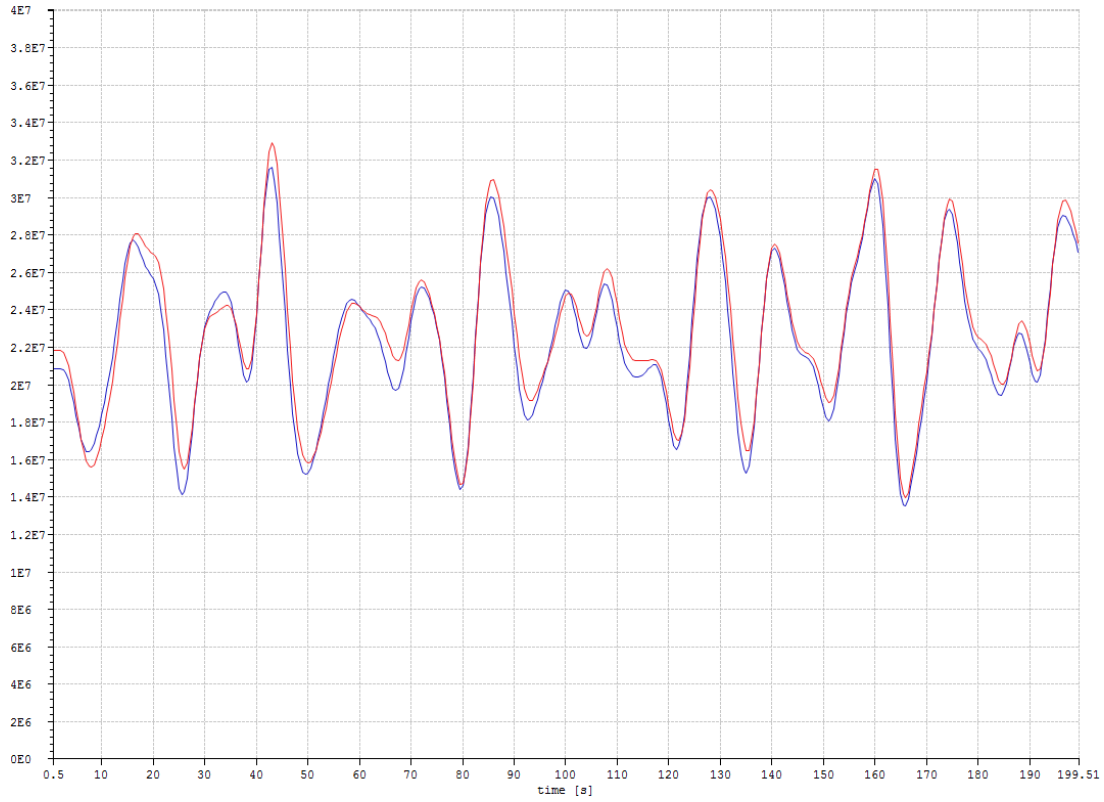

Figure 61 Floater vertical displacement (M) (scaled by 10^7) time series for case 1.1 (blue) and case 2.1 (red)

From figure 58, the case 2.1 locking occurs at a shorter translational distance than case 1.1 even the floater vertical position in case 2.1 is a little higher than case 1.1 in figure 61. From figure 58, the riser upper end position for case 2.1 approaches case 1.1 after the very beginning because of the relative speed between current velocity and floater velocity decrease from figure 60. Also between the case 1.1 and 2.1 there is drag coefficient difference. Considering the small difference between riser upper ends for case 1.1 and 2.1 at the beginning, it is concluded that the upper end position is not sensitive to the current. The locking criteria is based on the relative distance between the floater and riser upper end reaches max stroke. Since both end positions don't

vary much, this case 2.1 which locks at the shorter distance is acceptable.

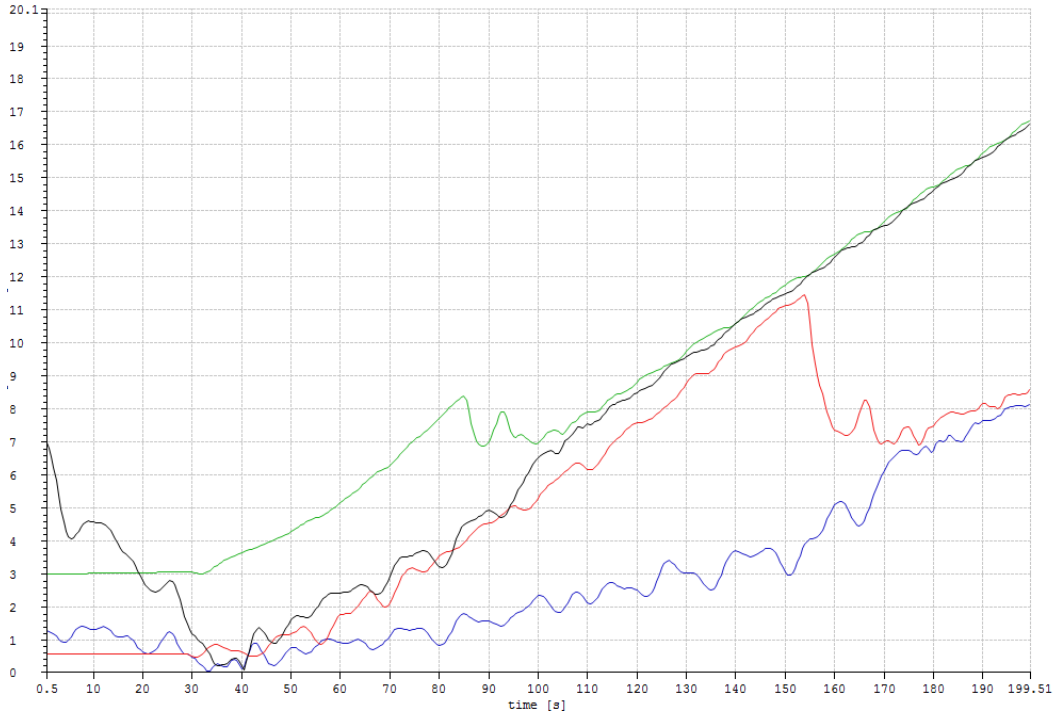

Figure 62 Upper and lower end angels (DEG) time series for case 1.1 (lower red and upper blue) and case 2.1 (lower green and upper black)

From figure 62, current have a great influence on the angles at the beginning that angles in case 2.1 are larger than case 1.1.

From figure 62, the upper and lower angles approaches each other at 110 to 120 S for case 2.1 and 170 to 180 S for case 1.1. From figure 59, the translational displacement for case 2.1 at 110 to 120 S and case 1.1 at 170 to 180 S are very close. It's concluded that horizontal displacement have a great influence on the asymptotic angle.

From figure 62 for the upper ends, current induced angle and offset induced angel are in the opposite direction. As offset increases and the relative speed between the current the floater decreases, the angle will reach a minimal at around 40 S. However from figure 62 for lower ends, there is no current so the offset effects dominate.

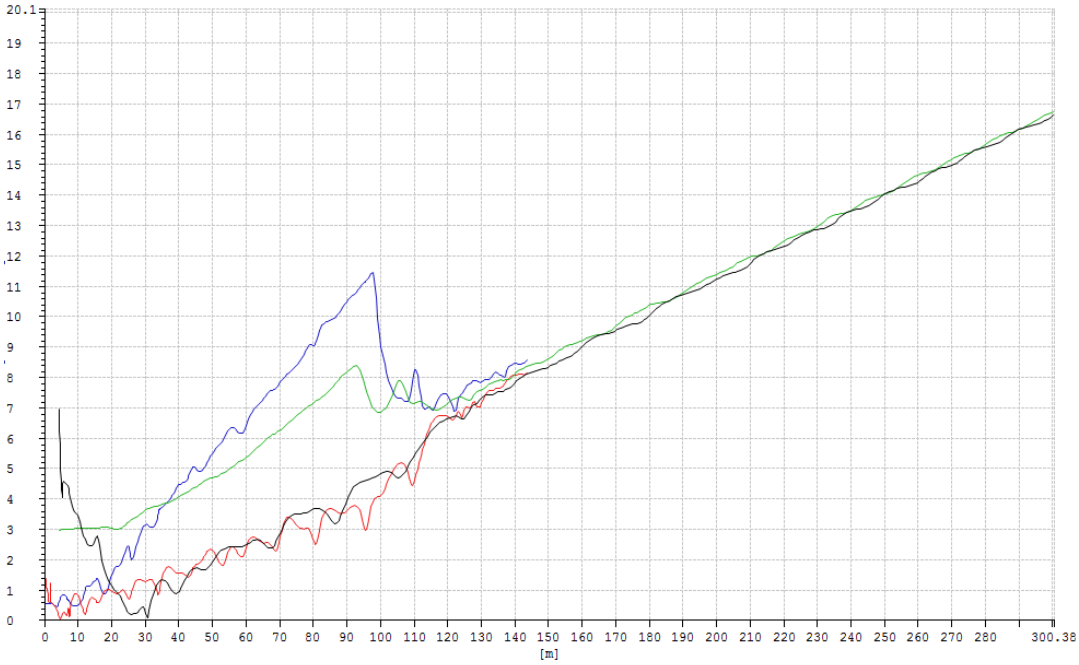

Figure 63 Upper and lower end angels (DEG) with translational displacement as x-axis for case 1.1 (lower blue and upper red) and case 2.1 (lower green and upper black)

From figure 63 it can be seen the angles are dominated by offset. Because of the difference drag coefficient between case 1.1 and 2.1, it can be seen that the lower end is very sensitive to the current on the upper part of the riser. Upper angles on the other hand is dominated by the floater motion since the difference between case 1.1 and 2.1 are quite small.

11.1.6 Load case comparison between case 1.1 and 3.1

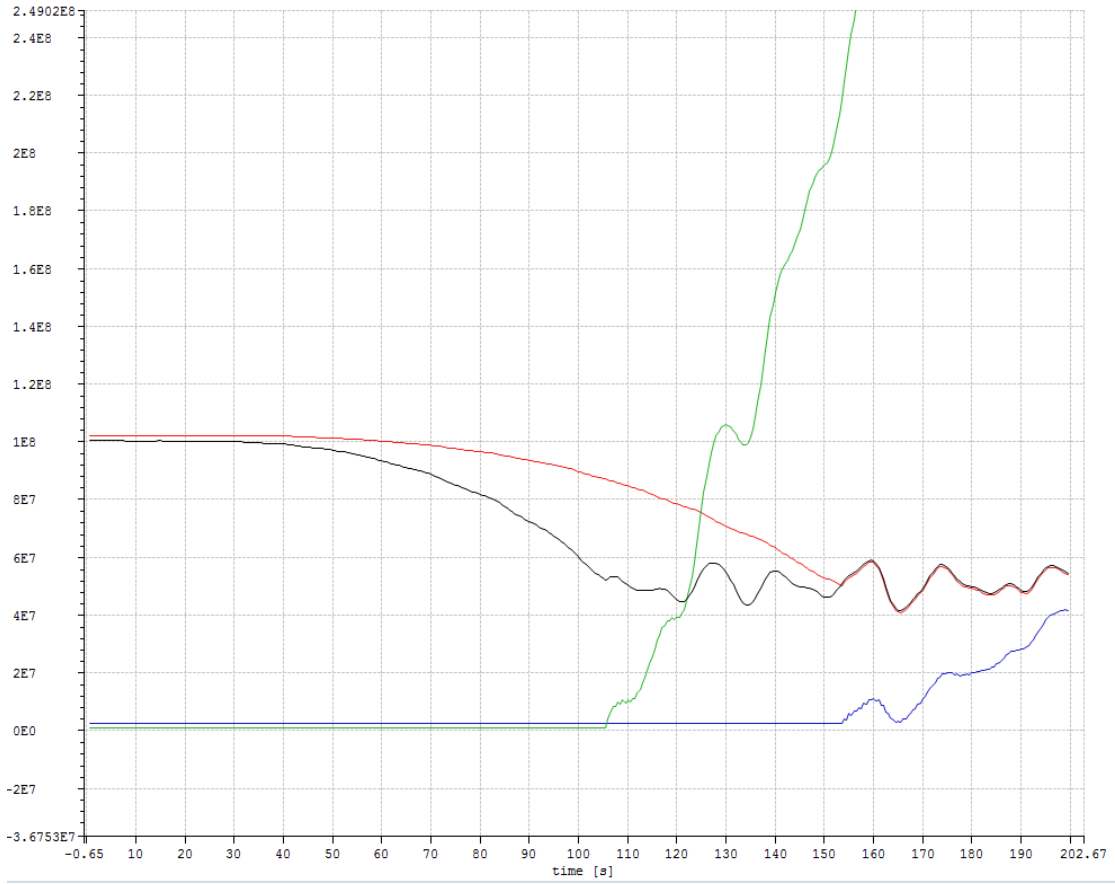

Figure 64 Riser upper end tension (N) and vertical displacement (M) time series for case 1.1 (displacement scaled by 10^7 red and tension blue) and case 3.1 (displacement scaled by 10^7 black and tension green)

From figure 64 the upper end tensions difference before lock is because of the different top tension.

From figure 64 it can be seen in case 3.1 lock occurs earlier and tension rises faster than case 1.1.

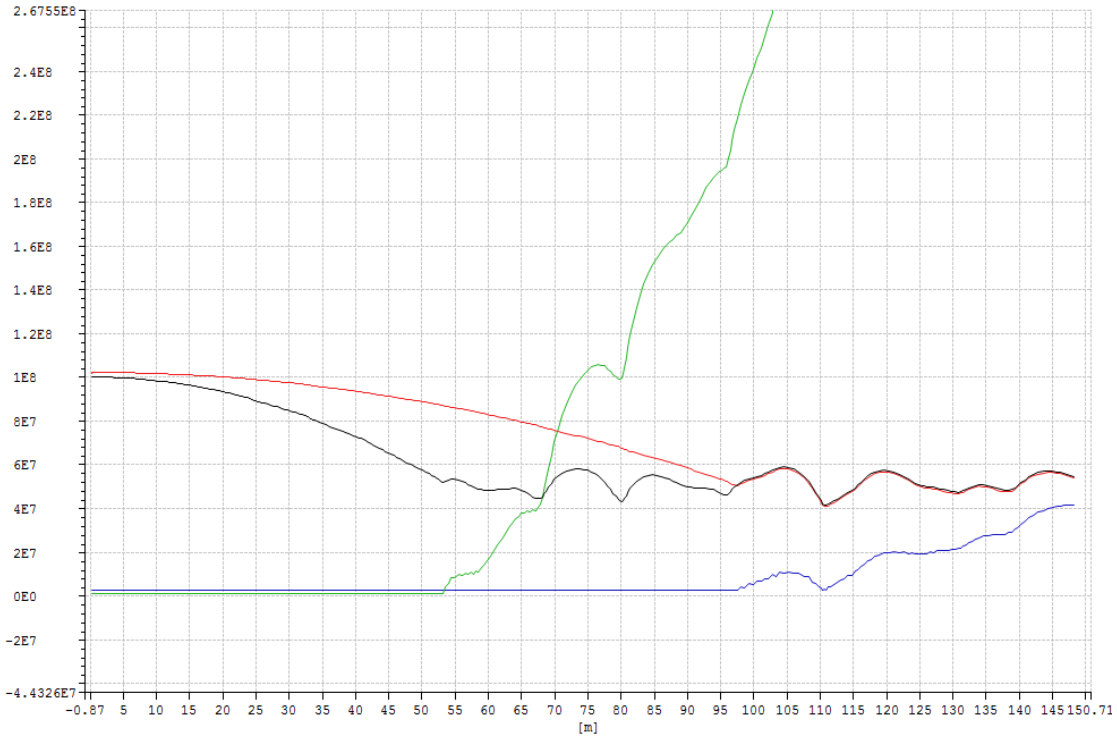

Figure 65 Riser upper end tension (N) and vertical displacement (M) with translational displacement as x-axis for case 1.1 (displacement scaled by 10^7 red and tension blue) and case 3.1 (displacement scaled by 10^7 black and tension green)

From figure 70 it can be seen in case 3.1 the upper end tension and displacement are more sensitive to water depth than case 1.1.

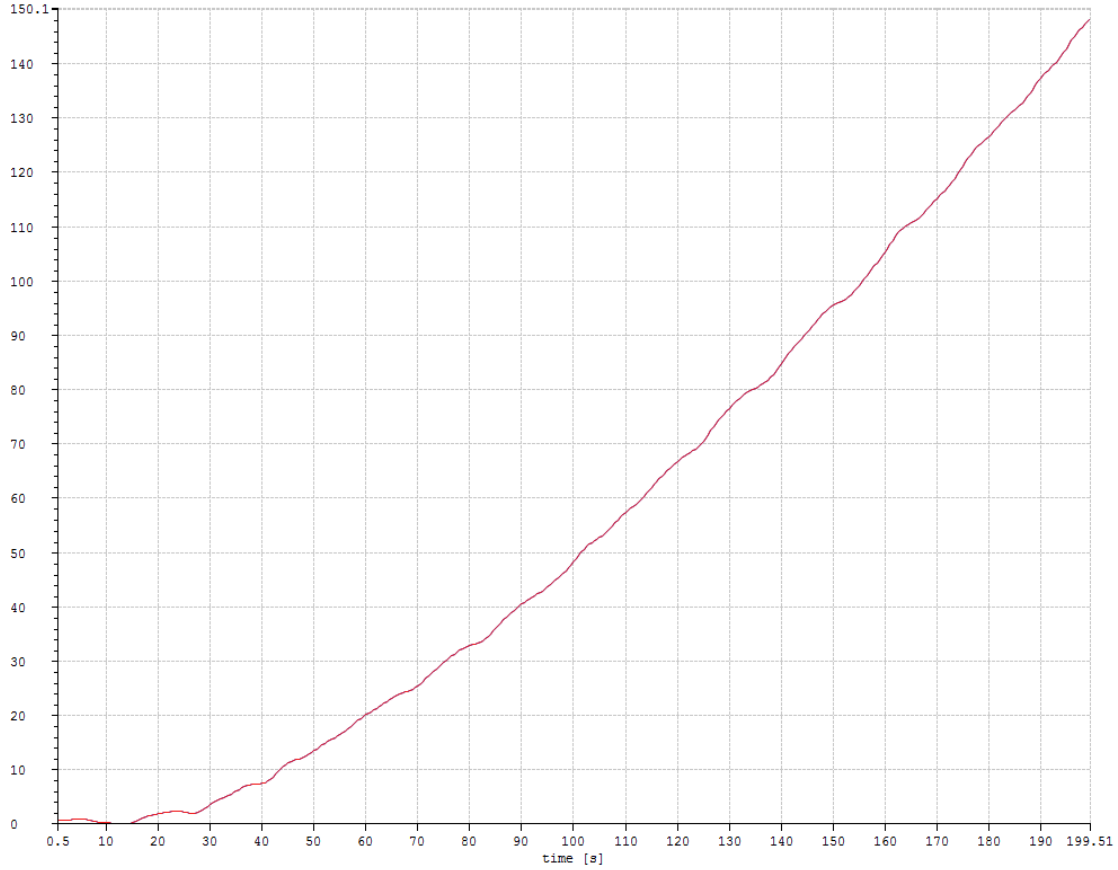

Figure 66 Floater translational displacement (M) time series for case 1.1 and case 3.1

From figure 71, the case 1.1 and 3.1 are indistinguishable. The surface current speed between case 1.1 and 3.1 are same but the there is a small current speed difference downwards. It can be seen the floater translational displacement is very insensitive the small current variation.

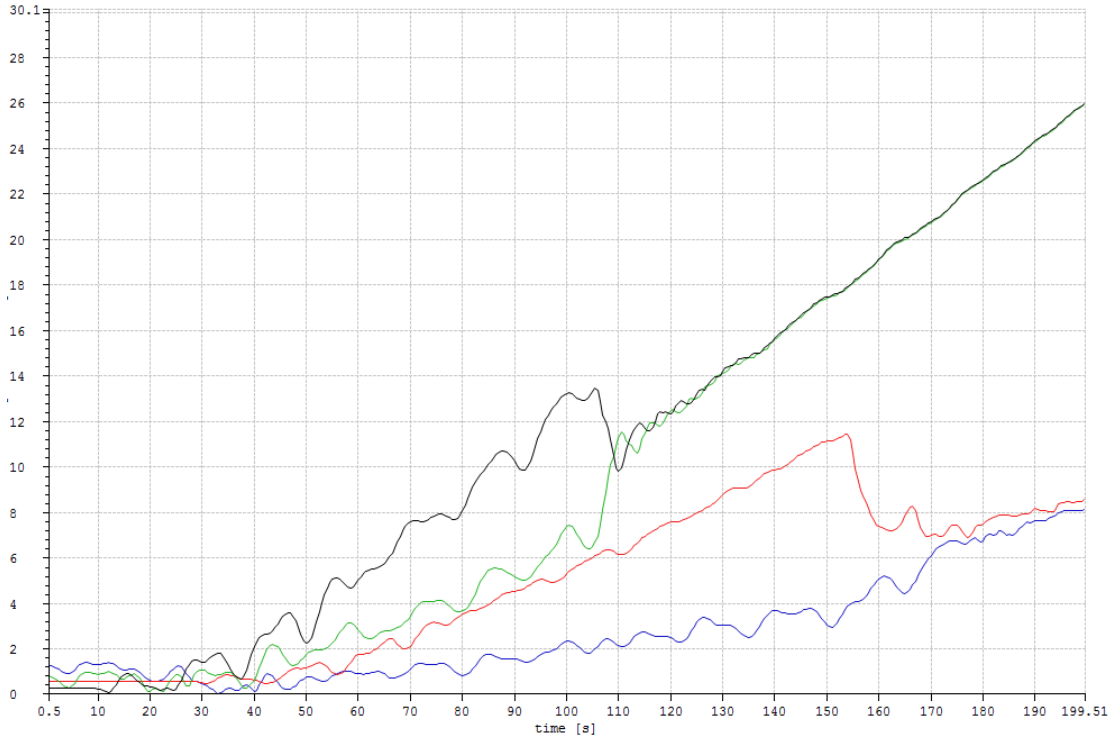

Figure 67 Upper and lower end angels (DEG) time series for case 1.1 (lower red and upper blue) and case 3.1 (lower black and upper green)

From figure 72 it can be seen in case 3.1 angles changes faster than in case 1.1

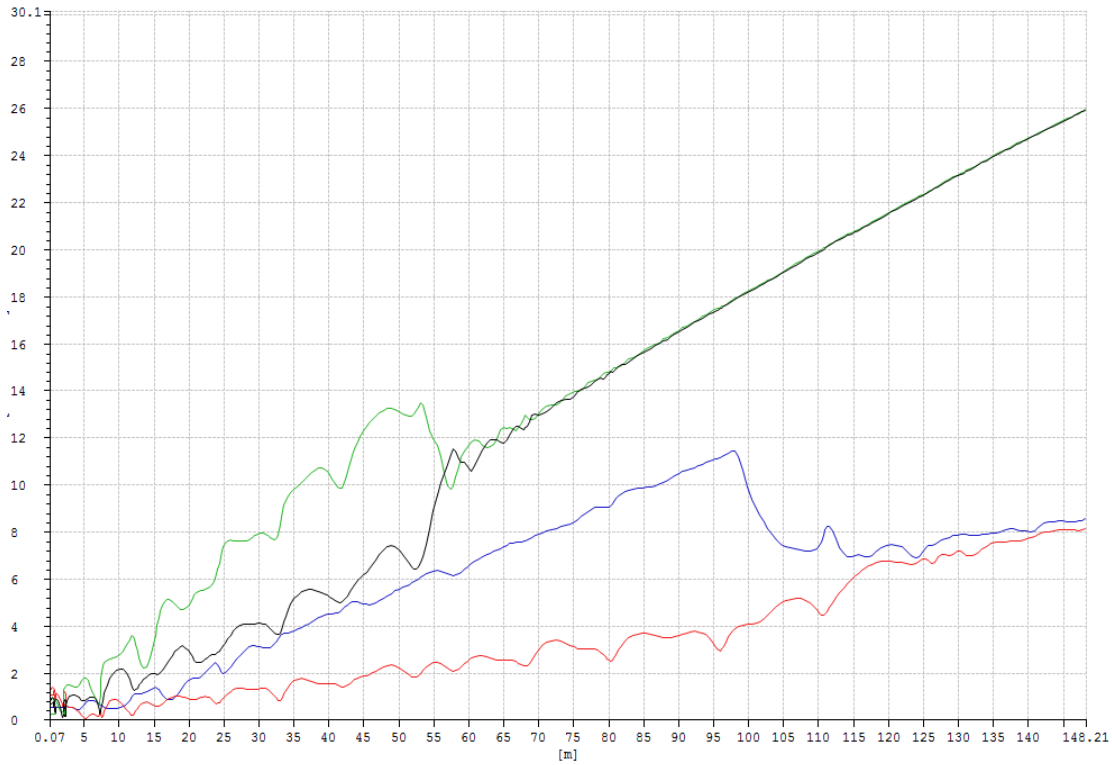

Figure 68 Upper and lower end angels (DEG) with translational displacement as x-axis for case 1.1 (lower blue and upper red) and case 3.1 (lower green and upper black)

From figure 73 it can be seen the angles are more sensitive to offset in case 3.1 than in case 1.1.

11.1.7 Load case comparison between case 1.2 and 2.2

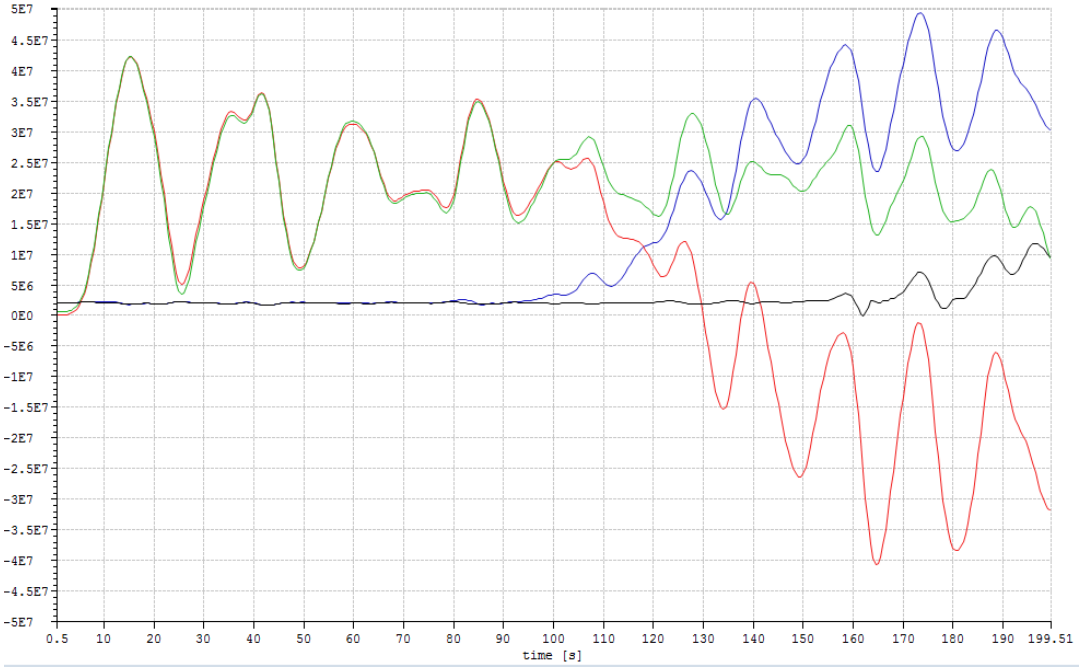

Figure 69 Riser upper end tension (N) and vertical displacement (M) time series for case 1.2 (displacement scaled by 10^7 green and tension black) and case 2.2 (displacement scaled by 10^7 red and tension blue)

From figure 69 for case 2.2, the locking occurs at around 90 s which is a little more delayed than the case 2.1. This is similar to the difference between case 1.2 and 1.1.

From figure 69 seen from the displacement difference between case 1.2 and 2.2, current has very minimal effects on the floater motion as seen from period before the locking. This is similar to the case 1.1 and 1.2.

From figure 69, the tension in case 2.2 develops much faster than case 1.2 and the floater vertical displacement drops dramatically consequently. This is similar to the uncoupled analysis.

From figure 69, it is confirmed as in chapter 10.1.3 that after locking the tension and vertical displacement fluctuation amplitude reaches a peak. This phenomena can be explained by tension geometric stiffness. After locking as tension becomes higher, this make tension geometric stiffness decreases. However, after locking the vertical displacement decreases, this decrease the tension geometric stiffness. At around 175 S, the conflicting effects reaches a peak.

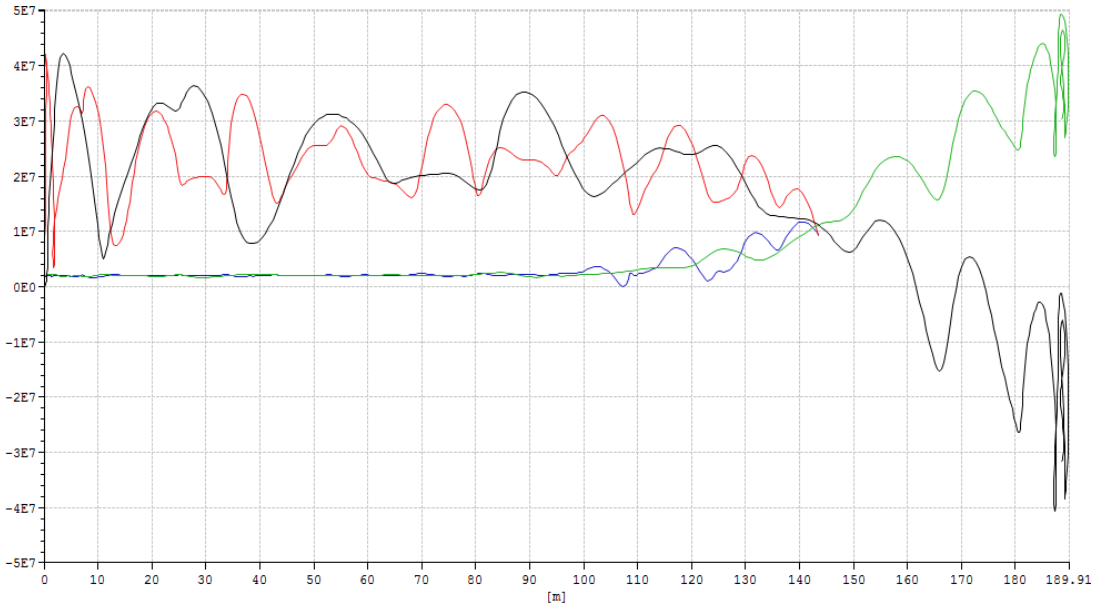

Figure 70 Riser upper end tension (N) and vertical displacement (M) with translational displacement as x-axis for case 1.2 (displacement scaled by 10^7 green and tension black) and case 2.2 (displacement scaled by 10^7 red and tension blue)

Comparing figure 70 with 69, it can be seen that the floater heave fluctuation amplitude is seldom influenced by current and offset but highly influenced by wave.

From figure 70 at the very beginning, the case 1.2 heave motion experienced a snap-through because of the floater translational negative velocity. From figure 70 at the end, the case 2.2 values experienced snap-through because of the equilibrium of horizontal component of top tension and hydrodynamic forces.

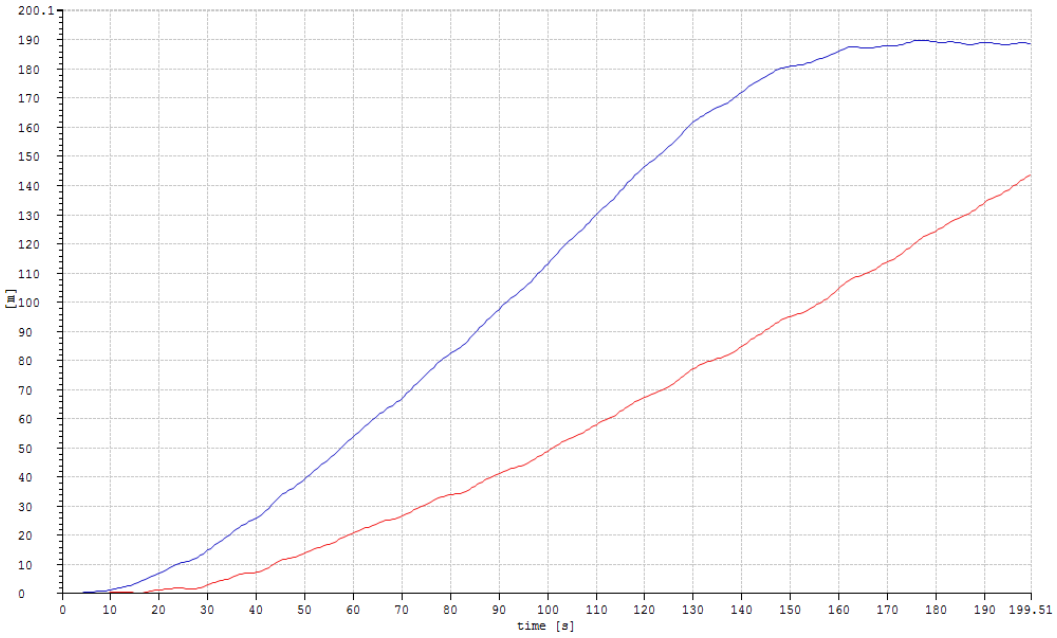

Figure 71 Floater translational displacement (M) time series for case 1.2 (red) and case

2.2 (blue)

From figure 71, platform move horizontally faster in higher current speed.

From figure 71, the translational displacement don't change much for case 2.2 because the horizontal component of upper end tension is in equilibrium with the hydrodynamic force.

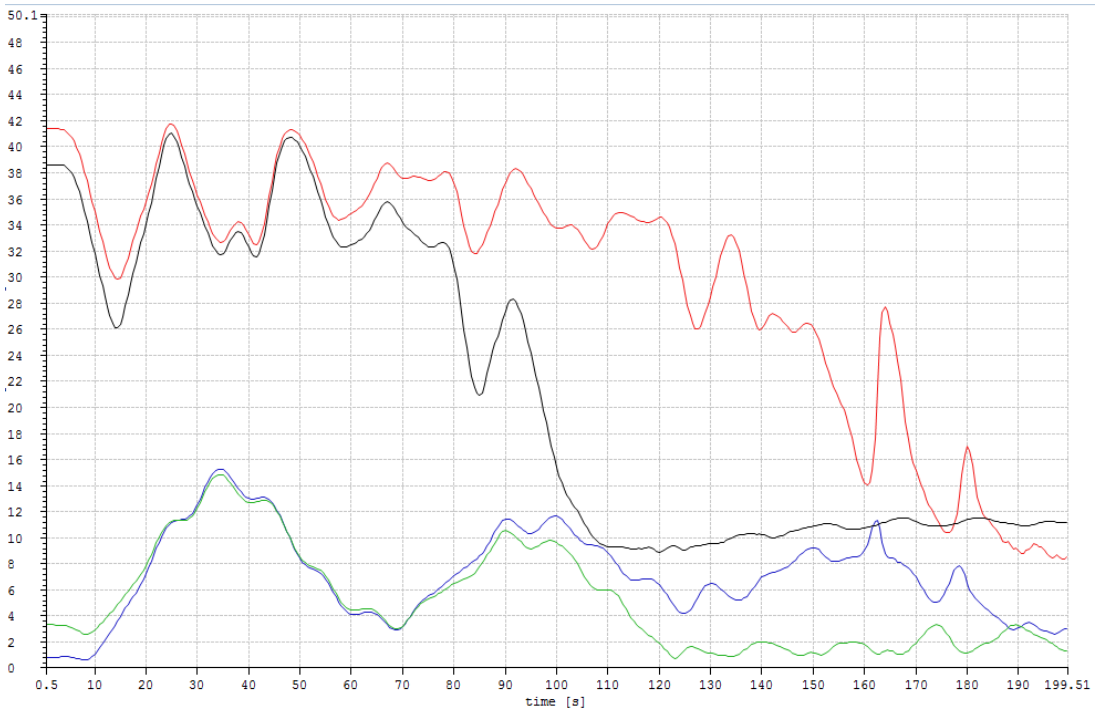

Figure 72 Upper and lower end angels (DEG) time series for case 1.2 (lower red and upper blue) and case 2.2 (lower black and upper green)

From figure 72, locking for case 2.2 occurs earlier than case 2.1 and hence the dramatic angles drop occurs earlier for case 2.2.

From figure 72 for upper ends, because the coupling is started from the beginning, the upper end angle is dominated by the floater motion until locking when tension increases.

From figure 72 for lower angles at the early period, it can be seen that the fluctuation is dominated by wave motions. From figure 72 for lower angles the difference between 1.2 and 2.2 can be explained that, the at the very beginning the current and riser relative velocity difference between case 1.2 and 2.2 is bigger, this makes the angles difference at the beginning big. Later when the current and riser relative velocity become smaller, the angles difference become smaller. The difference of offset between case 1.2 and 2.2 is becoming larger as time goes by, such the lower angle difference become bigger later.

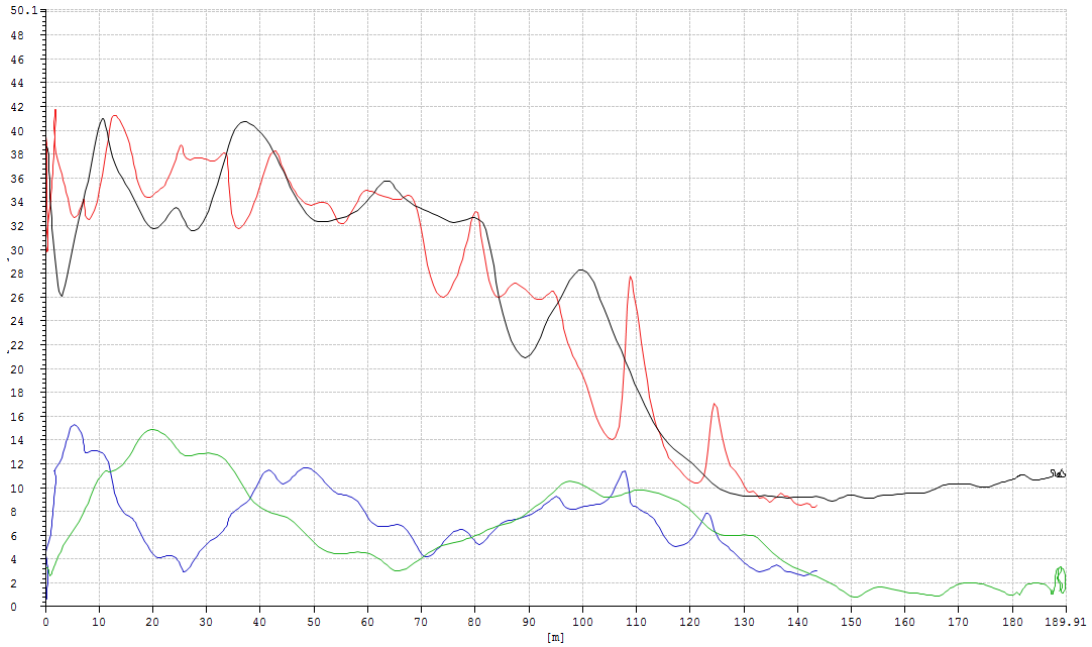

Figure 73 Upper and lower end angels (DEG) time series for case 1.2 (lower red and upper blue) and case 2.2 (lower black and upper green)

From figure 73 it can be seen that the offset dominate the angles.

11.1.8 Load case comparison between case 1.2 and 3.2

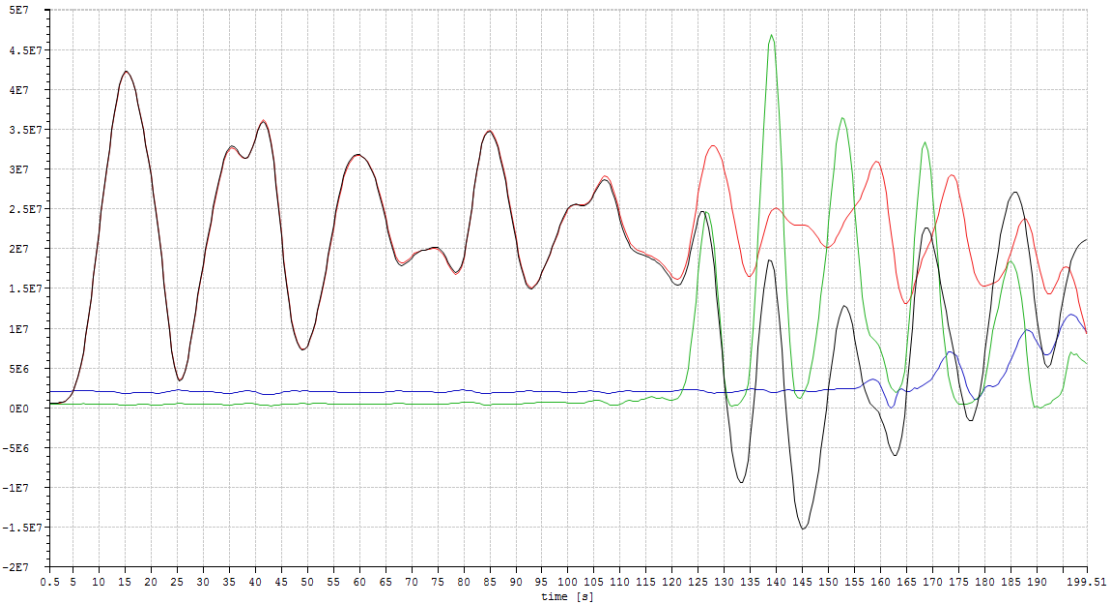

Figure 74 Riser upper end tension (N) and vertical displacement (M) time series for case 1.2 (displacement scaled by 10^7 red and tension blue) and case 3.2 (displacement scaled by 10^7 black and tension green)

From figure 74 the upper end tensions difference before lock is because of the different riser weight.

From figure 74 the lock occurs earlier in case 3.2 than in case 1.2.

From figure 74 average level of the tension did not increase but the tension fluctuate in a very big amplitude.

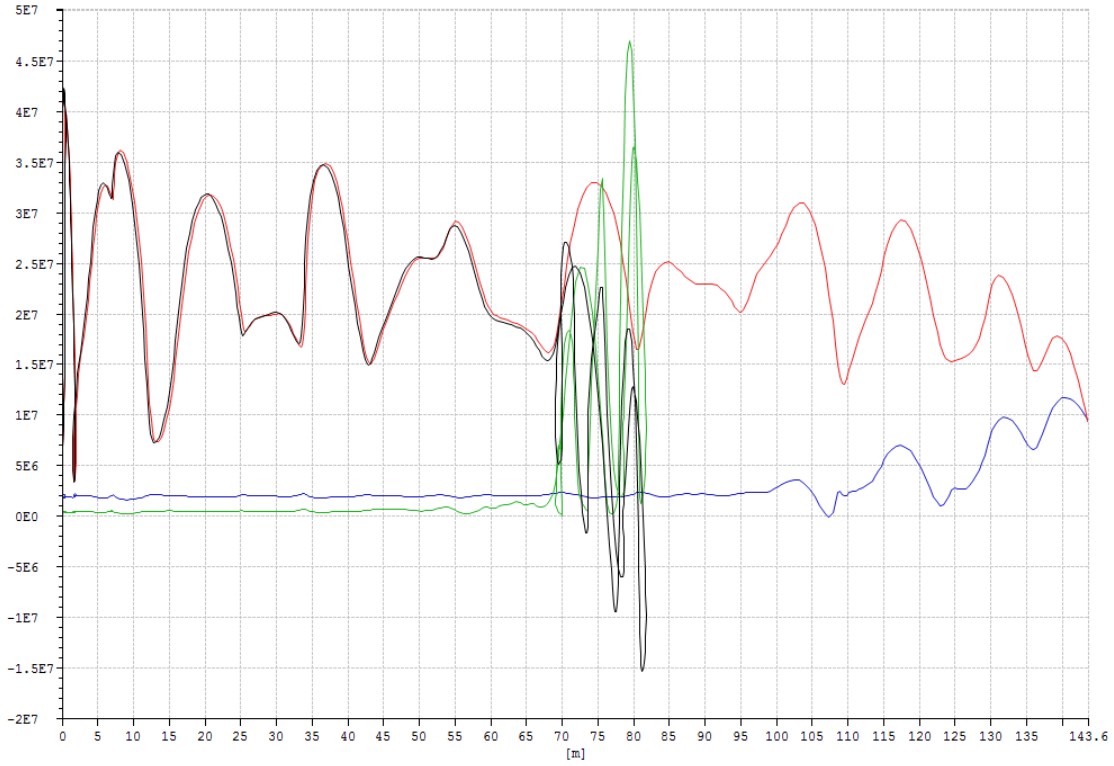

Figure 75 Riser upper end tension (N) and vertical displacement (M) with translational displacement as x-axis for case 1.2 (displacement scaled by 10^7 green and tension black) and case 3.2 (displacement scaled by 10^7 red and tension blue)

From figure 75 it can be seen the coupling effects and hydrodynamic forces reach an equilibrium at a shorter translational distance in case 3.2 than in case 1.2.

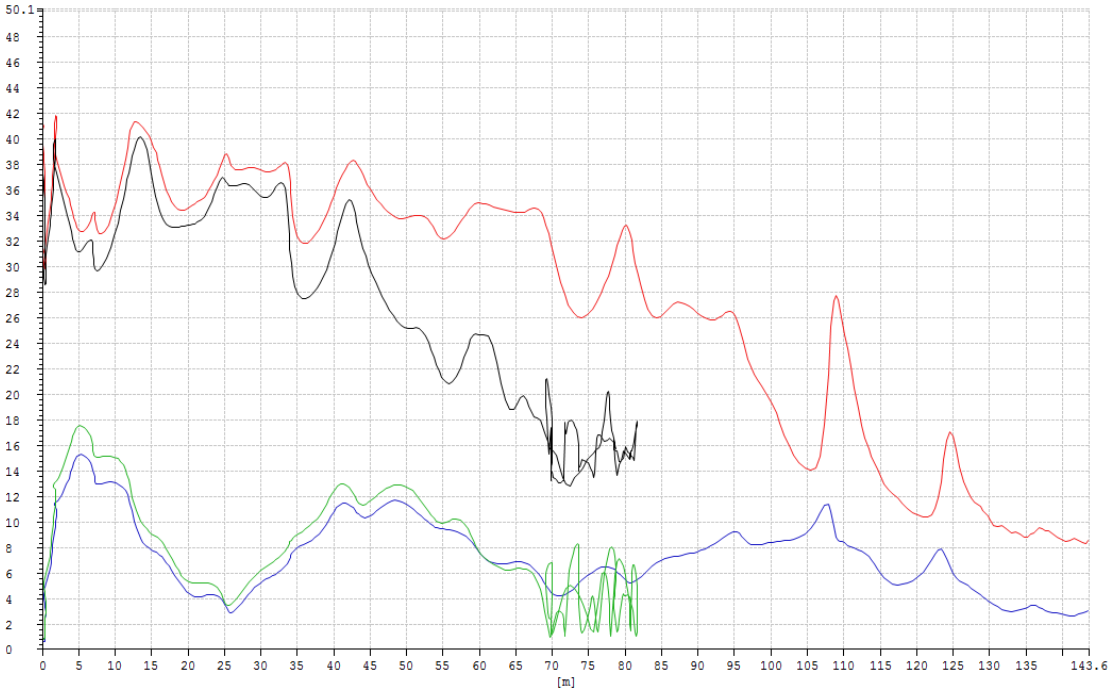

Figure 76 Upper and lower end angels (DEG) with translational displacement as x-axis for case 1.2 (lower red and upper blue) and case 3.2 (lower black and upper green)

From figure 76 it can be seen the angles are more sensitive to offset in case 3.2 than in case 1.2.

11.1.9 Locking moment

Table 5 Locking moment

Load case number	1.1	1.2	2.1	2.2	3.1	3.2	4.1	4.2	5.1	5.2	6.1	6.2
Locking moment (s)	153.5	About 155	85	About 90	106	About 120	58	About 66	224	About 245	138	About 140
Locking time difference (S)	1.5		5		14		8		21		2	

11.1.10 Comparisons between 1.1 and the corresponding analytical solution

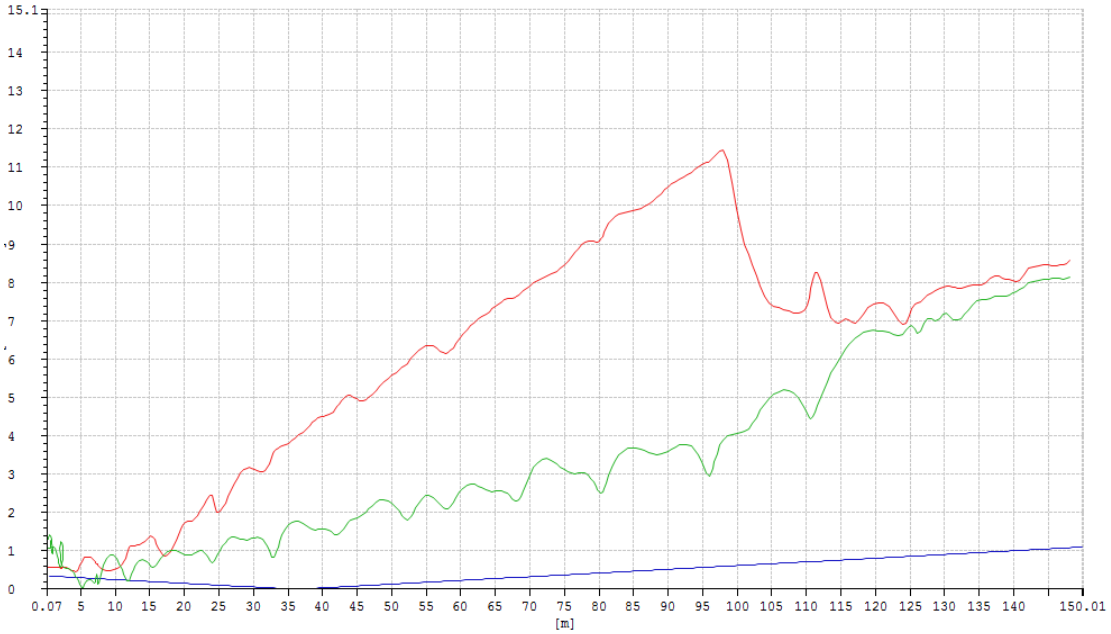

Figure 77 Sima upper and lower end angels (DEG) with translational displacement as x-axis for case 1.1 (lower red and upper green) and the corresponding upper end (blue) analytical angle solution

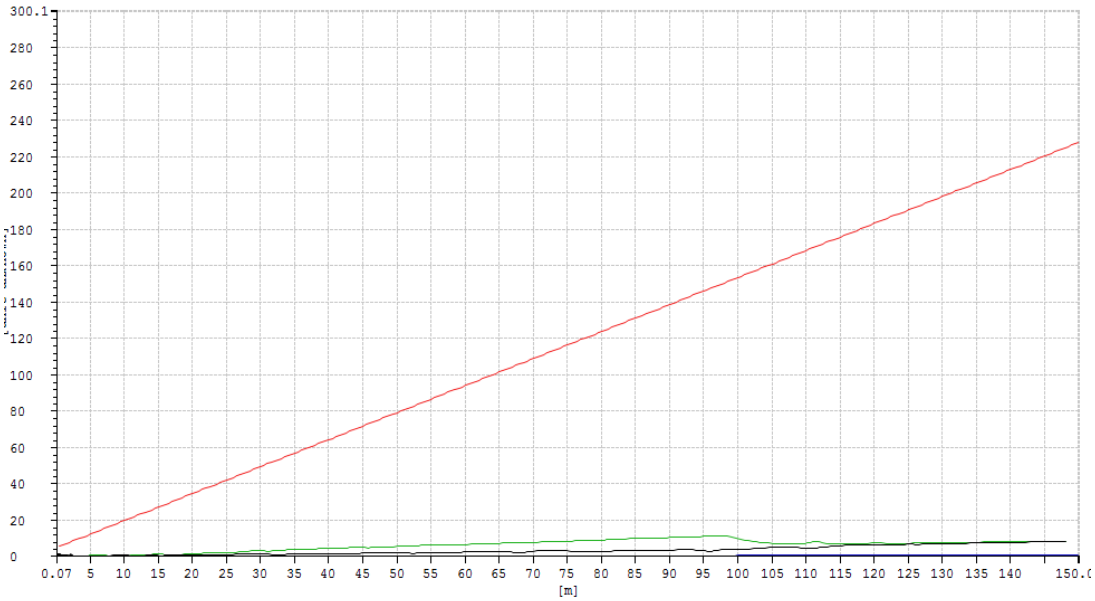

Figure 78 Sima upper and lower end angels (DEG) with translational displacement as x-axis for case 1.1 and the corresponding upper and lower (red) ends analytical angle solutions

Because tension is constant in the analytical solution so uncoupled analysis is to be compared with.

The upper end angle by analytical analysis is too small for but the upper end angle feature which first decrease to zero then increase is captured in figure 77. When four angles are put in one plot, the lower angle is too big that the rest angles are barely visible in figure 78. Combing with the equations (10.2.8) and (10.2.9), the analytical solution difference between upper and lower end is the tension. It can be seen the importance of tension effects on the end angles.

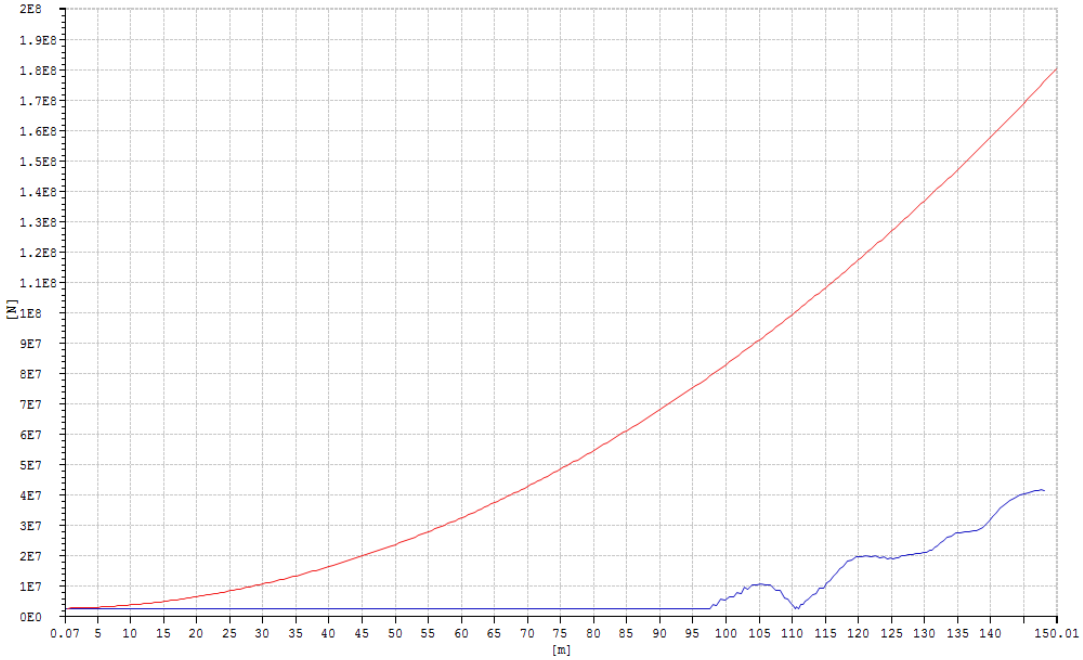

Figure 79 Sima upper end tension with translational displacement as x-axis for case 1.1 (blue) and the corresponding upper end analytical tension solution (red)

The analytical tension seems only comparable for small offset. For large offset the result would be way too conservative. The reason should be that the riser setdown in analytical solution is based on small angle hypothesis. But for large offset, the riser stretch would be much lower than riser setdown.

The rest case comparisons are in appendix (uploaded in DAIM zip file).

11.1.11 Results discussion

After locking, tension average level depends on the offset. The larger the offset, the larger the average tension. The tension fluctuation is caused by waves.

Lower end angle is very sensitive to the current at the upper surface.

Displacement and tension have a great influence on both end angles.

11.1.11.1 Coupling effects influence

For both coupled and uncoupled analysis, the environmental forces influence on the tension are very small.

After locking the tension increases faster in the uncoupled analysis than coupled one.

In table 5, the locking time for coupled analysis always occurs a bit later than uncoupled case.

Considering the translational distance where the locking occurs, the uncoupled analysis always occurs at a shorter distance than coupled analysis. The reason is that locking criteria for the uncoupled analysis is that locking is kept on after stroke run out. But locking could be mainly due to the heave motion and there is still some spare stroke during the floater move downwards.

Before locking, the coupling effects on the floater translational displacement and velocity is very small but have a noticeable influence on the vertical motions which increase the vertical amplitude.

11.1.11.2 Current speed influence

Current have a great influence on the floater translational displacement and velocity. Floater in higher surface current speed moves faster and further. Therefore the locking occurs earlier and the tension increase faster after locking. On the other hand current influence on the floater heave motion is very limited.

Higher surface current effects on riser configuration are only obvious at the very beginning, including lower upper end vertical position, larger end angles. Those effects will diminish because the as floater speed increase as the relative speed between riser and floater will decrease.

For higher surface current speed, the locking time difference between coupled and uncoupled are smaller. This means the less translational coupling effects in higher surface current speed.

11.1.11.3 Water depth influence

Locking occurs earlier and tension increase faster in shallower water.

Angles changes faster and more sensitive in shallower water.

Tension fluctuation amplitude depends on the water depth. Shallower water have larger fluctuation amplitude.

11.1.11.4 Simple modelling discussion

The current analysis scope is to simulate the floater motion in the program Simo, then the generated times series of the riser upper end is input into the program Riflex. In Riflex a simple riser model is modelled without using pipe-in-pipe model. Then the riser will follow the time series of the upper end till the moment stroke reaches maximum. The corresponding modelling will be that the riser follows the horizontal motions but the vertical motions till the stroke lock. Then riser follows the complete motions of the floater. Thus the stroke reactivation is ignored.

As the floater motions are oscillating, tensioners may reach the lock position (piston bottom& no stroke) firstly. Then stoke restored because of the oscillating motions in which floater heave motions have the most significance for example if the heave motion is at the crest by the time when tensioners lock firstly. Finally as the offset increasing, the tensioners lock status will not change.

The riser tension difference between the pipe-in-pipe situation and simple-model situation can be illustrated by the figure 77 below.

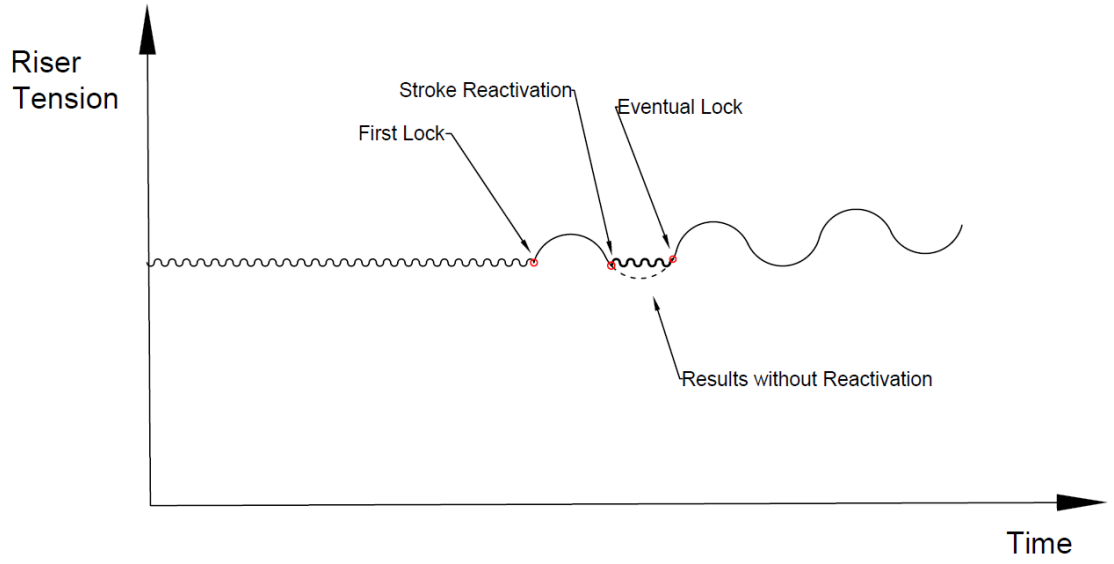

Figure 80 Simple locking modeling

The difference can be figured by riser tension variation. If the tensioner is functioning with spare stroke, the riser tension will stay almost constant varying in a smaller range. After the first lock, the two models will increase identically with larger tension variation until the first stroke reactivation happens. This is where the difference resides that stroke reactivation (pipe-in-pipe model) will make riser tension restore to the former constant state whereas lock (simple model) will increase the tension slowly with larger variation. Then lock and stroke reactivation will alternate even several times before the eventual lock. Thereafter, the two models will behave identically.

The detailed modelling difference can be seen as below. (The modelling below assumes no “yaw” motions of the risers)

The pipe-in-pipe model (realistic modelling) is illustrated in the figure 78. The upper end of the tensioner is pinned to the floater such that it will follow the floater translational motions. The pipe-in-pipe model will be effective until the stroke lock as phase 1.

Phase 2 is the moment just before the stroke lock. With the stroke lock and reactivation alternating, tensioner will finally reach the phase 3 when stroke is locked eventually.

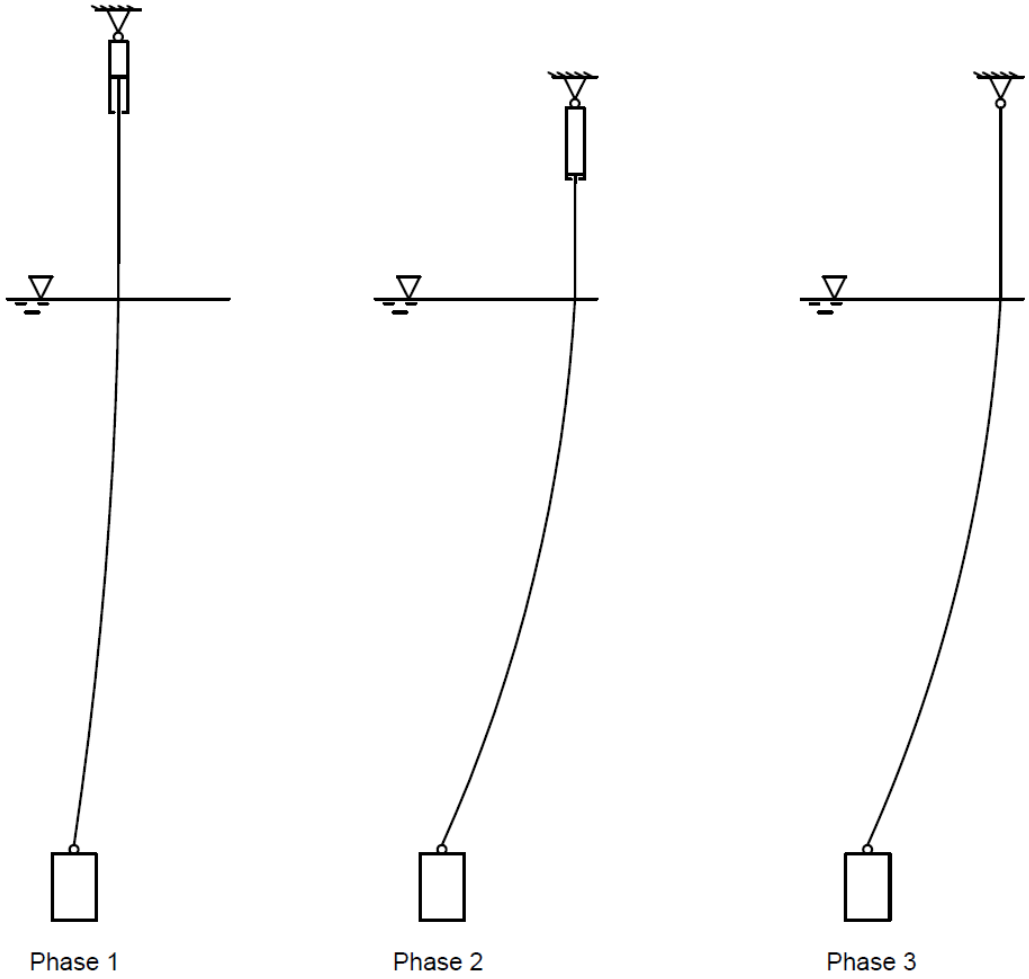

Figure 81 Riser realistic modelling

11.1.11.5 Further scope of study

For further improve the accuracy, some aspects can be improved regarding modelling in the future. First the connection between tensioners and floater should be modelled, it can smooth the sudden tension change after locking. Second the pipe-in-pipe

modelling should be adopted for tensioners as it account for the realistic mechanisms. Thirdly to see the critical local stress that motions from the pipe-in-pipe model should be input to Abaqus.

When Sima have some modification regarding the boundary condition change in coupled analysis in the future, the current analysis in the thesis should result in better comparisons.

For post processing, the thesis have used the post processing function in the Sima which turns out to be rather efficient when processing multiple comparisons. But the Sima post processing function is very convenient for the clarifying the relationships and testing results for improvement. Therefore multiple data processing should be done in Matlab in the future.

The equations and figures numbering and the corresponding references in the text needs to be changed with the thesis processing. The field function in the text editing software should be taken care of in the future.

The horizontal component of the riser upper end tension should be adopted as a comparison parameter in the future. This came into notice when discussing the results and not too much time for including this.

The sea component distribution over time seems to depend on time of analysis. The theories regarding the sea state realization in the program and hydrodynamic forces effects on the floater should be studied in the future.

For simple modelling in Riflex, the tensioner is omitted which is drawn in dash line to enlighten the differences between the two modelling in figure 79.

The upper end of simple modeling is located a little below the tensioner at the upper end of the outer barrier of the telescopic joint. This assumes that connection between upper end the tensioner and upper end of the outer barrier is rigid. Since the distance is not long this is a good approximation is assumed. The upper end of the out barrier of the telescopic joint follows the motions parallel to the sea surface (x-y plane) and the direction perpendicular to the sea surface (z direction) is assumed to be free with constant tension.

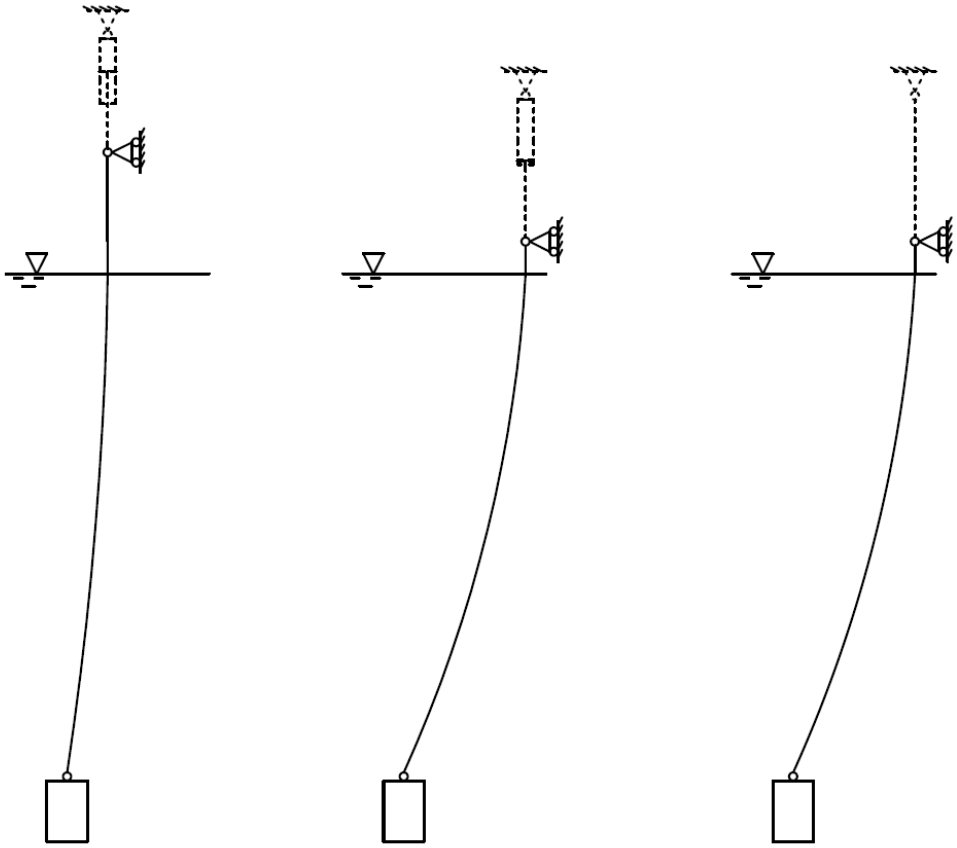

Figure 82 Riser simple modelling

References

BAI, Y. and BAI, Q. (2005) *Subsea pipelines and risers*. 2nd Edition. Amsterdam: Elsevier Science

FACTPAGES (2015) Field production yearly [Online] NPD. from: http://factpages.npd.no/factpages/Default.aspx?culture=en&nav1=field&nav2=TableView%7cProduction%7cTotalNcsYear [Accessed 21/08/2015]

ZHAN J.P. (2010) *Review and verification of marine riser analysis programs*. Thesis (MSc), NTNU.

STEN, R. (2012) *Dynamic simulation of deep water drilling risers with heave compensating system*. Thesis (PhD), NTNU.

ORCINA (2009) *Orcaflex theory manual*. Version 9.3c. Cumbria: Orcina Ltd.

Patel, M.H. (1995) Review of flexible riser modelling and analysis techniques. *Engineering Structures,* 17(4), pp. 293-304.

FALTISEN O.M. (1990) *Sea loads*. Cambridge: Cambridge University press, pp. 259-265.

LARSEN C.M. (1996) *Static analysis of non-vertical marine risers by simplified methods*. Lecture notes, NTNU.

PEYROT A.H. and GOULOIS A.M. (1979) Analysis of cable structures. *Computers and structures*, 10(5), pp. 805-813.

ARANHA J.A.P. (1997) Analytical approximation for the dynamic bending moment at the touchdown point of a catenary riser, *IJOPE.* 7(4).

CAMPBELL, I.M.C. and WEYNBERG, P.A. (1980) *Measurement of parameters affecting slamming: final report*. Technology Reports Centre No. 0T-R-8042 Wolfson Unit for Marine Technology Report No. 440. Southampton: Wolfson Unit for Marin Technology.

NESTEGÅRD, A., KALLEKLEV, A.J., HAGATUN, K., WU, Y.L., HAVER, S., and LEHN, E. (2004) Resonant vibration of riser guide tubes due to wave impact. In: *23rd International Conference on Offshore Mechanics and Arctic Engineering, Vancouver, June 2004.* pp. 987-994.

HERMANRUD L. (2014) *Dynamic analysis of workover riser under unexpected conditions*. Thesis (MSc), NTNU.

GRØNEVIK A. (2013) *Simulation of drilling riser disconnection-recoil analysis*. Thesis (MSc), NTNU.

KAVANAGH K., DIB M., BALCH E., and STANTON P. (2002) New revision of drilling riser recommended practice. In: *2002 Offshore Technology Conference. Houston, May 2002.*

NGUYEN C., THETHI R., and LIM F. (2006) Storm-Safe Deepwater Drilling. In: *IADC/SPE Asia Pacific Drilling Technology Conference and Exhibition. Bangkok, November 2006.*

DOPHIN DRILLING (2013) *Dolphin drilling internal documents.* Stavanger: Dolphin Drilling Ltd.

YOUNG R.D., HOCK C.J., KARLSEN G., MILLER J.E. (1992) Analysis and design of anti-recoil system for emergency disconnect of a deepwater riser: case study. In: *1992 Offshore Technology Conference*. *Houston May 1992.*

LARSEN. C.M. (Circa April 2015) *Conversation during guidance.*

AKER KVÆRNER STORD AS (2007) *Drilling riser analysis*. Doc. No. H600-ED465-R-CA0001, rev 02.

SPARKS, C. P. (2011) *Fundamentals of marine riser mechanics - basic principles and simplified analysis.* Oklahoma: PennWell

WAJNIKONIS C.J. and LEVERETTE S.J. (2009) Improvements in dynamic loading of ultra deepwater catenary risers. In: *2009 Offshore Technology Conference*. *Houston May 2009.*

THORY G. (1998). *Controlled pressure multi-cylinder riser tensioner and method*, Google Patents.

GRYTOYR G., SHARMA P., and VISHNUBOTLA S. (2011) Marine drilling riser disconnect and recoil analysis. In: *2011 AADE National Technical Conference and Exhibition*. *Houston April 2011.*

SINTEFF (2013) *RIFLEX user manual.* Trondheim: SINTEFF.

HDFGROUP (2011) WHY HDF? [Online] HDFGROUP Available from: https://www.hdfgroup.org/why_hdf/ [Accessed 21/08/2015].

MARINTEK (2015) Sima in-program help contents. Trondheim: Marintek.

API (2004) *Specification for Control Systems for Drilling Well Control Equipment and Control Systems for Diverter Equipment, Upstream Segment*. 2nd Edition. Washington, D.C.: American Petroleum Institute.

MCgINTY B. (2012) Continuum Mechanics [Online] Available from: http://www.continuummechanics.org/cm/index.html [Accessed 15/07/2015].

WANG, Y.J. (1986) Incremental virtual work equation for geometric nonlinear analysis. *Applied Mathematics and Mechanics,* 8(5).

RMSETH, S.N. (1978) *Nonlinear Static and Dynamic Analysis of Space Structures*. Thesis (PhD), NTNU.

BERGAN, P.G. et al. (1985) *FENRIS System Manual, Theory-Program Outline-Data Input*. Report 83-6064. Høvik.

MOLLESTAD, E. (1983) *Techniques for Static and Dynamic Solution of Non-linear Finite Element Problems*. Report No. 83-1. Trondheim: Div. of Structural Mechanics of Norwegian Institute of Technology.

LARSEN, C.M (1990). *Response modelling of marine risers and pipelines.* Trondheim: The University of Trondheim.

LANGEN I. and SIGBJØRNSSON R. (1986) *Dynamisk analyse av konstruksjoner*. Trondheim: Tapir.

MATHISEN, K.M (2012). *TMR 4190 lecture notes.* Trondheim: Dept of Structural Engineering.

MOAN, T (2003). *TMR 4190 finite element modelling and analysis of marine structures.* Trondheim: Dept of Marine Technology.

ORMBERG, H and LARSEN, K (1997). *Coupled analysis of floater motion and mooring dynamics for a turret-moored ship.* Trondheim: MARINTEK.

GRECO, M. (2012). *TMR 4215: sea loads lecture notes.* Trondheim: Dept of Marine Hydrodynamics.

HAVER, S.K. (2007) *Prediction of Characteristic Response for Design Purposes*. Stavanger: Statoil.

WIKIPEDIA. (2015) *Swell (ocean).*[Online]. Available from: http://en.wikipedia.org/wiki/Swell_%28ocean%29 [Accessed 21/08/2015]